University of Calgary

PRISM Repository **https://prism.ucalgary.ca**

The Vault Open Theses and Dissertations

2012-10-03

Gait Analysis for Pedestrian Navigation Using MEMS Handheld Devices

Susi, Melania

Susi, M. (2012). Gait Analysis for Pedestrian Navigation Using MEMS Handheld Devices (Master's thesis, University of Calgary, Calgary, Canada). Retrieved from https://prism.ucalgary.ca. doi:10.11575/PRISM/26254

http://hdl.handle.net/11023/272

Downloaded from PRISM Repository, University of Calgary

UNIVERSITY OF CALGARY

Gait Analysis for Pedestrian Navigation Using MEMS Handheld Devices

by

Melania Susi

A THESIS

SUBMITTED TO THE FACULTY OF GRADUATE STUDIES

IN PARTIAL FULFILMENT OF THE REQUIREMENTS FOR THE

DEGREE OF MASTER OF SCIENCE

DEPARTMENT OF GEOMATICS ENGINEERING

CALGARY, ALBERTA

SEPTEMBER, 2012

© Melania Susi 2012

Abstract

Advances in Micro-Electro-Mechanical Systems (MEMS) technology play a central role in the design of new generation of smartphones. Indeed MEMS sensors, such as accelerometers and gyroscopes, are currently embedded in most smart devices in order to augment their capabilities. In the near future, it is expected that these sensors will be further exploited for pedestrian navigation purposes. However, the processing of signals from MEMS sensors cannot provide accurate navigation solutions without external aiding, e.g. from GNSS (Global Navigation Satellite Systems) signals, since their signals deteriorate due to significant errors, principally biases and drift which requires frequent sensor resets.

When GNSS is not available and the sensors are mounted on the user's foot, periodic zero velocity updates can be performed during the identified stance phases of the foot, namely the periods when the foot is flat on the ground. In the case of handheld devices, this approach cannot be adopted, since zero velocity periods are not present. Furthermore, when the sensors are held in a hand, the sensed motion can be decoupled from the global user's motion rendering the situation much more complex to deal with. For this reason previous studies on pedestrian navigation are mainly focused on the body fixed sensor case.

In this thesis, algorithms for characterizing the gait cycle of a pedestrian holding an IMU (Inertial Measurement Unit) in hand are proposed but without constraining the user in its behaviour and thus taking into account several sensor carrying modes. In view of the variety and complexity of human motions, the recognition of the user's global

motion from handheld devices is first thoroughly examined. A classifier able to recognize several different motion modes, including standing, walking, running, climbing and descending the stairs, is designed and implemented. Then an algorithm for evaluating the linear displacement of a pedestrian walking on a flat plane using only a handheld IMU is proposed. The complete algorithm comprises the following three modules: (1) Characterization of the user's activity and recognition of the sensor carrying mode, (2) Step detection and (3) Step length evaluation.

The analysis leads to a novel step length model combining the user’s height, the step frequency and a set of three constants. First a universal model is proposed where the three constants have been trained with 12 different test subjects. Then, the same model is used for 10 different subjects to calibrate individually the set of constants. The validity of both universal and calibrated models is assessed in position domain using the above 10 test subjects. The fitted solution achieves an error between 2.5 and 5 % of the travelled distance, which is comparable with the performance of models proposed in the literature for body fixed sensors.

Preface

This thesis includes a number of figures and tables previously published in two conference papers (Susi et al 2011a, Susi et al 2011b) and one journal paper (Renaudin et al 2012). All these figures and tables have been produced by the thesis author on the basis of this thesis research. The co-authors' valuable feedback on the above figures and tables is acknowledged. The publication of the above material in this thesis is allowed by co-authors and journal publishers.

Acknowledgements

I would like to express my sincere gratitude to Professor Gérard Lachapelle for giving me the chance to conduct my studies under his supervision. His continuous encouragement and his generous knowledge sharing were essential during my master studies. Furthermore, the care with which he reviewed the chapters of this thesis really improved the quality of the work. His commitment to the work will be an example and an inspiration for my future work.

I wish to also thank my co-supervisor Dr. Valérie Renaudin for believing in me and for her enthusiastic approach to this research work. Her detailed review of my thesis and useful comments enhanced the value of this dissertation. I greatly appreciated her help during the numerous and long data collections performed for this thesis.

The financial support of Research In Motion (RIM), the Natural Science and Engineering Research Council of Canada, Alberta Advanced Education and Technology and Western Economic Diversification Canada is acknowledged.

I am sincerely grateful to Dr. Daniele Borio for his valuable advices, helpful discussions and support during my first year of studies in Calgary. Thanks to Dr. Aiden Morrison for designing and realizing the NavCube, the sensor platform used for many

field tests of this thesis. This tool was essential for my research work. I also want to thank him and Dr. Haris Afzal because they were kindly available to help me during many data collections.

Thanks to my friends of the PLAN group for the good time spent together and the discussions about my research. In particular, I would like to thank Peng Xie, Martin Ma, Da Wang, Anup Dhital, Billy Chan, Yuhang Jiang and Zhe He. Thanks to all of the PLAN group members also because almost everyone acted as test subjects for the experiments of this thesis. Special thanks to Martin Ma, who was available to act as a test subject at any time and with any temperature (even below -30°C!). I also want to thank many visiting students with whom I shared good moments: Sophie Damy, Leslie Montloin, Leila Kleiner, Rahul Godha, Antonio Angrisano, Salvatore Gaglione, Nicola Linty, and Cyril Pedrosa.

I owe thanks to my family and my friends in L'Aquila for their constant and unconditional support.

Finally, I wish to express my most heartfelt gratitude to my beloved and missed grandmother Adalgisa and grandfather Mazzini who taught me the most important lesson of my life, the only one that I am sure I will never forget. Thank you because you made me the person I am today.

Dedication

I dedicate this thesis

to my beloved grandmother Adalgisa and grandfather Mazzini.

.

Table of Contents

List of Tables

List of Figures and Illustrations

List of Symbols, Abbreviations and Nomenclature

Abbrevations	Definitions
AR	Auto-Regressive
COM	Centre Of Mass
DFT	Discrete Fourier Transform
DoF	Degree of Freedom
DR	Dead Reckoning
FFT	Fast Fourier Transform
GNSS	Global Navigation Satellite Systems
GPS	Global Positioning System
IMU	Inertial Measurement Unit
INS	Inertial Navigation System
LPC	Linear Prediction Coding
MEMS	Micro Electro-Mechanical Systems
PDA	Personal Digital Assistant
PDR	Pedestrian Dead Reckoning
PSD	Power Spectral Density
RFID	Radio-Frequency Identification
RLS	Recursive Least Square
STFT	Short Time Fourier Transform
UWB	Ultra Wide Band

WiFi	Wireless Fidelity
ZUPTs	Zero velocity UPpdaTes
ZARUs	Zero Angular Rate Updates

Symbols	**Definitions**
$\mathbf{a}$	acceleration vector
a_k	linear predictor coefficients
$d_{(\bullet)}$	distance computed at the time $(\bullet)$
$E_{(\bullet)}$	energy of the quantity $(\bullet)$
f_s	sampling frequency
f_{step}	step frequency
f_{stride}	stride frequency
$\mathbf{H}$	design matrix
k	constants for the step length model/number of nearest neighbours
n	time index of discrete samples
N	analysis window length
$p_{(\bullet)}$	position computed at the instant $(\bullet)$
P_{det}	probability of detection
P_{fa}	probability of false alarm
P_{md}	probability of miss detection
$\hat{P}_x$	estimated spectrum

s	step length
$\mathbf{s}^a$	output of the tri-axis accelerometer
$\mathbf{s}^\omega$	output of the tri-axis gyroscope
$\tilde{\mathbf{s}}$	filtered IMU signal norm
$\tilde{\mathbf{s}}_0$	unbiased filtered IMU signal norm
ϑ	heading
$\boldsymbol{\eta}^a$	noise vector associated to the gyroscope output
$\boldsymbol{\eta}^\omega$	noise vector associated to the accelerometer output
$\sigma^2_{(\bullet)}$	variance of the quantity $(\bullet)$
$\boldsymbol{\omega}$	angular rate vector
$[\square]^T$	transpose operation of the quantity $(\bullet)$
$[\bullet]^{-1}$	inverse operation of the quantity $(\bullet)$
$\lVert\square\rVert$	norm of the quantity $(\bullet)$

Chapter One: Introduction

The increasing demand for smart-phones motivates manufacturers to provide innovative and competitive capabilities to these mobile devices. Embedded sensors are foreseen to be used to track the position of a mobile phone user walking in a shopping centre, downtown or in other critical environments where Global Navigation Satellite Systems (GNSS) signals are hardly available. The possibility to track pedestrians indoors extends location based services not only for mobile phone applications but also to other domains, including search and rescue services, enhanced E-911, health monitoring services and many other applications (e.g. Bancroft 2010).

Currently navigation services provided by mobile devices are mainly based on GNSS signals and, subsequently, are more confined to outdoor environments. Indeed indoors or in light indoor environments the accuracy, the availability and the continuity of GNSS services cannot be guaranteed since satellite signals are strongly attenuated and affected by multipath. This represents a major limitation for pedestrian navigation applications as in general, people spend the majority of their time in indoor or urban environments. To overcome this limitation, it is possible to use hybridisation techniques and for example combine GNSS receivers with an Inertial Measurement Unit (IMU). The latter is composed of a tri-axis accelerometer and gyroscope providing acceleration rate and angular rate measurements of the rigid body with respect to the navigation frame. These measurements have to be integrated in order to estimate body's position and orientation by applying a strap-down approach (Titterton & Weston 2004).

However, due to the integration operation, small errors can produce a significant error growth that is directly proportional to the operation time. This aspect is particularly critical for Micro Electrical Mechanical Systems (MEMS) sensors whose signals are affected by large errors. Indeed, for low cost sensors the error growth is proportional to the cube of the operation time (Skog et al 2010). Consequently, the navigation solution provided by MEMS accelerometers and gyroscopes requires external constraints, for example, obtained from frequent GNSS updates. When the latter are not available, approaches alternative to the double integration of inertial data, implemented by the strap-down method, should be applied. In the pedestrian navigation case, the characteristics of human gait can be exploited in Pedestrian Dead Reckoning (PDR) which is presented in Section 1.1.

1.1 Pedestrian navigation: general overview

Pedestrian navigation refers to the act of guiding a person moving on foot from a starting point to a prefixed destination by means of diverse technologies. This challenging task relies on the continuous localization of pedestrians in ubiquitous environments and addresses a wide range of applications. Each application requires a specific level of accuracy that is maximum for safety related services (Bancroft 2010) and lower for the consumer grade market. Due to the unpredictability of human motion and the variety of involved environments, the quality of pedestrian navigation services cannot easily be guaranteed everywhere. In open sky environments, GNSS is certainly the primary technology for navigation but in indoor spaces or in urban canyons the

situation is much more complex. Indeed buildings and manmade infrastructures are blocking and attenuating satellite signals, which complicates their tracking and processing.

High sensitivity GNSS receivers can be used to acquire weak signals even inside buildings or in urban canyons but their quality is often still too low for computing a reliable position estimate in the above adverse environments (Lachapelle 2007).Consequently, the integration of GNSS with other technologies is necessary. Radio based positioning systems using Wireless Fidelity (WiFi), UltraWide Band (UWB) or Radio-Frequency Identification (RFID) are possible options for tracking pedestrian indoors (Alonso et al 2009, Inoue et al 2009, Luimula et al 2010, Shen et al 2010). The main drawback of all above systems is that they are usually limited to specific areas because they rely on dedicated infrastructures, which are expensive.

Another possible option is to combine GNSS with inertial sensors following a dead reckoning (DR) approach. This method evaluates the current position of a moving object starting from the previous one. It was originally applied to ship navigation and is named PDR when it is adapted for pedestrian navigation.

PDR offers an interesting strategy because it uses inertial sensors by exploiting the kinematic of the human gait (Beauregard 2007, Renaudin et al 2007) instead of doubly integrating the inertial data as it is classically done in a strap-down approach. As explained in the Introduction, the latter method is not recommended for pedestrian navigation using low cost sensors, since even if the subject is not moving the double integration increases the noise components proportionally to the operational time.

Instead the PDR allows bounding the sensor errors growth using information extracted through the pedestrian gait analysis.

Human gait analysis refers to the study of human locomotion involving the estimation of spatial and temporal parameters (Tao et al 2012, Do & Suh 2012) such as step length or walking speed for several application domains, including sport, healthcare and entertainment applications. When PDR algorithms are applied, the gait information is used to propagate the user's position. The process computes the user's position starting from an initial known position using the heading estimate and the user travelled distance or speed. Traditionally, linear displacement is evaluated by first detecting the user's steps and then determining their length.

1.2 Limitations of previous works

Published techniques for pedestrian navigation are very effective when the sensor is fixed on the user's body, especially when it is located on the foot. In this case the stance phase of the foot, i.e. when the foot is flat on the ground, can be identified. Periodic Zero velocity UPdaTes (ZUPTs) and/or Zero Angular Rate Updates (ZARUs) are then performed to bound the position error accumulation (Foxlin 2005, Skog et al 2010, Godha & Lachapelle 2008, Suh & Park 2009). This approach is based on the biomechanical observation stating that during normal walk the user's foot touches periodically the ground. The same approach is used for sensor mounted on the user's ankle, since also in this case static periods can be identified.

Many authors have addressed the cases of sensors placed on the user belt or torso. These sensor locations are also very suitable for pedestrian navigation since the motion of the sensor reflects the motion of the subject's Centre Of Mass (COM) and consequently the global user's motion (Alvarez et al 2006, Jahn et al 2010). However, body fixed locations are generally not realistic for common users that are usually carrying their mobile devices in their hands, trouser pockets, or handbag.

For the above cases, especially when the sensor is in the hand, the situation is much more complex. Few authors deal with the unmounted sensor case. The majority of them consider sensors placed in the user's pocket (Steinhoff & Schiele 2010, Bylemans et al 2009). This situation is less complex than the handheld device case. Indeed the patterns of the recorded IMU signals are generally undistorted and can be directly related to the motion of the user's leg and consequently to the user's foot. When the sensor is held in a hand, the main challenge is that the hand motion can be highly decoupled from the user's motion. Consequently, the motion of the hand can mask the accelerations due to the user displacements. In addition, when the sensors are not body fixed, not only their orientation is unknown but it can rapidly change when the subject moves the hands. For this reason, in the case of a handheld device, a continuous identification of the global user's motion mode and of the hand motion is required to properly tune the navigation algorithms constraining the computation of the subject's trajectory to real displacements.

In Gusenbauer et al (2010), the case of a mobile device carried in the user's hand and orientated toward the current line of sight is considered. This corresponds to the typical mobile phone orientation when the subject is looking at the screen to read navigation instructions. However the cited work is restricted to the above sensor position and does not consider any different carrying mode. Another approach for handheld devices is based on the integration of IMU signals with a camera, which is generally already embedded in smart phones. In Hide et al (2010) the case of a walking user carrying the mobile device in front of him and with the camera pointing toward the ground is considered; the paper exploits the extracted images to evaluate the translation between frames and consequently to bound the error accumulation due to the use of the inertial sensors. This approach is limited by the estimation of the orientation of the camera, the lightning conditions and the uniqueness of features in the frames.

Consequently the few works dealing with the non body fixed sensor case are generally assuming that the sensor is relatively stable while the user is walking and are generally ignoring the swinging hand case. The above assumption strongly limits the applicability of these algorithms to real scenarios where portable devices are held without any constraint and are, consequently subjected to a great variety of hand motions.

1.3 Main contribution

In view of the limitations of published works, the overall purpose of this research is to contribute to the development of PDR algorithms for handheld IMU devices. It is worth mentioning that this thesis work does not deal with the estimation of the heading required for PDR algorithms, but focuses on the evaluation of the user's linear displacement. All the proposed algorithms are working with sensors that are freely carried by the user, without any restriction on the device's orientation and considering that the sensor carrying mode could change suddenly. The major contributions of this work are summarized as follows:

1. **Analysis of techniques for processing the IMU signal and extracting human gait characteristics:** Since this work proposes algorithms for pedestrian navigation based on gait analysis, the characteristics of IMU signals are extensively analyzed in the time, frequency and time-frequency domains. The different signal patterns produced by different sensor carrying modes are also examined. In particular, how human gait characteristics are reflected into IMU signal patterns is investigated. Finally, different signal pre-processing techniques are considered in order to cope with the noisy nature of low cost sensor signals.

2. **Classification of user's global motion mode using handheld IMU devices:** Different sensor locations are subject to different cyclic dynamics occurring during diverse human activities. The knowledge of these dynamics can help tuning the correct propagation of the user's position estimate. For this reason, the

recognition of user global motion modes is deeply analyzed herein for the case of handheld devices. The following motion modes are considered: standing, walking, running, climbing and descending stairs. The recognition of the mentioned motion modes is considered as a classification problem and is performed by extracting several features from the sensor signal. The extracted features are integrated in three different classifiers, namely the Naïve Bayesian, the *k*-nearest-neighbour and the decision tree classifiers. Performance of the above classifiers is compared through several field tests. The results of this research have been presented in Susi et al (2011a).

3. **Characterization of the walking case**: A specific analysis of the walking case has been conducted. The characterization of the walking case consists in recognising the sensor carrying mode of a walking subject. In particular, the following states have been considered: walking with the sensor in the swinging, texting and phoning hand or keeping the sensor in a handbag. The recognition of irregular motions has also been studied and defines an additional state in the activity classification process. It represents a novel element with respect to existing contributions in this field. This class of motion refers to parasite motions that do not reflect a real variation of the user's displacement and that have consequently to be removed from the navigation process. Some of this work has been published in Susi et al (2011b).

4. **Step detection algorithms for a walking subject using handheld IMU devices:** Different step detection algorithms are proposed for the walking case.

The algorithms are adaptive, i.e. properly tuned according to the sensor carrying mode and are based on low pass filtering and peak detection techniques. Furthermore, the use of an adaptive threshold makes the peak detection algorithms independent of the variations of the signal energy and consequently of any change of the user pace.

5. **Step length estimation for a walking subject using handheld IMU devices:** In order to evaluate the user step length, a model has been designed. It combines the user step frequency and user height with a set of three variables. The step frequency is extracted directly in the frequency domain through a dedicated analysis of the IMU signal. In particular, the relationship between the frequencies extracted from handheld signals and step frequency is thoroughly investigated. A universal model is proposed where the three constants have been trained using 12 subjects. A calibration of these constants has also been performed for fitting the model to each subject. The performance of the proposed model is assessed with ten subjects. This novel step length model has been published in Renaudin et al (2012).

1.4 Thesis organization

The structure of this dissertation is now summarized.

Chapter 2 reviews the theoretical background of the human walking bio-mechanic. In particular, since the case of IMU handheld sensors is the target of this

work, focus is made on the bio-mechanic theory describing the synchronization between arms and legs during the walk. An extensive analysis and comparison of different techniques for processing the IMU signals is proposed. Furthermore, the signal pre-processing techniques adopted to cope with low cost sensors' noise are described.

Due to the complexity of the human motion, knowing the user's context, in terms of motion, can help bounding the position errors. Since in this work the recognition of the user motion is considered as a classification problem, **Chapter 3** recalls the basis of classification theory. In particular the Naïve Bayesian, the *k* nearest neighbours and the decision tree classifiers are illustrated. The implementation of the classification theory for recognising human motion is described.

First of all, the cases of the user's global motion identification are described. Several features, extracted from the IMU signal and for different sensor carrying modes, are presented. All extracted features are integrated in the three previous mentioned classifiers. Then, the recognition of different sensor carrying modes for a walking subject is investigated. A new motion mode is introduced, namely the irregular motion. The features extracted for the characterization of the walking case are deeply examined. Finally the complete decision tree classifier, which has been designed and implemented for recognizing the above states, is presented.

Chapter 4 is focusing on the evaluation of the pedestrian linear displacement that traditionally consists of two elements: first detecting the user's steps and then evaluating

their length. A general overview of existing step detection techniques using body mounted sensor is reported. Furthermore, algorithms to detect step events by using IMU handheld devices are proposed.

Specifically, two different algorithms are presented: one for users carrying the device in a swinging hand and one for users texting, phoning or carrying the device in a bag. It is shown that the latter cases can be grouped in a unique class, since the signal patterns produced in these cases are comparable with the ones obtained for body fixed sensors. Then, the novel step length model for handheld IMU devices is proposed. The derivation of both the universal model and the model fitted to each test subject is described.

Chapter 5 describes the field tests performed for training and assessing all proposed algorithms. Finally **Chapter 6** draws some conclusions and proposes research directions for future work. In Figure 1-1 a scheme representing the thesis structure is shown. In particular, the interconnections (in red) among conceptual subsections of different chapters and the interconnections (in blue) among subsections of the same chapter are represented.

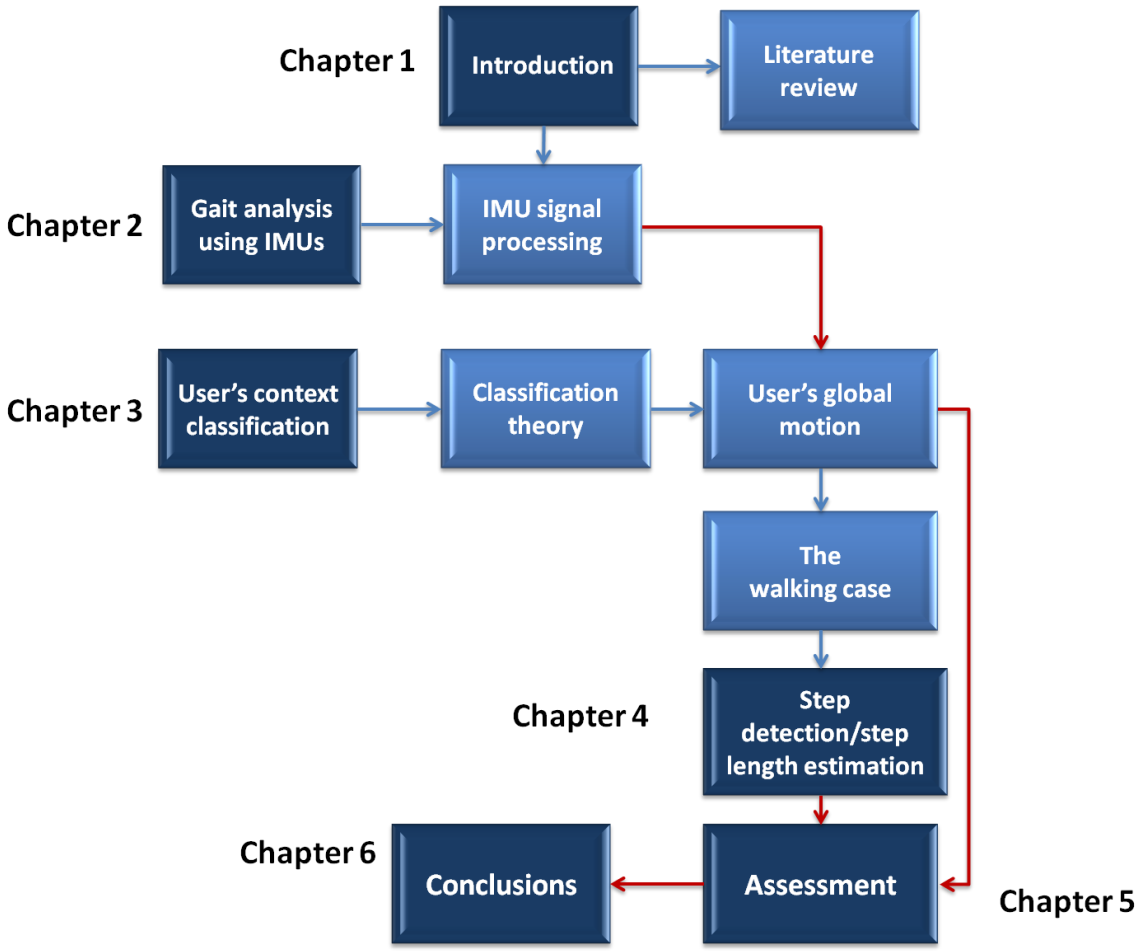

Figure 1-1: Structure of the thesis and logic interconnections among chapters

Chapter Two: Human gait analysis by using inertial handheld devices

This chapter introduces the main characteristics of human gait that can be exploited for navigation purposes in PDR algorithms. The IMU that is used to detect human gait and design the proposed algorithms is first described. In particular, the error sources affecting the IMU signals are presented. Since these errors can degrade the performance of the navigation algorithms, a dedicated signal pre-processing phase is required and described. Finally, different signal processing techniques, in the time, frequency and time frequency domains, are proposed to extract relevant information from the IMU signals.

2.1 Human gait

Human gait analysis refers to the study of human locomotion through the evaluation of kinematic, kinetic and spatial/temporal parameters (Do & Suh 2012). This field of study finds application in a large variety of domains, including entertainment, healthcare and pedestrian navigation.

The act of walking involves the coordination of different human body parts, such as the skeleton, the muscle and the neural systems. Various factors can affect the complex interaction between the body parts, for example any pathological nature will require a distinction between "**normal gait**" and "**pathological gait**". "Normal gait" refers to the naturalistic and general human walking parameters without differentiating the age, sex or individual physical parameters. Conversely, "pathological gait" refers to an

abnormal gait, for example affected by pathologies such as muscle weakness or skeleton deformities (Rose & Gamble 2006).

In this thesis, only the normal gait case is considered. Indeed it has been shown that a normal gait is characterized by a fundamental pattern that is not subjected to inter and intra individual variations. Specifically the normal human gait is marked by the periodic repetition of two main phases, the **stance phase**, when the foot is in contact with the ground, and the swing phase, when the foot is in the air. These two phases are represented in Figure 2-1. The stance phase occurs between two events: the foot strike and the ipsilateral (same foot) foot off. Complementary, the swing phase starts with the foot off event and ends when the second ipsilateral foot strike (Rose & Gamble 2006).

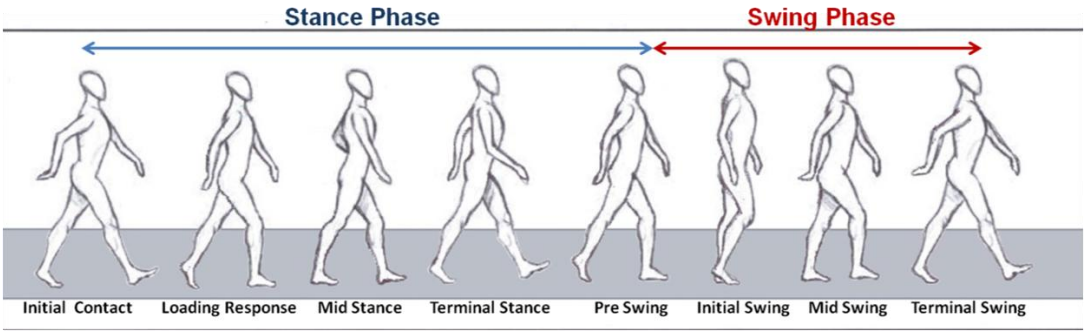

Figure 2-1: Human gait cycle and its phases

As shown in Figure 2-1, in the case of normal gait, the stance and swing phases can be further divided in eight sub phases as follows:

- Initial contact: refers to the precise instant when the foot touches the ground. The initial contact marks the beginning of the stance phase.

- Loading responses: corresponds to about 10% of a gait cycle. During this phase the foot comes in full contact with the ground and the stance limb supports all the body's weight.
- Mid-stance: starts when the foot leaves the ground and ends when the body advances over the stance limb.
- Terminal stance: starts when the heel leaves the ground and ends when the contra-lateral foot touches the ground.

- Pre-swing: in this phase the knee flexes before the swing phase and the body's weight is loaded to the opposite limb.
- Initial swing: represents the first third of the swing period. It starts when the foot leaves the ground and ends when the maximum knee flexion occurs.
- Mid swing: is the middle third of the swing period. It starts with the maximum knee flexion and ends when the tibia is vertical.
- Terminal swing: is the third swing period during which the knee fully extends before the heel's contact.

The repetition of the same event for the same foot marks the occurrence of the **stride** event. The repetition of the same event for different feet marks **step** events. In general, the period when the foot is flat on the ground is assumed as reference event since it is the most easy to be identified.

The running gait shows some differences with respect to the walking gait. While in the walking case there is at least one foot that touches the ground, in the running case, aerial phases, when both feet are in the air, can be identified. For this reason, in the running mode, the vertical component of the ground reaction assumes bigger values than in the walking mode. More specifically, during running the stance phase decreases by 35% while the peak ground reaction force increases by 50% (Rose et al 2006). These different values of the stance phase and the ground reaction force are reflected in different patterns of the **Centre Of Mass** (COM), which is the point of the body where the entire mass can be considered concentrated (Rose & Gamble 2006). In walking mode the centre of mass assumes its biggest value at the middle of the stance phase. Conversely, during the running mode, the centre of mass reaches its lowest values at the middle of the stance phase. Indeed the different profile drawn by the centre of mass during motion can be used to distinguish running and walking modes (Rose & Gamble 2006).

However, this approach will not be used in this thesis. The COM plays an important role in gait analysis. In Winter (2004), the COM is considered as the intersection of the sagittal, the transverse and the frontal plans cutting the human body as shown in Figure 2-2. Although the COM varies dynamically according to the performed motion, when the subject is static, it can be considered placed close to the hip. Indeed, since the COM's motion reflects the global motion, it is common to place the sensor used for gait analysis close to the hip. However, this location is not suitable for mobile devices. Indeed mobile devices are generally held in hand. In order to track the

global user's motion even if the sensor is held in the hand, it is necessary to analyze how the motion of the body's upper and lower parts are related. Generally, human gait analyses are focused on the motion of the body's lower part. For this reason, gait models are generally designed excluding the subject's arm contribution. A few studies have analyzed the arms' swing in conjunction with the foot's vertical moment.

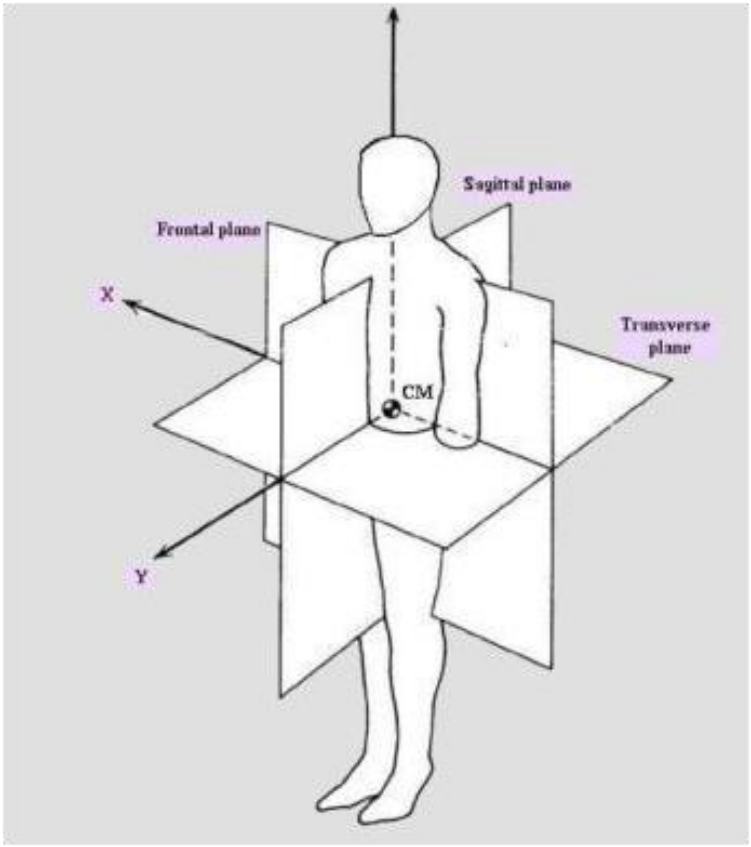

Figure 2-2: Representation of the human body and the three plans defined by the body's COM - adapted from Winter (2004)

Specifically, it has been observed that during normal walk, coordination between upper and lower parts of the human body exists. Indeed, the arms' swing has the purpose of decreasing the reaction momentum of the vertical axis of the foot (Park

2008). For example, when the left foot is on the ground (during the stance phase), a positive torque induced by the arm swing allows advancement of the right leg. The same event happens for the right leg. Consequently, this coordination can be exploited to track the lower part motion even if the sensor is handheld.

2.2 Inertial sensors for detecting human gait

In this thesis, gait analysis is performed using data from a MEMS IMU. MEMS technology is based on the integration of mechanical micro structures, sensors, actuators and electronics on a single chip realized with micro fabrication techniques used in the semiconductor industry (Park & Gao 2008).

The term IMU indicates a device including three accelerometers and three gyroscopes fixed in orthogonal triads. In Figure 2-3 an IMU (left side) and the scheme of its internal structure (right side) are shown. The use of one or more IMUs to characterize human gait is a very common approach (Sabatini et al 2005, Mathie 2003). Indeed an accelerometer and a gyroscope allow providing the body's angular rate and acceleration, which can be processed for tracking motions.

MEMS IMUs are particularly appealing for consumer grade applications thanks to their advantageous properties. They are low cost, low power consumption, small size and light weight. All these characteristics allow these sensors to be embedded in unobtrusive devices, such as smart phones or Personal Digital Assistants (PDAs). Conversely, the main drawback is that their signal is affected by various noises and biases degrading the IMU's performance. In this section, first of all the accelerometer

and gyroscope sensors are described. Then the error sources affecting their signals are detailed. Finally, various techniques to process the IMU signal, and subsequently cope with their noisy nature, are illustrated.

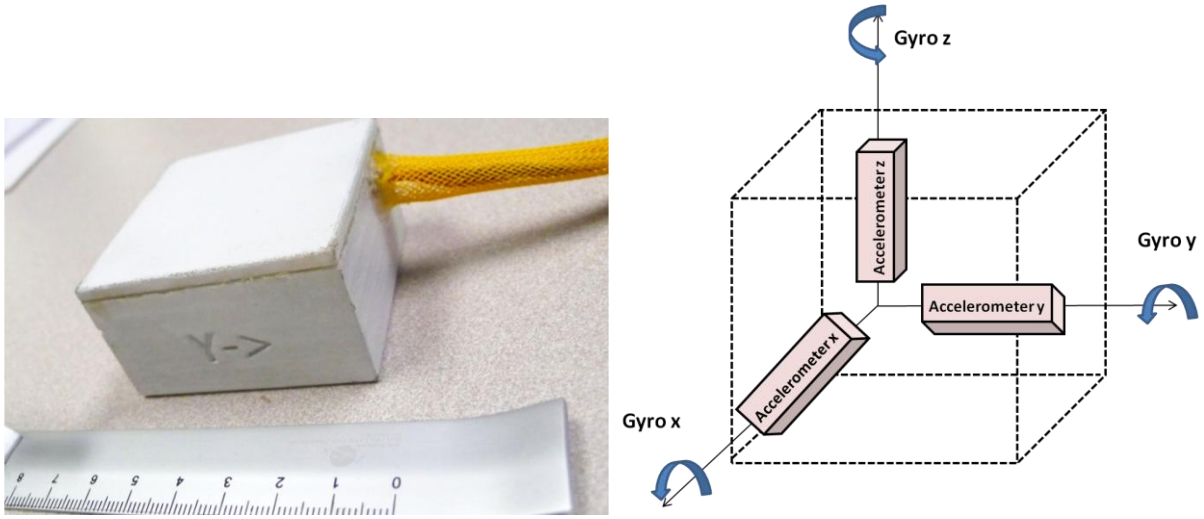

Figure 2-3: (Left) Inertial measurement unit (IMU); (Right) IMU's scheme showing the three accelerometers and the three gyroscopes mounted in an orthogonal triad (adapted from Gabaglio 2002).

2.2.1 Accelerometer

An accelerometer is a sensor able to provide the acceleration of a body, whose mass is known, by exploiting Newton's second law (**F** = m**a**). Different types of accelerometers can be implemented (Titterton & Weston 2004). The pendulum accelerometer is the most commonly implemented using MEMS technology and is composed of a proof mass suspended by springs and constrained to move only along a predefined axis. Furthermore, the mass is placed in the middle of two electrodes. When acceleration occurs along the predefined axis, the proof mass is moving from its equilibrium position. The displacement's change can be evaluated by measuring the

capacitance's change. The latter is then used to evaluate the amplitude of the force inducing the proof mass's displacement (Kraft 1997).

2.2.2 Gyroscope

Gyroscopes are sensors able to provide the angular rate of a body with respect to a reference frame. There are different varieties of gyroscopes, namely mechanical, optical and vibrating gyroscopes. An extensive survey can be found in (Titterton & Weston 2004). While the realization of mechanical and optical gyroscopes is still expensive, vibrating gyroscopes can also be low cost if manufactured with MEMS technology. Gyroscopes exploit the Coriolis effect according to which an object with velocity $\boldsymbol{v}$ and angular rate $\boldsymbol{\Omega}$ will experience an acceleration $\mathbf{a}_{cor}$. The Coriolis acceleration can be expressed by

$$\mathbf{a}_{cor} = 2\mathbf{v} \times \boldsymbol{\Omega} \quad (2.1)$$

The vibrating gyroscope impresses a velocity to a proof mass by inducing a vibration on the above mass. Due to the Coriolis principle, if an angular rotation is induced along a direction perpendicular to the velocity's plane, a Coriolis acceleration is produced. The resulting acceleration vector, lying on the plane perpendicular to the velocity and angular rate vectors, modifies the motion of the proof mass. The Coriolis acceleration can be sensed by electrical circuits able to detect a variation of the electrical capacitance. Subsequently, the angular rate can be computed by using the equation (2.1).

2.3 Inertial sensor errors

MEMS Inertial sensor signals are affected by various errors requiring specific pre-processing. These errors can be classified in two main classes: deterministic and non-deterministic or stochastic errors. Calibration techniques can be applied to remove the first type of errors while non deterministic errors require stochastic modelling. In this section more details about the main type of errors characterizing inertial sensors are given.

2.3.1 Noise

Noise refers to random errors in the sensor measurement that can be intrinsic, namely produced by the sensors itself, or external, that is induced by electronic external device's interference. Due to the non systematic nature of the noise, deterministic modelling cannot be applied and stochastic modelling is required (El-Sheimy 2004).

2.3.2 Sensor bias

A bias is composed of two parts, a deterministic one, indicated as bias offset, and a stochastic one indicated as bias drift. The bias offset is the component generated directly by the sensors and, in light of its deterministic nature can be evaluated through calibration processes. This component is particularly significant for low cost sensors, for which frequent calibration is necessary. The bias drift, that is the error accumulated over time, is random and requires stochastic modelling (El-Sheimy 2004).

2.3.3 Scale factor errors

The ratio between the sensor's signal output and the sensor's input to be measured is indicated as scale factor error. This error is deterministic and can be removed with specific calibration techniques (El-Sheimy 2004).

2.3.4 Non-orthogonality errors

This error is produced by an imperfect mounting of the sensors, usually due to non-orthogonality of the axes. Consequently, the measurements along each axis are affected by those of the other two axes in the body frame (El-Sheimy 2004). This type of error can be modelled in the INS error equation or calibrated

2.4 IMU signal model and pre-processing

As introduced in Section 2.2, a six degree freedom (6DoF) IMU is composed of a tri-axis accelerometer and a tri-axis gyroscope sensing respectively acceleration and angular rate of the body frame. Consequently, the digital output of the IMU can be modelled as a six-dimensional vector given by the response to the experienced inertial force and a noise term (Skog et al 2010) as

$$\mathbf{s}[n] = \begin{bmatrix} \mathbf{s}^{a}[n] \\ \mathbf{s}^{\omega}[n] \end{bmatrix} = \begin{bmatrix} \mathbf{a}[n] \\ \boldsymbol{\omega}[n] \end{bmatrix} + \begin{bmatrix} \boldsymbol{\eta}^{a}[n] \\ \boldsymbol{\eta}^{\omega}[n] \end{bmatrix} \tag{2.2}$$

where

- $n \in \mathbb{N}$ is the temporal index of the signal with sampling frequency $f_s = 1/T_s$. For the experiments conducted in this thesis, f_s is equal to 100 Hz.

- $\mathbf{s}^{a}[n] \in \mathbb{R}^{3}$ is the digital output of the tri-axis accelerometer composed by the acceleration vector **a**[n] and the related noise vector $\boldsymbol{\eta}^{a}[n]$.
- $\mathbf{s}^{\omega}[n] \in \mathbb{R}^{3}$ is the digital output of the tri-axis gyroscope composed by the angular rate vector $\boldsymbol{\omega}[n]$ and the related noise vector $\boldsymbol{\eta}^{\omega}[n]$.

Human walking gait is a low-frequency activity and the most useful information is contained in the frequencies below 15 Hz (Mathie 2003). For this reason, the raw IMU data has been low pass-filtered by using a Butterworth filter with a cut-off frequency of 15 Hz. This type of filter has been selected in view of its simplicity and maximally flat magnitude response in the pass band.

The following notation is used to denote the filtered acceleration components:

$$\tilde{\mathbf{s}}_{x}[n], \tilde{\mathbf{s}}_{y}[n], \tilde{\mathbf{s}}_{z}[n] \tag{2.3}$$

Since accelerations and angular rates are defined in an arbitrary system of axes, two main approaches can be adopted for processing, namely:

- The measurements can be projected in a local frame where an axis, generally indicated as the z axis, is parallel to the gravity vector and the other two axes, parallel and perpendicular with respect to the motion's direction, lie in the horizontal plane.
- Computation can be performed on the signal norm (Kwakkel 2008).

The first approach is suitable when the sensor is body fixed (Karantonis et al 2006, Veltink et al 1996). In this case, the orientation of the sensor in the local level frame is solved by alignment techniques.

When the orientation of the sensor cannot be easily determined or is changing over time, like with handheld sensors, the signal's norm is usually preferred and is used in this thesis.

The signal norm is expressed as

$$\tilde{s}[n] = \sqrt{\tilde{s}_x^2[n] + \tilde{s}_y^2[n] + \tilde{s}_z^2[n]} \tag{2.4}$$

Furthermore, the presence of a non-zero DC component, which is present in the signal, can hide important information and reduce the effectiveness of the frequency domain estimation techniques described in Section 2.5.2. Thus, the DC component is removed as follows:

$$\tilde{s}_0[n] = \tilde{s}[n] - \frac{1}{L}\sum_{l=0}^{L-1}\tilde{s}[n-l] \tag{2.5}$$

The second term of (2.5) is the signal mean computed using a moving average filter and *L* represents the length of the analysis window. The criterion to select the length of the analysis window will be detailed in Sections 3-2.

2.5 IMU signal analysis

In this thesis the analysis of IMU signals is performed in the time, frequency and time-frequency domains. Indeed, as detailed in this section, the above domains offer different points of view to study the signal properties.

2.5.1 Time domain analysis

The analysis in the time domain is the most intuitive and direct approach to study the properties of a signal. As described in Section 2.1, when the inertial unit is placed on the foot and the user is performing a cyclic activity, such as walking and running, it is possible to distinguish several motion phases (Mathie 2003, Kwakkel 2008).

This enables different approaches for improving the accuracy of the user location, including the determination of the stance phase, i.e., when the foot is leaning on the ground. Indeed, this gait event can be exploited bounding the error growth of inertial sensors as introduced in Section 1.2.

Figure 2-4 shows the norm of the accelerations measured by two synchronised MEMS **accelerometers placed on the foot** (upper part) **and in the hand** (lower part) of a user walking at normal speed. The two signals show clear periodicities reflecting the cyclic nature of the walking motion performed by the user. For the foot mounted sensor, the periods when the acceleration is close to the value of gravity (g) correspond to the stance phases of the foot. When the sensor is foot mounted the signal dominant component is produced by the cyclic repetition of the stride events. When the sensor is in the user hand, the periodicity of the signal is due to the combined effect of the lower

body motion and the arm swing. However, from the time domain analysis it is not possible to extract all the signal's different components. In order to analyze the contribution of these components, a frequency analysis is required and detailed in Section 2.5.2.

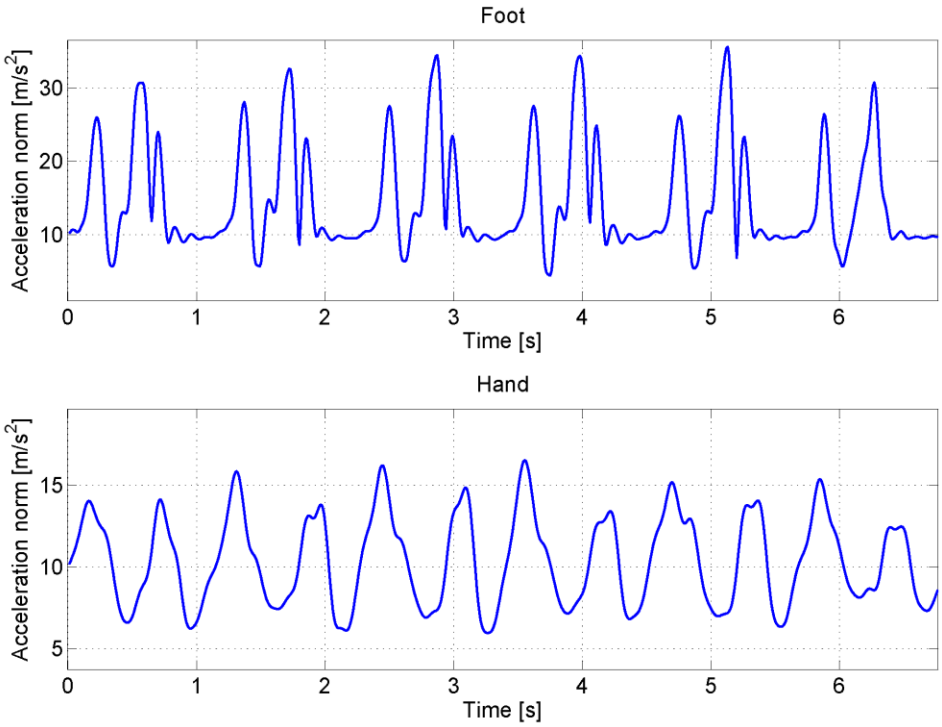

Figure 2-4: Time domain representation of the accelerometer signal extracted from a sensor on the foot (upper part) and in the swinging hand (lower part) of a walking subject.

2.5.2 Frequency domain analysis

As shown by J.B. Fourier almost two hundred years ago, any real waveform can be considered the sum of a unique combination of different sine waves. These different contributes can be analyzed in the frequency domain by evaluating the signal spectrum. The latter indicates how the signal energy is distributed among different frequencies. For

periodic signals the spectrum is discrete while for a-periodic signals the spectrum is a continuous function of the frequency. In Figure 2-5 the relationship between a periodic signal and its frequency representation is illustrated.

.

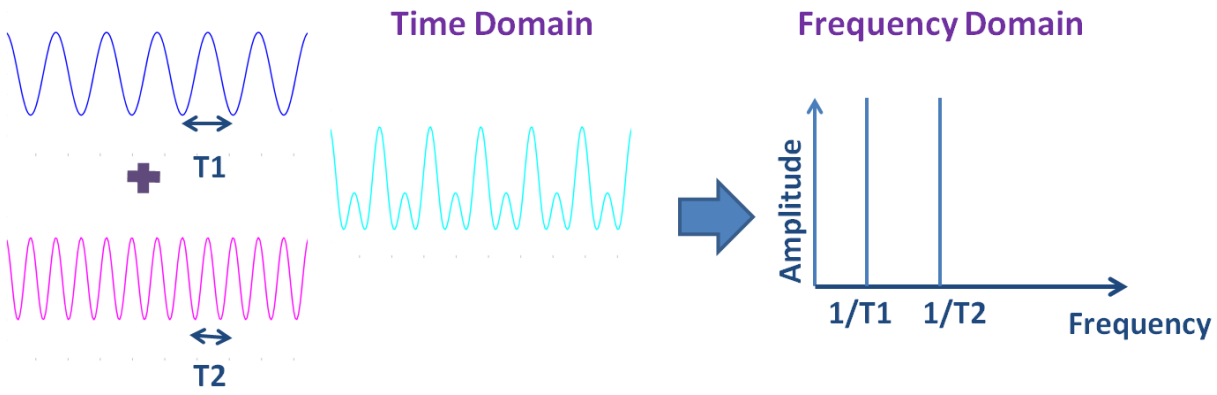

Figure 2-5: Relationship between time and frequency domains for a periodic signal

In order to analyze the different components constituting the IMU signal, and consequently extract the signal "hidden periodicities", when the sensor is handheld the frequency domain analysis can be adopted.

The spectrum of a signal can be estimated by applying two main methods: **parametric and non-parametric techniques**. Parametric techniques are based upon the mathematical properties of the signal while non parametric techniques, which are implemented in this thesis, rely on the direct analysis of empirical data.

2.5.2.1 Parametric techniques for spectrum estimation: the Linear Predicti Coding (LPC) technique

An example of parametric technique is given by the LPC. The latter method models the signal as the output of a linear system driven by white noise. In particular, the version of the LPC based on a AutoRegressive (AR) model represents the signal as a linear combination of its p past values. Such model can be used to represent the quasi periodic signal recorded by an accelerometer during cyclic activities.

Indeed, an example of accelerometer signal LPC frequency analysis for motion mode detection applied to pedestrian navigation can be found in (Chowdary et al 2009). This approach allows predicting a digital signal x[n] by using a linear predictor of order p (Proakis & Manolakis 1996) so represented

$$\hat{x}[n] = -\sum_{k=1}^{p} a_k x[n-k] + e[n] \tag{2.6}$$

where

-a_k are the linear predictor coefficients

-e[n] is the approximation error at the instant n

A unique set of linear predictor coefficients can be computed, for example, by minimizing the sum square of the prediction error as detailed in (Proakis & Manolakis 1996). Finally, taking the z transform of the (2.6) the spectral envelope of the signal can be found as

$$H(z) = \frac{E(z)}{1 + \sum_{k=1}^{p} a[k] z^{-k}} \tag{2.7}$$

Then the signal spectrum can be estimated as

$$\hat{P}_x(z) = |H(z)|^2 \tag{2.8}$$

In Figure 2-6 the spectrum of the accelerometer signal, estimated by applying the LPC, is reported for the case of a subject walking with the sensor in a swinging hand. MS

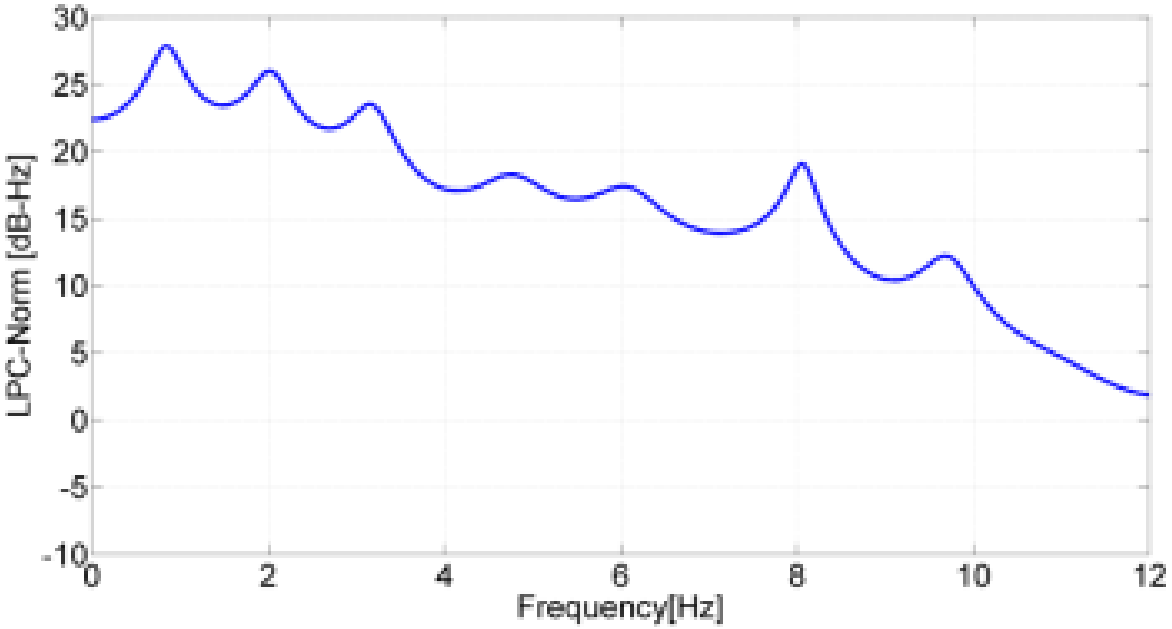

Figure 2-6: Spectral Envelope computed with the LPC (order p =30) -MEMS on the foot of a walking subject

Parametric models allow achieving a superior frequency resolution than non parametric techniques. However, since parametric techniques are based on a mathematical model, if the model does not fit well the data, the obtained results can be

inaccurate or misleading. For example, if the choice of the order of the interpolation p is not appropriate false peaks could be detected in the signal spectrum.

2.5.2.2 Non parametric techniques for spectrum estimation: the periodogram

Non-parametric methods rely on the direct use of the available data. A classical non parametric spectrum estimator is the periodogram. It estimates the Power Spectral Density (PSD) of a finite sequence $\{x[n]\}_{n=0}^{N-1}$ by applying the following:

$$\hat{P}_x(\omega_k) = \frac{|X(\omega_k)|^2}{N} \tag{2.9}$$

where $X(e^{j\omega})$ is the Discrete Fourier Transform of $\{x[n]\}_{n=0}^{N-1}$ given by

$$X(\omega_k) = \sum_{n=0}^{N-1} x[n]\, e^{-j\omega_k n} \tag{2.10}$$

where $\omega_k = \frac{2\pi k}{N}$, with $k = 0,1,\ldots N-1$.

The Discrete Fourier Transform is generally computed by using the **Fast Fourier Transform** (FFT) in order to reduce the computational complexity from $O(N^2)$ to $O(N\log_2 N)$ with N representing the length of the analysis window. Specifically, to apply the FFT technique a window $N = 2^n$ is required.

The windowing process implies that the estimated spectrum is the convolution of the true spectrum and the spectrum of the window function. The convolution operation is responsible of an effect indicated as *leakage* that spreads the energy in the main lobe of a spectral response into the side lobes. This effect can be reduced by using windows

with non uniform weighting. On the other side, these types of windows will decrease the spectral resolution.

In this thesis the analysis of the IMU signal is performed using a specific type of periodogram indicated as **Welch periodogram**. This technique is applied by using an Hamming window (Proakis & Manolakis 1996) to divide the signal $x[n]$ in overlapped blocks and by averaging the squared magnitude FFTs of the signal blocks. The main advantage of this approach is the reduction of the variance when compared with the standard periodogram. In Figure 2-7, the Welch periodogram is represented for the case of an IMU placed in the swinging hand of a walking subject. Three main peaks are clearly visible in the periodogram. The relationship of these peaks with different gait events will be analyzed later in this thesis.

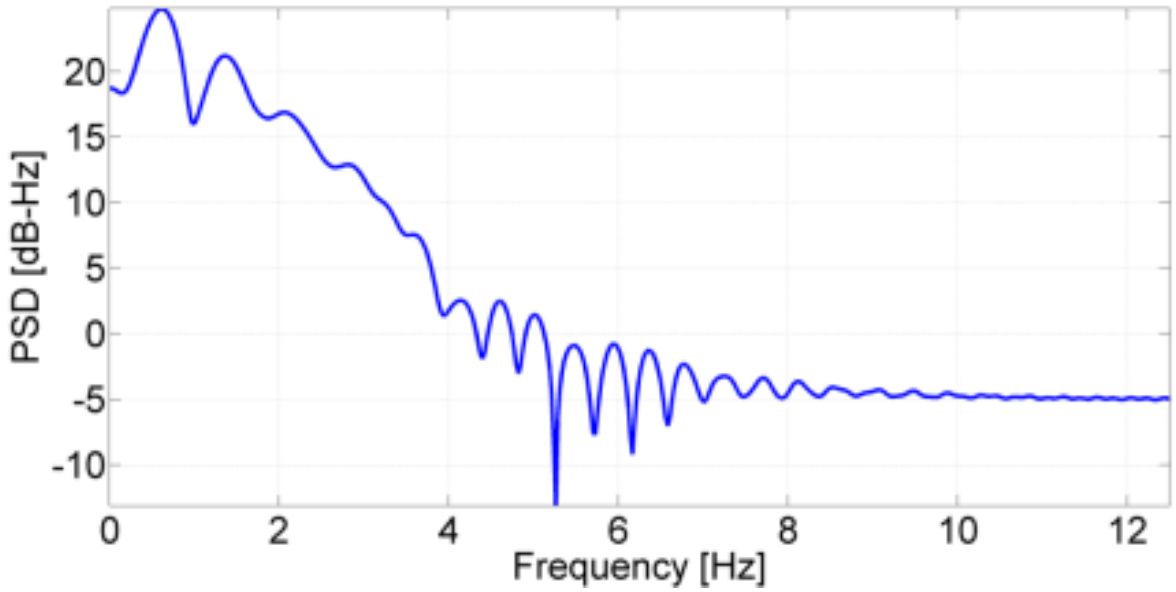

Figure 2-7: Periodogram computed with the Welch method (MEMS sensor in the swinging hand of a walking subject)

However, since the IMU signal is non stationary, i.e. the signal's first order statistics change over time, it is necessary to observe how the frequency components change over time too. Subsequently, an analysis in the time-frequency domain, described in Section 2.5.3, is required.

2.5.3 Time-frequency domain analysis

For non-stationary signals the representation in the frequency domain is unable to capture signal changes over time. A standard method to analyze a non-stationary signal is the Short Time Fourier Transform (STFT) whose underlying basic assumption is that the signal can be regarded as stationary for short durations (Cohen 1995). In particular for a a finite sequence $\{x[n]\}_{n=0}^{N-1}$, the STFT is defined by

$$STFT(\omega,\tau) = \sum_{n=0}^{N-1} x[n]w[n-\tau]e^{-j\omega n} \qquad (2.11)$$

where $w[\square]$ is the analysis window.

Despite the poor time-frequency localization properties of the STFT, this transform has two main advantages, namely its low computational requirement and the non-parametric nature. By computing the square modulus of the STFT, the signal's spectrogram is further obtained. The properties of the spectrogram are strictly related to the **analysis window**.

The window should be long enough to obtain a good frequency resolution but without capturing significant signal components that would belong to transient periods. Subsequently **a trade off between time and frequency resolution is imposed**. In

Figure 2-8 the spectrogram of the accelerometer signal is reported for the case of a user walking with the sensor in a swinging hand. It can be seen that this method is able to clearly show the dominant frequencies and their variations over time.

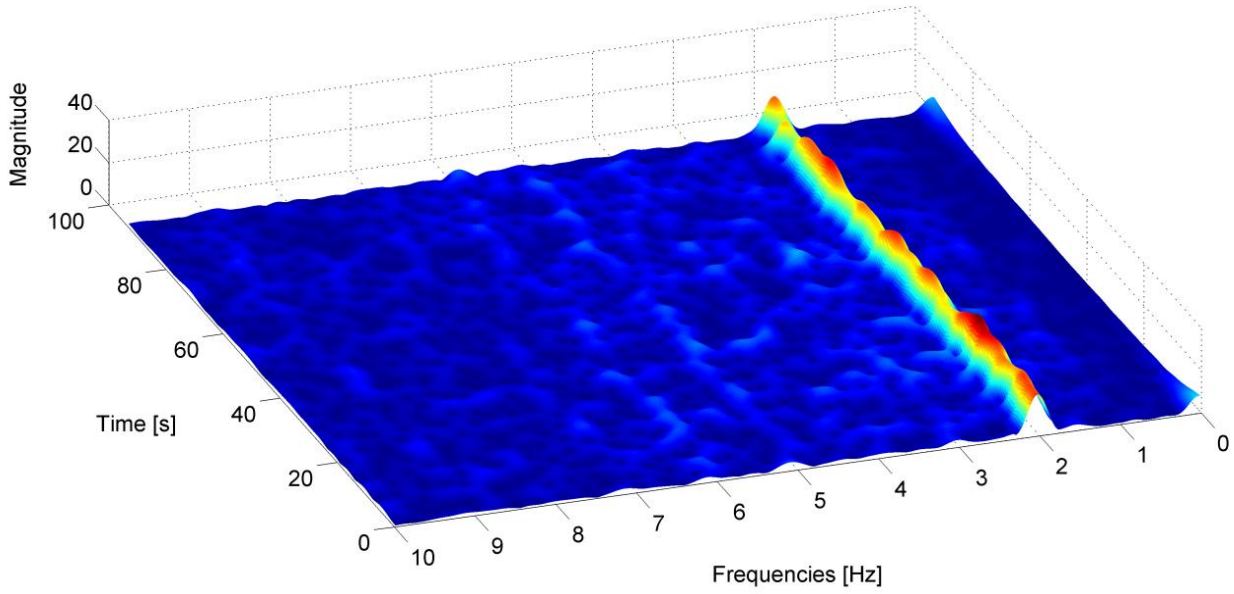

Figure 2-8: Spectrogram of the accelerometer signal (MEMS sensor in the swinging hand of a walking subject)

2.6 Summary

In this chapter it has been shown that inertial sensors are effective tools for gait analysis. However, due to the low cost nature of the inertial sensors considered in this thesis, a specific processing of their signals is required. Different signal processing techniques

have been presented in order to thoroughly analyze the IMU signal in different domains and extract useful information for gait analysis. In particular, these techniques will be exploited in Chapter 3 in order to extract meaningful signal features for the user's global motion mode recognition.

Chapter Three: Motion mode recognition for navigation purposes

When GNSS is not available, information about the user context, such as his motion mode, can be very useful to reduce the uncertainty about his location. Indeed the pedestrian navigation algorithm should be adapted to the specific user's motion mode. The advantages of constraining the PDR solution by exploiting the user motion knowledge have been showed for the case of body fixed sensors (e.g. Pei et al 2011). Similar results are expected with handheld sensors. However, the identification of the user's motion mode with handheld inertial sensors introduces new issues requiring specific processing.

In this chapter, algorithms for identifying the user's global motion from signals sensed by a handheld IMU are proposed. The user motion mode identification is considered as a **classification/pattern recognition problem**, where the classes/patterns correspond to different human activities. To render this chapter self-contained, first a general overview of classification theory is proposed. Then, the features used for identifying different user's activities, such as **standing, walking, running, climbing/descending stairs** are presented. Finally, the mentioned classifiers for motion mode recognition are detailed.

3.1 Human activity recognition: literature review

Human activity recognition using inertial sensors is a rich and proliferating research field, especially for clinical analysis (Nijsen et al 2010, Yin et al 2008). Indeed

the identification of human activity is exploited in biomechanics (Sabatini, 2006), medical diagnosis, rehabilitation, sport science (Ermes et al 2008), and the monitoring of physically and mentally impaired people. An example of such application is given by the implementation of systems alerting if the monitored subject shows reduced activity signs or unusual behaviours such as a fall. In the context of indoor positioning and navigation, the human activity identification can help to constrain the user position or to adapt the navigation algorithms according to the user's activity.

However, according to the type of application for which activity recognition is performed, different issues arise. They strongly depend on diverse features.

- **The number of available sensors**: activity recognition using multiple inertial sensors is a common approach for medical applications because the latter guarantees higher performance and increased reliability of the identification process. However, the processing of multiple sensors requires higher computational cost, which may not be compatible with real time applications. Moreover, the use of multiple sensors is not suitable for smartphone/mobile devices based applications, which is the target of this thesis.

- **The sensors position**: sensor signal patterns strongly depend on the sensor's mounting location. Indeed, the sensor output can be very different for different sensor positions, even if the monitored subject is performing the same activity. A common assumption for human activity recognition is that the sensor is rigidly attached to the user's body. In many studies, the sensor is located close to the

COM, for example near the pelvic region or mounted on the user's belt. In fact, as explained in Section 2.1, the forces experienced by a sensor close to the COM reflect the global user motion mode. However, handheld devices are freely carried and, consequently, the sensor orientation and position can change suddenly rendering the activity recognition complex.

- **The activities to be recognized:** the complexity of the activity to be identified can be very different. Human activities can be classified as primary activities, such as walking, standing, running and complex activities, generally involving the manipulation of objects. In the case of handheld devices, the user can interact in different ways with the smartphone, i.e. phoning, texting, or reading navigation instructions on the screen's device. As underlined in Chapter 4, for pedestrian navigation applications, these kinds of activities should be identified and distinguished from the user's primary activity. It is obvious that the complexity of the classification algorithm is positively correlated with the complexity of the activity to be recognized.

Most of existing studies have explored the use of multiple inertial sensors, especially accelerometers, to perform motion recognition. One of the most complete studies involving multiple accelerometers was performed by Bao & Intille (2004). Five bi-axial accelerometers were placed in five different locations on the user's body and their algorithm was able to recognize 20 different human activities, including walking, running,

watching TV and eating. In order to detect various activities, different classifiers, such as a decision tree, Nave Bayes and nearest neighbour algorithm, were used to compare their performance. The results of this study showed that the decision tree classifier achieved the best performance. A smaller number of studies use single accelerometers for context detection.

For example, Ravi et al. (2005) used a single tri-axial accelerometer located near the pelvic region, comparing the performances of various classifiers. Eight human activities are analyzed, namely standing, walking, running, climbing/descending stairs, sit-ups, vacuuming and brushing teeth. A few research studies exploit gyroscopes' capabilities for motion modes recognition. In Tuncel et al. (2009), two single axis gyroscopes are mounted on the test subjects' leg to identify different leg's motions for rehabilitation purposes. In Bourke & Lyons (2006) a dual axis gyroscope mounted on the user torso is used to discriminate normal activities from falls by applying a threshold algorithm to the peaks in the angular rate signal, angular acceleration and torso angle change.

A survey of recent studies in the area of activity recognition by using inertial sensors can be found in (Lara & Labrador 2012). Although the literature shows that inertial sensors are effective tools for recognizing human activities, the case of handheld sensors has been only marginally examined. Principally because the handheld situation is much more complex than the body fixed one. Indeed **a mobile device held in hand is subjected to various types of motions that are uncorrelated with the global locomotion**. Therefore the pattern of the sensor signal is hardly predictable, which renders the classification process a difficult task. In light of these limitations, this thesis

analyses the recognition of different human activities by using handheld devices and considering real life-scenarios typical for mobile device users.

3.2 Pattern recognition

A system able to automatically identify different motion modes can be modeled as a pattern recognition system. In general, the goal of pattern recognition systems (Fukunaga 1972) is to automatically assign a given input pattern to a known class of objects, according to specific decision rules. Given an input pattern, that is a set of initial measurements, it is necessary to select significant features able to characterize the observed samples in an unambiguous way.

By extracting the above features, a mapping process is performed from the input *m*-dimensional space of the measurements to the *n* (with $n < m$) dimensional space of the features. In this way, since the input to the classifier becomes smaller, the design of the pattern recognition system becomes simpler. In this study the design and the implementation of classifiers for human activities recognition has been performed using different statistical approaches. For this reason, Section 3.2.1 recalls the theory of statistical pattern recognition.

3.2.1 Statistical pattern recognition

Statistical pattern recognition is based on the underlying statistical model of pattern and pattern classes (Jain et al 2000). In the statistical approach, the selected features can be represented by a vector, $\mathbf{x} = [x_1, x_2, .., x_n]$, in the *n*-dimensional space

where *n* is the number of input features. If the features are properly selected, the feature space should be divided into disjointed regions corresponding to different pattern classes. Then, by analyzing the input feature vector, the classification process assigns each vector to one among the *c* possible pattern classes, $\boldsymbol{\omega} = [\omega_1, \omega_2, ..., \omega_c]$.

In Figure 3-1, the conceptual scheme of a pattern recognition system is reported and, as shown below, a mapping process is performed from the input pattern to a hidden state by observing the feature vector and according to a specific decision rule characterizing the classifier.

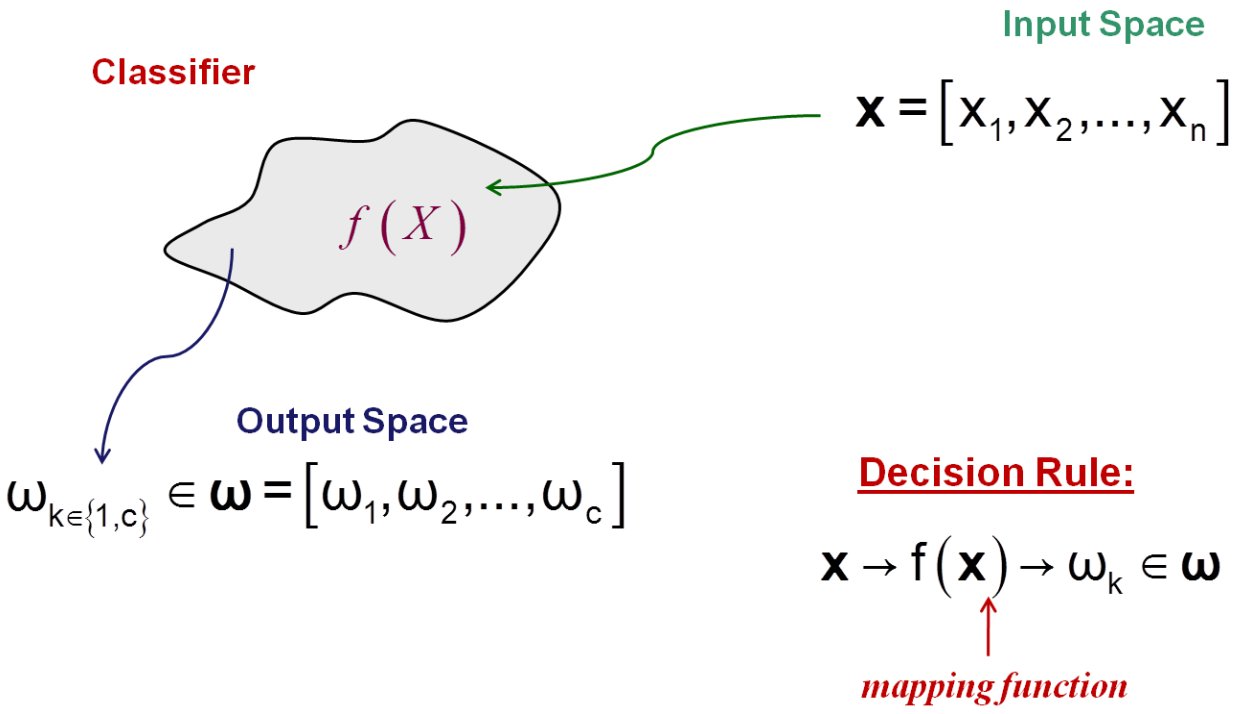

Figure 3-1: General scheme of a pattern recognition system: a hidden state is assigned to an input pattern by observing the feature vector and according to the decision rule defined by the classifier

Figure 3-2 illustrates the general model of a statistical pattern recognition system. A pattern recognition system (or classifier) is composed of two phases: **the training (or learning) phase** (represented in yellow) and **the classification (or testing) phase** (represented in green).

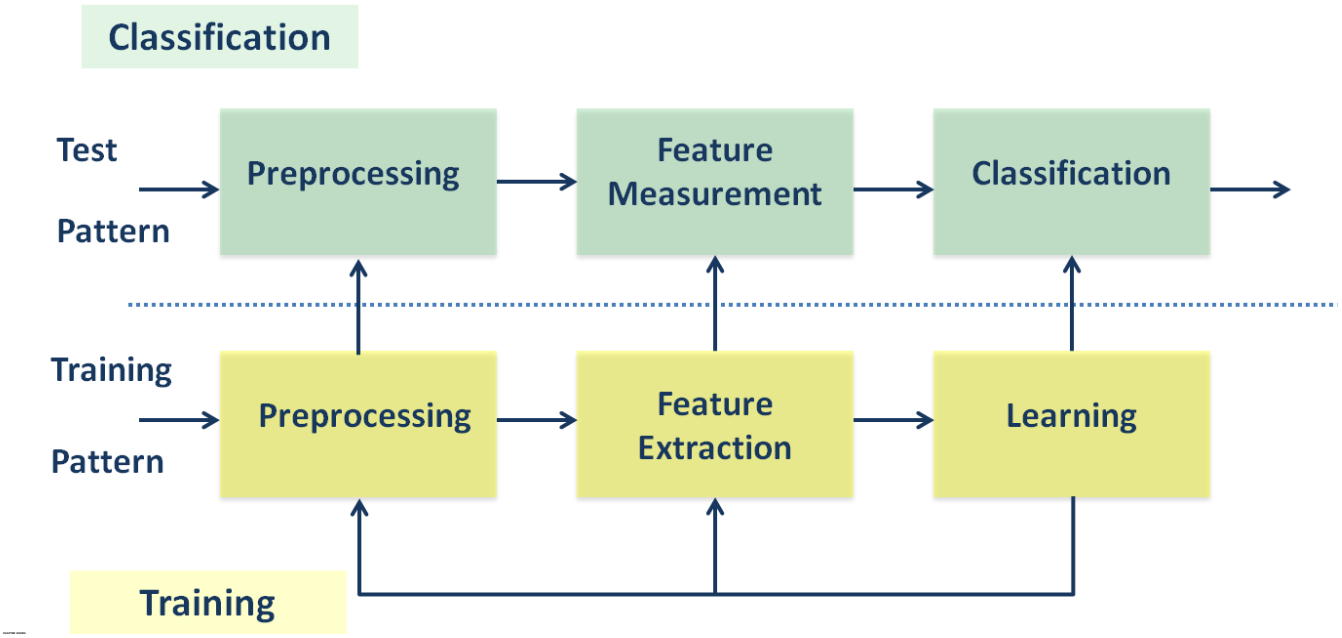

Figure 3-2: Model for statistical pattern recognition (adapted from Jain et al (2000))

In the **pre-processing phase**, the acquired data are used to obtain a compact representation of the pattern, reducing the impact of noise, and making the feature extraction (second phase) possible. The **features extraction** plays a key role in the design of a classifier. An ideal feature extraction process should be able to minimize the intra-set distance (distance among different features in the same class) and to maximize

the inter-set distance (distance among different features in different classes, as shown in Figure 3-3 (Jain 2000).

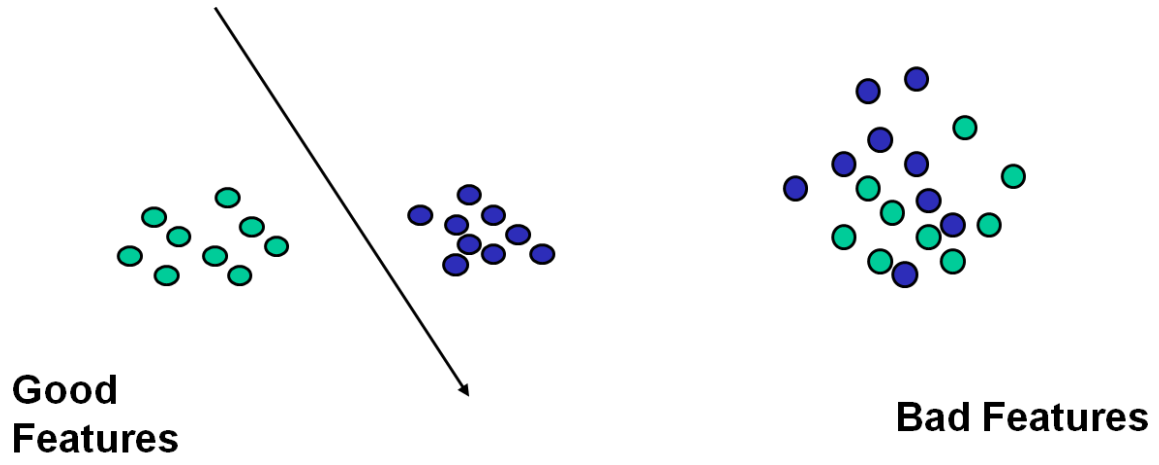

.

Figure 3-3: Different feature distributions: (left side) optimum distribution case with high inter-set separability and low intra-set separability, (right side) bad distribution case with low inter-set separability

In this way, the **classification** can be performed (third step) with a reduced error probability due to a good inter-class separability. As shown in Figure 3-2 the general model of a pattern recognition system includes also a feedback loop allowing optimization of the pre-processing and the feature extraction methods in the design phase. In statistical approaches, given the input vector, $\mathbf{x} = [x_1, x_2, .., x_n]$, and the *c* possible classes $\boldsymbol{\omega} = [\omega_1, \omega_2, ..., \omega_c]$, the probability that the vector belongs to the i^{th} class

is defined by the class-conditional probability function $p(\mathbf{x}|\omega_i)$. Several decision rules can be used to limit the decision regions, as shown in Figure 3-4.

The choice of the approach depends on the knowledge about the class conditional probability densities (Jain et al 2000). By traversing the tree in Figure 3-4 from left to right, the available information decreases and the design of the classifier becomes more difficult.

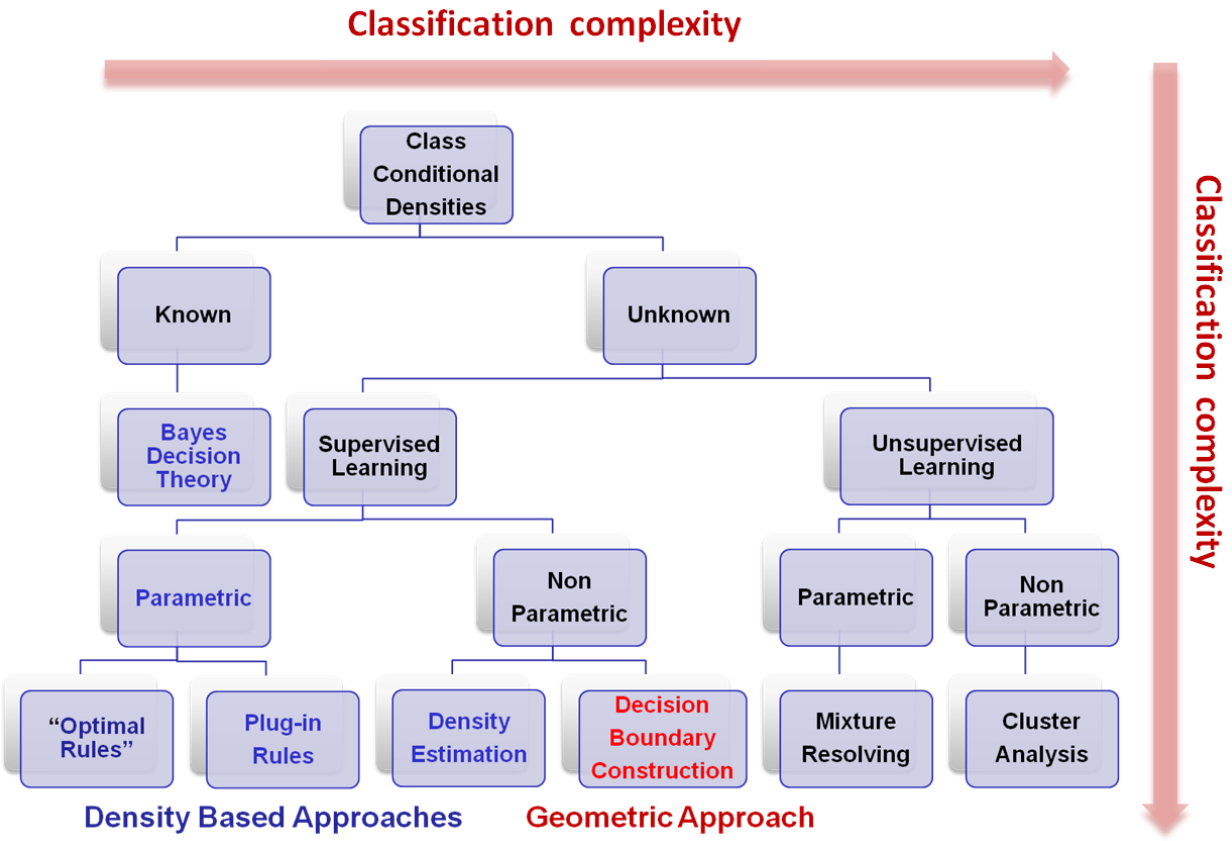

Figure 3-4: Possible approaches in statistical pattern recognition (adapted from Jain et al (2000))

If all the class conditional densities are known, the classifier can be designed by exploiting the Bayes rule that assigns the class with the highest a posteriori probability to the input pattern. Equivalently, it chooses the class that minimizes the conditional risk that is the conditional probability of making a wrong decision, defined by the following expression:

$$R(\omega_i|\mathbf{x}) = \sum_{j=1}^{c} L(\omega_i,\omega_j)\cdot P(\omega_j|\mathbf{x}), \qquad (3.1)$$

where $L(\omega_i,\omega_j)$ is the loss incurred in deciding ω_i when the true class is ω_j. The Bayes decision rule is defined as the optimum rule (Jain et al 2000) since it is, among all the possible rules, the one with the minimum probability of error. The weak point of this approach is that usually the class conditional densities are unknown and so this rule cannot be applied. Indeed if the class conditional densities are unknown, it is necessary to distinguish them on the basis of the kind of training samples available. The training samples can belong to labelled classes (**supervised learning**) or to unlabelled classes (**unsupervised learning**).

In the case of unsupervised learning, since the knowledge about the training data is lower, the classification process is more difficult. Concerning the supervised learning, if the distribution of the class conditional densities are known, but their statistical parameters, such as the mean or the variance, are not available, it is necessary to use a parametric approach. Conversely, if the form of the distributions is not available, a non-

parametric approach has to be used. In this case, two alternatives are possible: to estimate the form of the distributions or to use the training data to define the decision regions. By observing the tree diagram in Figure 3-4, it emerges that another distinction is made regarding the method used to define the decision regions. Two different approaches are possible: probabilistic and geometric. The former refers to the estimation of the probability density functions whereas in the latter, decision boundaries are determined by optimizing specific cost functions. The *k*-nearest-neighbour and the decision tree that will be described in the following sections, belongs to the second kind of techniques.

3.2.1.1 IMU signal pre-processing for motion mode recognition

Activity recognition requires the extraction of meaningful attributes indicated as features to univocally characterize each activity. These features are used as input to the classification scheme (Jain 2000). High performance of a pattern recognition system strongly depends on a good selection of these attributes. The feature extraction phase can be performed only after that the raw data have been represented in a compact form. With this aim a pre-processing phase able to reduce the noisy components has to be implemented. As explained in Section 2.4, since **gait is a low-frequency activity**, all the frequencies above 15 Hz have been removed by low-pass filtering the raw data with a 10^{th} order Butterworth filter whose frequency cut-off equals 15 Hz. The feature extraction is performed by dividing the filtered inertial data in windows of *N* samples.

Specifically, for our sampling frequency of 100 Hz, *N* was chosen equal to 128 corresponding to 1.28 seconds with 50% of overlap. In addition, this size allows the fast computation of the FFT, used for the frequency analysis of the examined signals. The selection of a suitable window is a critical phase. Long windows cannot capture a sudden change of motion. Instead, narrow windows are not suitable for the analysis in frequency domain performed by FFT. The features selected for the user's global motion mode recognition are illustrated in Section 3.3.

3.3 Features for global motion mode recognition

In this section the features used to identify different user's activities, namely standing, descending/ascending stairs, walking and running, are introduced. The use of accelerometers is the most widespread (Mannini & Sabatini 2010) approach for human activity recognition using wearable sensors. This method is here used for the identification of the user global motion mode. Indeed, in order to extract information useful for human activity recognition, the accelerometer signal has been thoroughly analyzed in the **time, frequency and time-frequency domains** using the techniques described in Section 2.5.

The identified accelerometer features allows recognizing the mentioned activities with high accuracy as detailed in Chapter 5 where the performances of the classifiers here presented are assessed. However, as detailed in Chapter 4, the capabilities of a gyroscope have been also exploited to better characterize the walking mode through the identification of the sensor carrying mode/hand motion.

3.3.1 Energy related features

The analysis of the energy over time is a traditional approach to perform activity recognition since this is the most direct parameter to evaluate the characteristics of the motion mode. In fact, it is obvious that activities such as running are characterized by higher energy values than walking. Conversely, sedentary activities, such as sitting or standing, are characterized by a decrease of the energy. In this thesis, the total energy is computed by squaring the magnitude of the pre-processed accelerometer data and integrating it according to the following expression:

$$E_{s_0^a} = \frac{1}{N}\sum_{n=0}^{N-1} s_0^{a\,2}[n] \tag{3.2}$$

where $s_0^a[n]$ is referring to the filtered norm of the accelerometer signal after the pre-processing phase, as expressed in Section 2.4, and *N* is the length of the analysis window. The weakness of this approach is that different subjects can perform the same activity with very different values of energy.

Furthermore, this feature can assume different values according to the sensor position. For example, a sensor in the user swinging hand experiences higher energies than a sensor in the user pocket. To overcome this limitation, the **sub-band energy ratios** distribution is also considered. This approach is based on the consideration that **faster motion mode induce higher energy frequency values**.

To obtain the energy in four different sub-bands an energy estimator has been implemented according to the scheme of Figure 3-5. The energy estimator evaluates the energy after that the signal has been filtered by a Butterworth filter-bank. Each filter has a different cut-off frequency with the aim of obtaining the energy in the following frequency sub-bands.

- 0-2 Hz
- 2-6 Hz
- 6-10 Hz
- >10 Hz

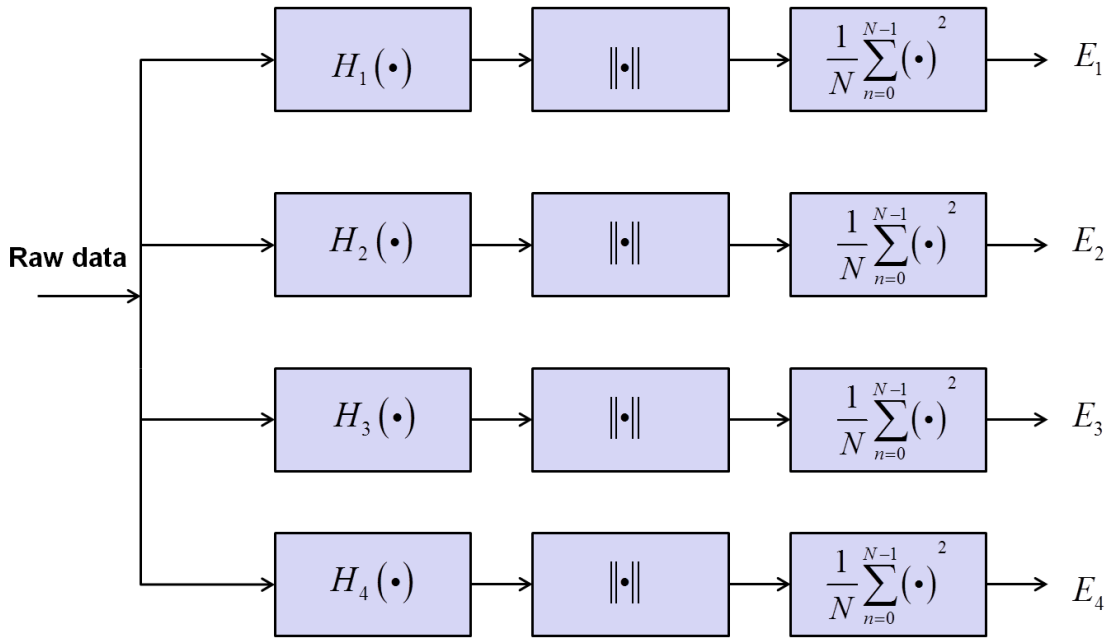

Figure 3-5: Energy estimator implemented as a filter bank

The choice of the above sub-bands is motivated by the empirical observation that in the running case the energy values in the sub-band between 2-6 Hz are significantly larger than the ones related to the first sub-band (0-2 Hz). This is clearly shown in Figure3-6 reporting the total energy and the sub-band energies for the case of the IMU in a swinging hand. This feature has the advantage of being less sensitive to variations of sensor locations or motion style than the total energy defined in (3.2).

Similar results have been obtained for the other examined sensor locations, i.e. pocket and foot, for all subjects used for the field tests described in Section 5.1.

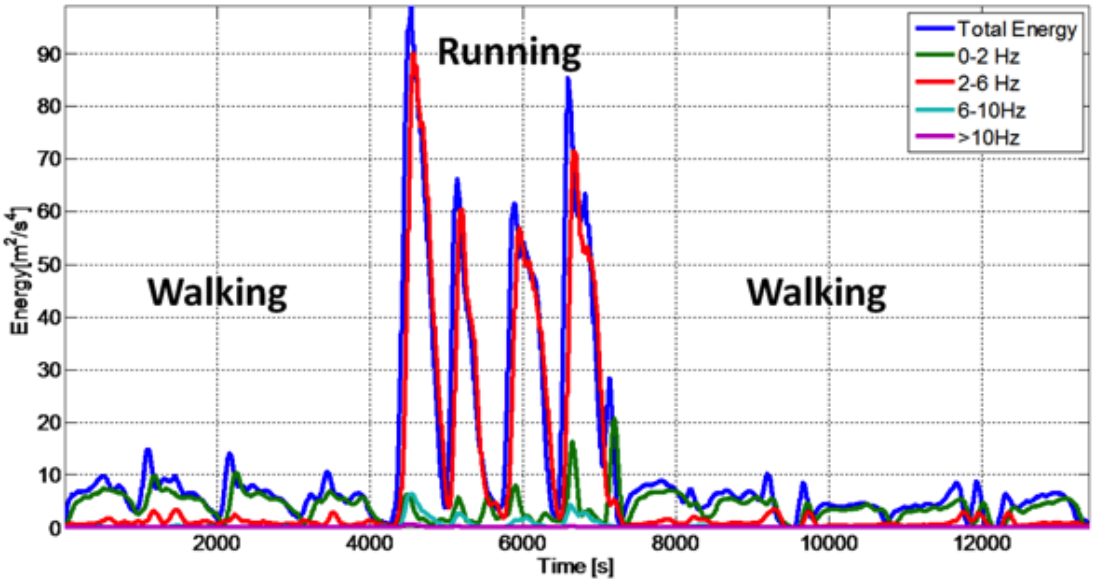

Figure 3-6: Total energy and sub-band energies for a user with the sensors in the swinging hand.

However, similar values of the sub-band energy ratios are also obtained for the stair case. In fact when the user is descending the stairs, as in the walking case, the energy values in the sub-band between 2-6 Hz are larger than the ones related to the first sub-band (0-2 Hz). Conversely, for a user climbing the stairs the energy sub-band ratio values are similar to the ones obtained for the running case. By comparing Figure 3-6 and Figure 3-7 it is clear that the use of the energy ratio can provide ambiguous results for the running and going down the stairs cases and for walking and going up the stairs cases even if the total energy is different for these two situations. For this reason, in order to increase the separability among the mentioned activities in Section 3.7.2 the correlation feature is also introduced

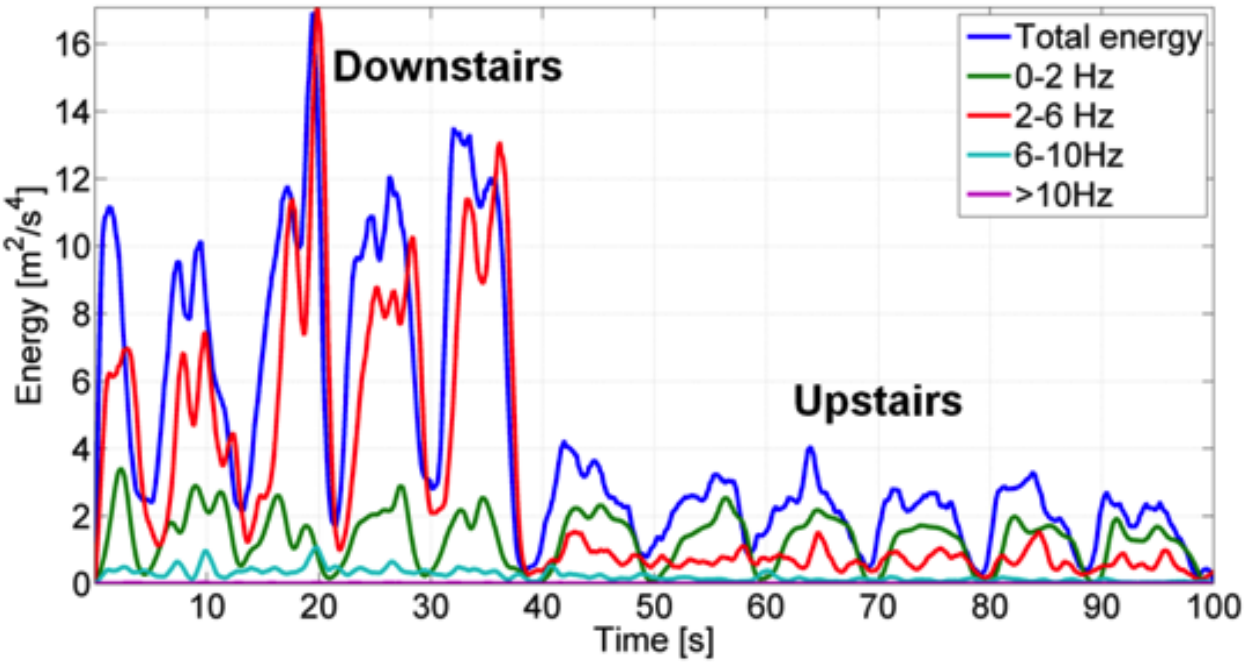

Figure 3-7: Total energy and sub-band energies for a user with the sensors in the swinging hand while he is descending and climbing the stairs.

3.3.2 Correlation

The correlation has been evaluated by applying the Pearson's correlation definition for each possible pair of accelerometer components defined as (Good 2009):

$$r_{xy} = \frac{\sum_{n=1}^{N}\left(x[n]-\bar{x}\right)\left(y[n]-\bar{y}\right)}{\sqrt{\sum_{n=1}^{N}\left(x[n]-\bar{x}\right)^2\left(y[n]-\bar{y}\right)^2}} \qquad (3.3)$$

Where $x[n]$ and $y[n]$ for n in range (1, N) are the samples of the two selected signals components and $\bar{x}$ and $\bar{y}$ are the sample means of the two components. The three accelerometer components in the sensor frame are indicated as **x**, **y** and **z** and are represented in Figure 3-8. As shown in Figure 3-8, since the sensor is freely carried, the sensor frame is different from the body frame which is associated with the pedestrian. The body frame, represented in figure 3-8, has its **X**' axis pointing along the walking direction, the **Z**' axis parallel to the gravity vector and the **Y**' axis directed so to constitute a right handed orthogonal triad.

Since the correlation measures the similarity among components it assumes larger values in the stair case for the vertical and the forward direction. The reason is that the motion in the stair case is mainly due to the combination of the motions of the forward and the vertical directions. In Figure 3-9 (left side), the plots of the correlation over time (correlogram) in the stairs case are reported when the sensor is in the user swinging

hand. By observing the following plots we can see that the largest values are related to the components indicated as z and y.

Even if do not know the sensor orientation with respect to the body frame, it is likely the named components are the vertical and the forward directions. Indeed, as mentioned, the motion on the stairs is due mainly to these components. It is interesting to observe that the correlation between the components indicated as x and y assumes lowest values but show some periodic peaks. This can be explained considering that between different flights on the stairs there is a small landing where the test subject has to transit before going on the next flight of stairs. So the user has to change orientation, splitting acceleration in the two horizontal components. Consequently, the periodic increase of the values in this graph is due to turns between different flights of the stairs.

If we consider the same kind of plots for the walking case on a flat surface, as reported in Figure 3-9 (right side) the correlation values are found to be lower than in the stairs case. This can be easily explained by the fact that in this case the motion is mainly along one direction (forward). Consequently, the level of the correlation values can be used to distinguish walking on a flat plane and walking on the stairs. However, this feature relies on the single components of the accelerometer signal and, consequently, its **effectiveness is related to the sensor orientation**. This is a critical aspect for freely carried whose orientation is a priori unknown. Indeed, as shown in Chapter 5, the performance of motion identification using this feature are higher for the foot and pocket case than for the sensor in a swinging hand case.

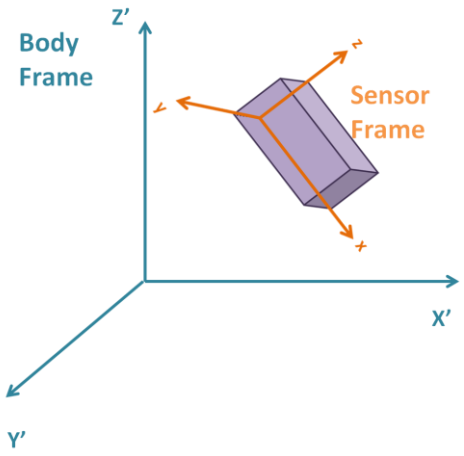

Figure 3-8: Representation of the sensor frame with respect to the body frame

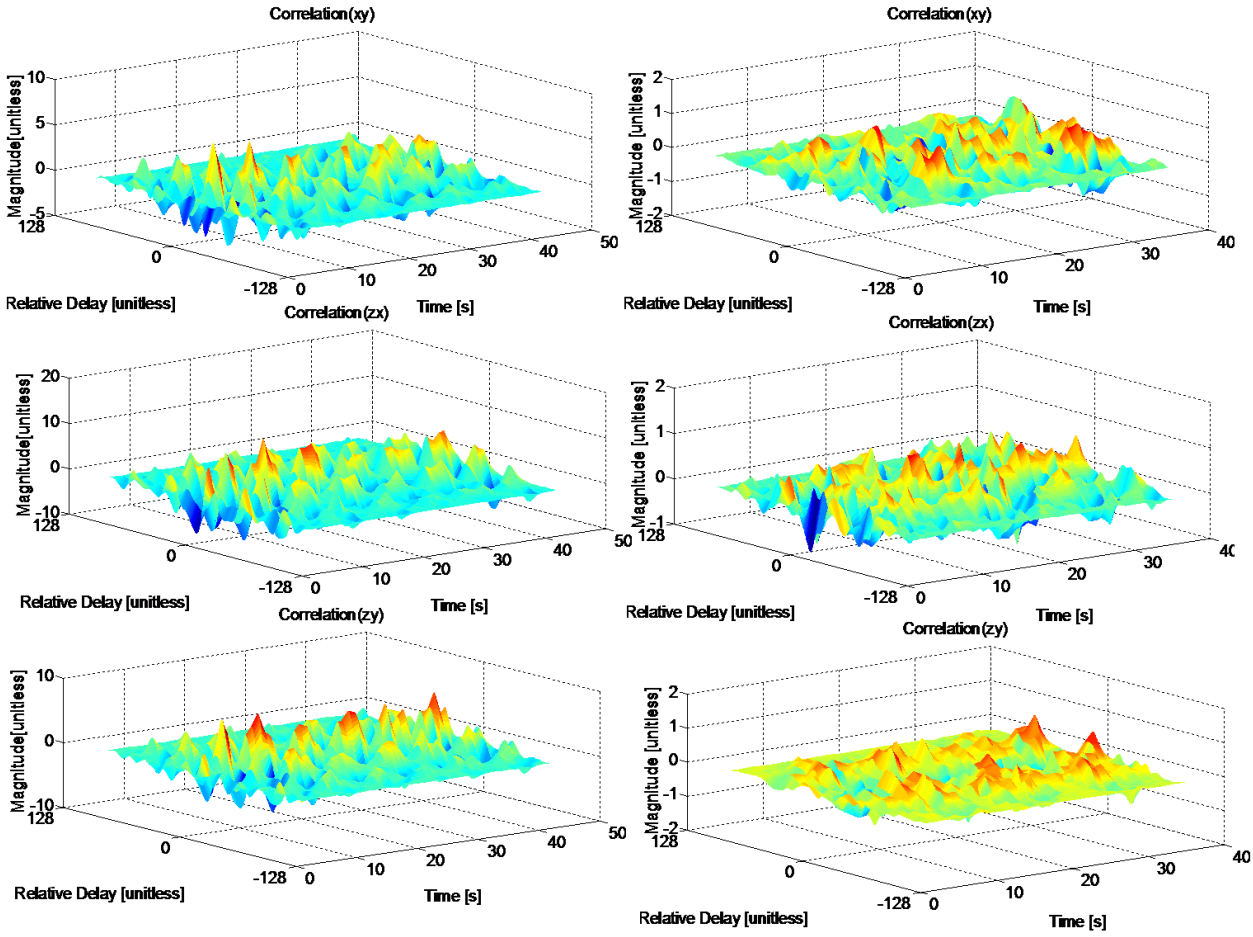

Figure 3-9: Correlograms of the accelerometer components for the stairs case (left side) and the walking case (right side)

3.3.3 Frequency domain features

As introduced in Section 2.5, by analyzing the accelerometer signal in the time domain, if the sensor is on the foot, it is possible to identify single stride events. On the other side, it has been shown (Susi et al 2010) that if the sensor is in the hand, the situation is more ambiguous and the motion mode requires the analysis of the IMU signals in different domains. For this reason, a frequency domain analysis has been performed following the approach described in Section 2.5. Since the signal is not stationary, the first three dominant frequencies, i.e. maxima in the spectrogram, are analysed over time. In Figure 3-10, the plots of the dominant frequencies over time are reported for the running and the walking cases.

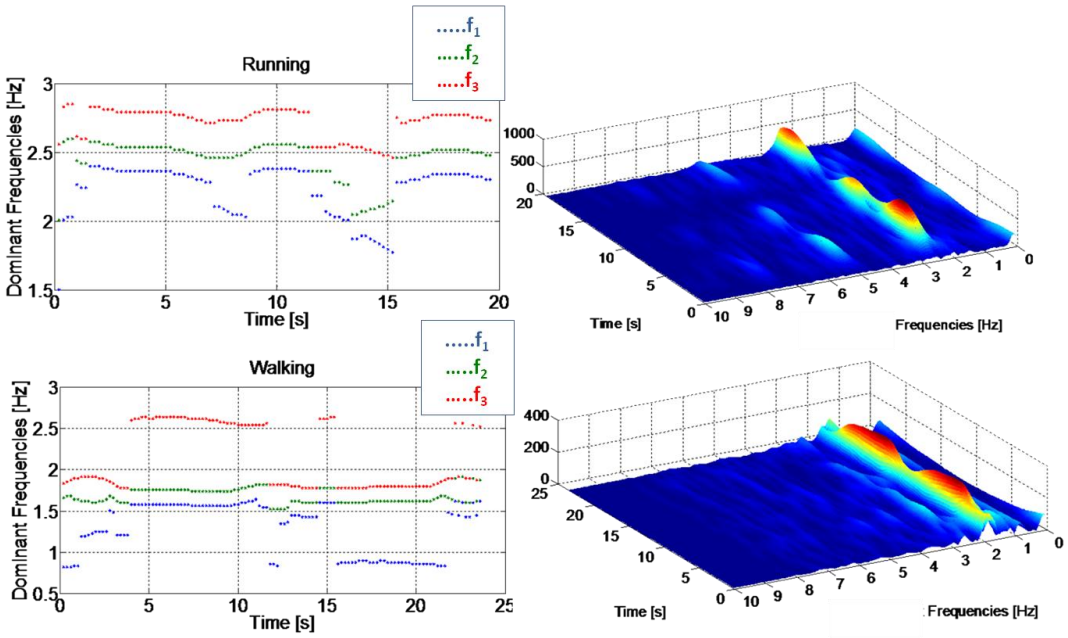

Figure 3-10: (Left) Dominant frequencies over time for the running and the walking cases; (Right) Spectrograms of the accelerometer signal for the running and the walking cases (sensor in the user swinging hand).

Comparing the plots in Figure 3-10, it is possible to see how in the running mode (Figure 3-10, lower part) the frequency peaks appear at higher frequency values than in the walking mode (Figure 3-10, upper part). By observing Figure 3-11, which reports the spectrogram of the accelerometer signal for a subject alternating running and walking with the IMU in the swinging hand, it is clear that **faster motion modes force the signal energy to migrate towards higher frequencies.**

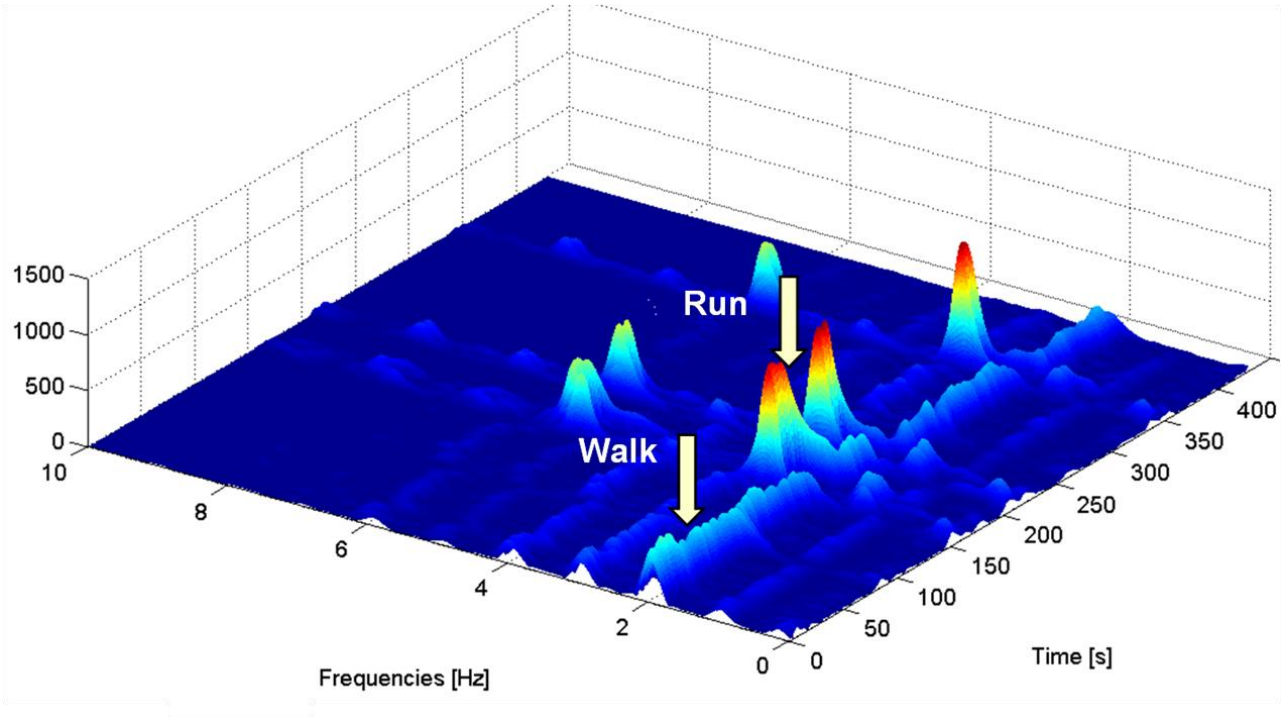

Figure 3-11: Spectrogram of the accelerometer signal for a subject with the IMU in his swinging hand.

In order to further investigate the relationship between dominant frequencies and user's speed, a test has been performed on a treadmill. Indeed, the treadmill allowed monitoring of how the dominant frequency values change by setting different controlled velocities. In Figure 3-12 (upper) the norm of the accelerometer signal and (lower) the dominant frequencies are reported for the sensor in the swinging hand.

Observing the plot of the dominant frequencies, it is clear that the increase of their values is directly proportional to the increase of user's speed. The first two frequencies (in blue and in red) assume constant values over time for fixed velocities. Instead, for the third frequency, a larger dispersion is visible. However, it should be noticed that the treadmill could affect the user's walking style making it unnatural. In view of this consideration, the relationship between dominant frequencies and gait events, i.e. user's step and stride, is more thoroughly examined in Chapter 5.

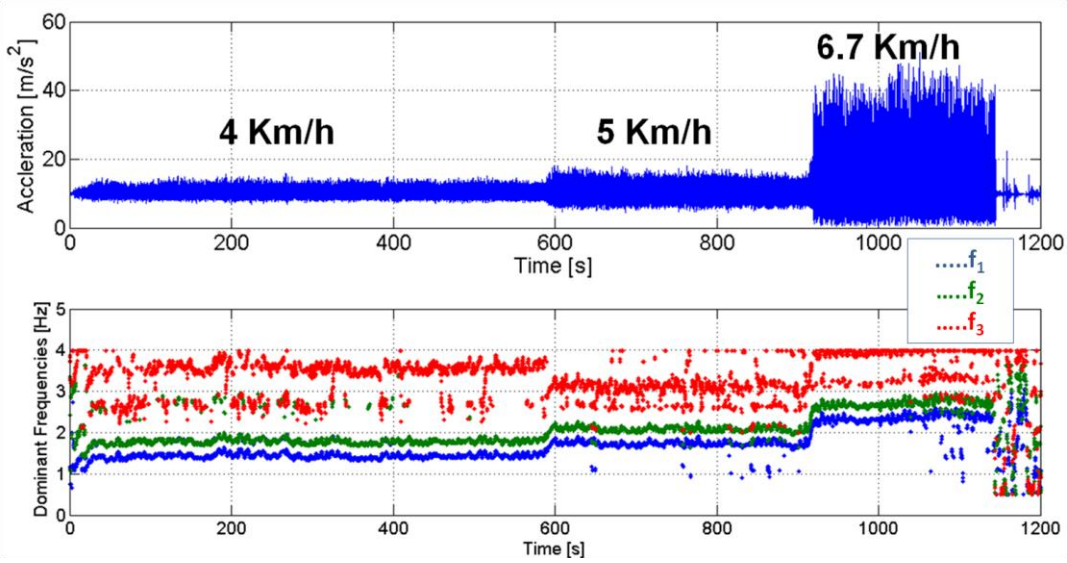

Figure 3-12: (Upper) Norm of the accelerometer signal for different user's speed; (Lower) Dominant frequencies for different user's speed.

3.4 Classifiers for global motion mode recognition

In this thesis, in order to compare the performance of different classifiers, the features presented in Section 3.3 have been integrated into three different classifiers, namely a **Naive Bayesian classifier**, a **decision tree algorithm** and a ***k*-nearest-neighbour** technique. A comparison of the classifier's performance is reported in Chapter 5. The considered algorithms are briefly described in the following. More details on these techniques can be found in (Jain 2000, Webb 2002).

3.4.1 Naïve Bayesian classifier

The Naive Bayesian classifier is a parametric technique relying on the hypothesis that all features used for the classification process are statistically independent (Jain 2000).

Consequently, the probability of observing a specific feature vector conditionally to its assignation to the j-th class is computed by multiplying the marginal conditional feature probabilities as

$$p\left(x_1, x_2, ..., x_d \mid \omega_j\right) = \prod_{i=1}^{d} p\left(x_i \mid \omega_j\right) . \qquad (3.4)$$

where **x** represents the feature vector and ω_j indicates one of the possible *c* classes as defined in Section 3.2.1. The final class is selected according to the Maximum A Posteriori (MAP) decision rule expressed as

$$\omega(x_1, x_2, ..., x_d) = \arg\max_{\omega_j} \left(\prod_{i=1}^{d} p(x_i|\omega_j) \cdot p(\omega_j) \right). \quad (3.5)$$

Here the different activities are considered equally likely so that the term $p(\omega_j)$ can be neglected.

The estimation of the likelihood function $p(x_i|\omega_j)$ is performed by the training data analysis and by applying a Kernel Density Estimation (KDE) method with Gaussian kernel (Silverman 1996). In Figure 3-13, the sub-bands energy likelihood functions are shown for a data set collected for a subject walking and running with the sensor is in a swinging hand.

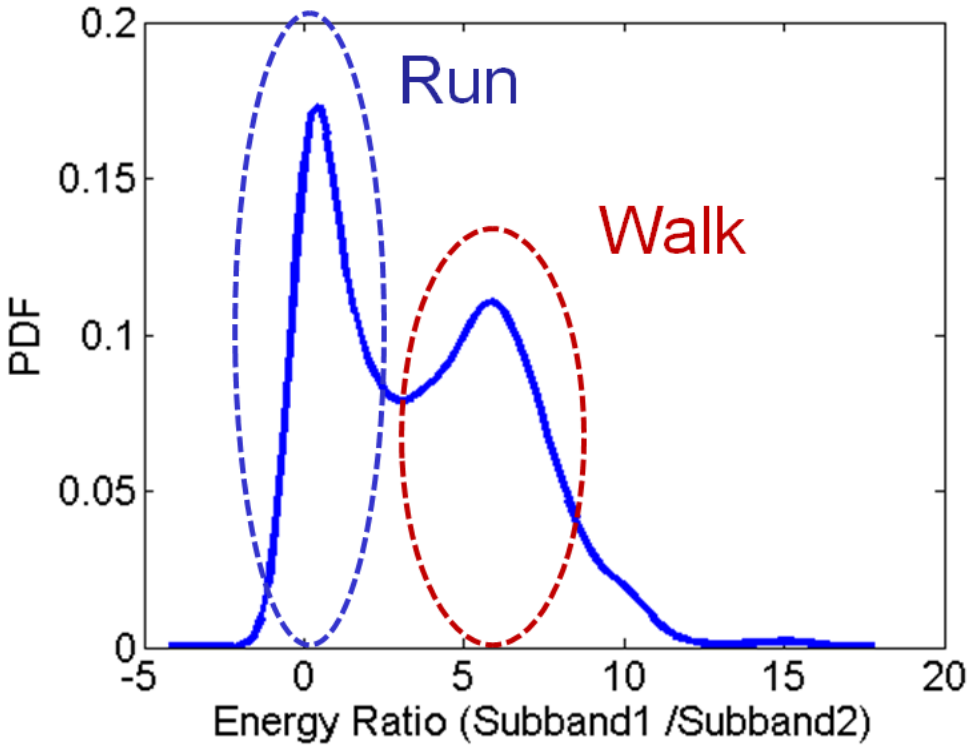

Figure 3-13: Sub-bands energy likelihood function for the walking and running modes

The distribution is a Gaussian mixture with modes related to walking and running activities. Each motion mode has a Gaussian distribution whose first order statistics, i.e. mean and variance, are estimated by fitting the mixture model with the empirical data.
A multivariate Gaussian likelihood function is used to describe jointly the cross-correlation features. Thus, the correlation among these features has been taken into account through the cross–correlation terms included in the covariance matrix of the multivariate distribution function. Finally, the feature joint conditional probability has been computed multiplying the single conditional distributions.

3.4.2 Decision tree classifier

The decision tree is a direct acyclic graph with the structure of a tree. The latter can be included in the class of non-parametric classifiers (Webb 2002). All classes that can be assigned to the input observations are represented by the leaves of the tree. Corresponding to each node, a test about one or more features is specified. Consequently, the full classification problem is divided in simpler classification tasks. Then, for each input, it is possible to assign a specific class by traversing the decision tree from the root to the leaves.

In order to identify the various motion modes a decision tree, valid for different sensor locations (e.g. **hand, pocket and foot**), has been designed and implemented according to the scheme in Figure 3-14. The total energy is the first feature evaluated, with the purpose to distinguish dynamic and static activities. If the total energy value is

higher than a trained threshold the activity is considered dynamic otherwise is classified as static. In the case of dynamic activities four instances are possible: walking, running, climbing down the stairs and climbing up the stairs. In order to recognize different types of dynamic activities further testes, involving multiple features, are necessary. First of all, the energy ratios between first and second sub-bands are evaluated.

To reduce the ambiguity between walking and climbing up the stairs and running and climbing down the stairs the cross-correlation terms are then computed. As explained in Section 3.3, usually this attribute assumes higher values when the user is walking down/up the stairs, since in that case the motion involves more dimensions. However, when the sensor is in the hand, its orientation can rapidly changes and the correlation terms can be split along the three axis of the sensor reference system. Thus, to make the classifier more robust also dominant frequencies and the total energy are evaluated and compared with trained thresholds.

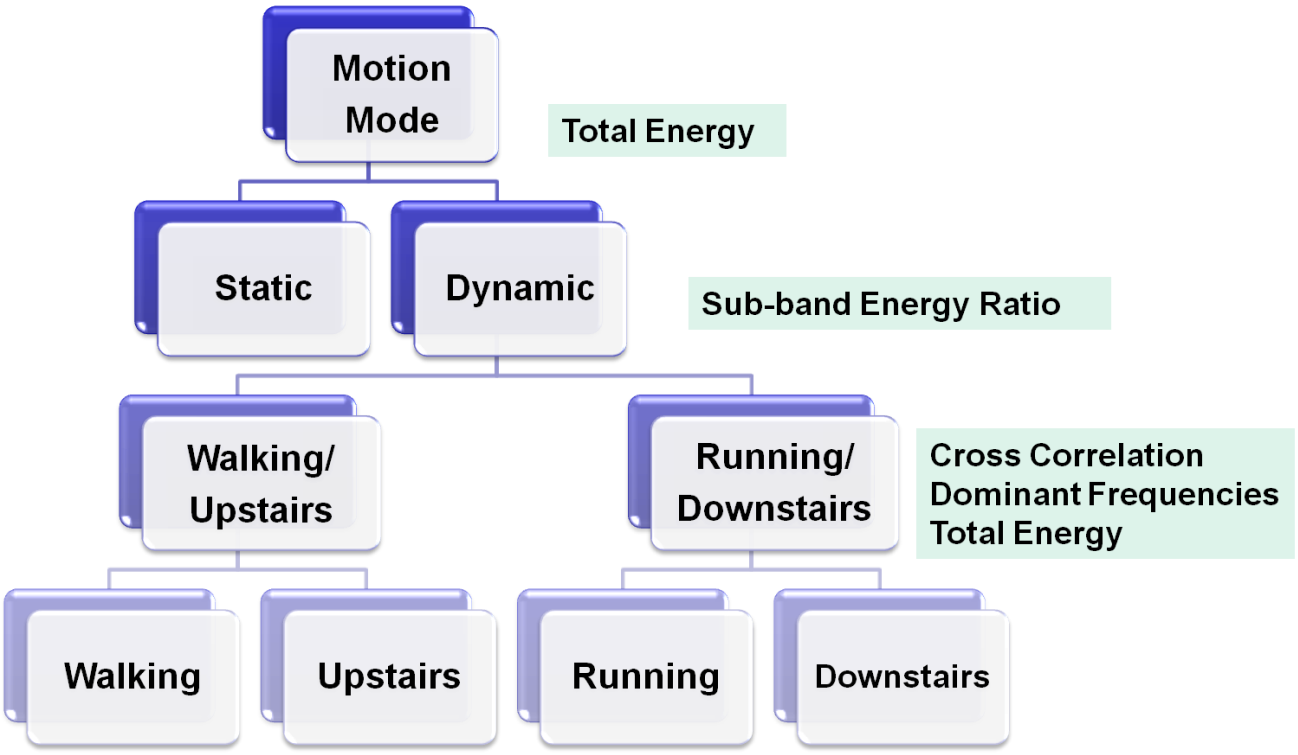

Figure 3-14: Decision tree for global motion mode recognition

3.4.3 K-nearest-neighbour classifier

The *k*-nearest-neighbour is a non-parametric classifiers. Starting from a unlabeled feature vector **x** and a set of labelled feature vectors this classifier searches for the *k* nearest neighbours of the input vector. Thus, it assigns to **x** the most frequent class among the classes of his neighbours. The *k*-nearest-neighbour decision does not require any knowledge about the class conditional probability distributions. Moreover, the classifier performance is related to the choice of the two following parameters:

1. **the value of k (number of considered neighbours)**
2. **the distance metric (used to find the k nearest neighbours)**

Higher values of *k* are less sensitive to noise but can reduce the separability among decision regions. The best value of *k* is generally selected empirically.

Concerning the distance metric, several distance metrics can be used but according to Weinberger et al (2005), "*the metric has to be optimized with the goal that the k nearest neighbours always belong to the same class while examples from different classes are separated by a large margin*".

It is possible to use a "weighted" version of this algorithm where the distance measurements are modified by weights selected according to the influence of each instance.

In this thesis, the selection of the k nearest neighbours is performed using the Euclidean distance, which is the most frequently used technique. It evaluates the root of square differences between coordinates of a couple of sample vectors, $\mathbf{x} = [x_1, x_2, ..., x_n]$ and $\mathbf{y} = [y_1, y_2, ..., y_n]$, according to the following definition:

$$d(x,y) = \sqrt{\sum_{i=1}^{n} (x_i - y_i)^2} \qquad (3.6)$$

For simplicity the *k* value adopted for this thesis has been chosen equal to one.

3.5 Summary

In this chapter different IMU signal features for motion mode recognition have been presented. Feature selection has been performed with the purpose to extract attributes able to characterize the different states regardless of the considered subject and sensor location. The above features have been integrated in three different classifiers. The main goal of this analysis was to compare the performance of these classifiers to select the most effective for motion mode recognition by using handheld devices. Results of such comparison can be found in Chapter 5. Finally, the approach used in this chapter to identify different human activities will also be adopted for the recognition of the sensor carrying mode and the user's hand motion presented in the next chapter. Thus, the knowledge of the sensor carrying mode will be exploited to adapt the pedestrian navigation algorithms proposed in Chapter 4.

Chapter Four: Step length estimation

PDR mechanization is an effective approach to propagate the user position and is commonly exploited with body fixed inertial sensors. However, the use of the PDR technique with handheld devices has been only marginally examined in the literature mainly due to the decoupling between hand and COM displacements. This chapter investigates the estimation of step lengths with handheld inertial sensors and proposes an algorithm for evaluating the travelled linear distance. In conjunction with the heading knowledge, this algorithm can be used to propagate the position of a pedestrian walking on a flat surface. Firstly, the chapter introduces the mathematical formulation of PDR mechanization. Then, the derivation of the algorithm for step length evaluation with handheld devices is given.

4.1 Pedestrian Dead Reckoning

PDR mechanization exploits human gait characteristics to propagate the user's position from the previous epoch to the current one. Specifically, starting from a known position, the PDR algorithm estimates the pedestrian's coordinates by combining the walking direction and the linear travelled distance between two epochs. The latter is generally computed by **first detecting pedestrian's steps and then evaluating their length**. The PDR mechanization is given by

$$\mathbf{p}_t = \mathbf{p}_{t-1} + s_t \begin{bmatrix} \cos\theta_t & \sin\theta_t \end{bmatrix}^T$$
$$\mathbf{d}_t = \sum_{t=0}^{end-1} \left\| \mathbf{p}_t - \mathbf{p}_{t-1} \right\| \quad (4.1)$$

where s_t is the step length, θ_t is the walking direction over one step, $\mathbf{p}_t$ the user's position at epoch t and $\mathbf{d}_t$ the travelled distance.. Figure 4-1 illustrates the PDR approach and its recursive nature where the computation of the actual user's position results from the previous displacements.

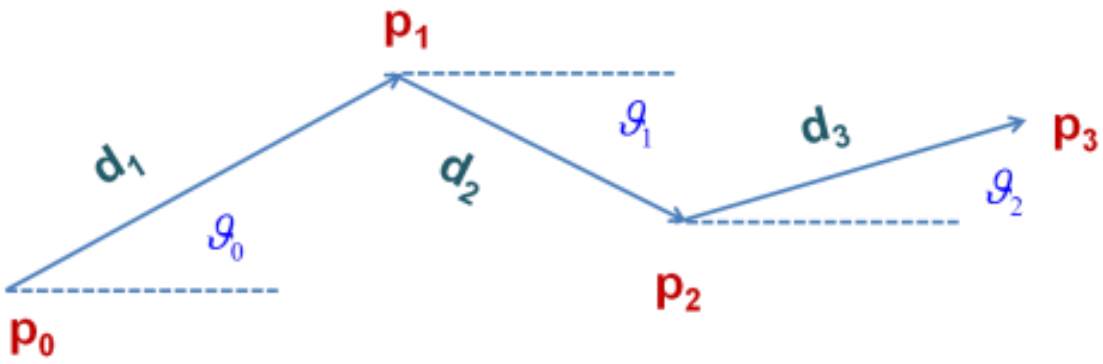

Figure 4-1: Representation of PDR approach

In order to apply the PDR approach, a novel step length model for handheld device, introduced in Section 5.2, is applied. The model requires the:

1. Identification of the sensor carrying mode and the hand motion,
2. Detection of step events,
3. Estimation of t step length.

The above stages are detailed in Sections 4-2-4-6.

4.2 Identification of sensor carrying mode and hand motion

A handheld IMU experiences different types of motions produced by the combination of the body's lower and upper parts. Furthermore, since the sensor is not rigidly fixed to the body, its position can suddenly change rendering the IMU signal pattern hardly predictable. For this reason the knowledge of the sensor carrying mode and hand motion can be exploited to adapt the navigation algorithms according to the detected mode and, consequently, to the IMU signal characteristics.

Moreover, all hand motions that are uncorrelated with the subject's global motion should be identified and removed in the PDR mechanization. These movements typically occur when the user is standing and looking for his/her phone in the bag or consulting the phone instructions. In these situations the subject is not changing his geographical position but is inducing a significant inertial force sensed by the IMU. In view of these considerations, the following six different modes have been identified and considered typical for mobile device users:

-**Static**: a subject is considered static if his/her location does not change during the analysis temporal window. This class includes also the case when the subject is slightly moving without changing his position. This is the case, for example, when the user is stepping on the spot while making a phone call.

- **Hand texting**: this class includes the situation when a user is walking while texting or reading a message on the phone or watching the mobile phone screen to

follow navigation instructions. In this case the device's motion is almost only due to the global motion of the user, while the user hand is quasi-stationary. This is why these cases can be considered very similar to the body fixed case, and subsequently, dealt with similar approaches.

-**Hand phoning**: the walking user is making or receiving a call.

-**Bag carrying**: the walking user is carrying the mobile device in a bag.

-**Hand swinging**: the walking user is holding the mobile device in a swinging hand.

-**Irregular motion**: this class refers to the motions that a subject performs without changing his position. This is the case when a subject is looking for the phone in a bag without walking.

Similarly to the recognition of the user global motion mode, the identification of the above states has been considered as a **classification problem**. As seen in Chapter 3, any classification algorithm requires three phases, namely data pre-processing, feature selection/extraction and decision making. These three steps are detailed in Sections 4.2.1- 4.2.3 for the states here defined.

4.2.1 Signal pre-processing

In order to evaluate the linear travelled distance the IMU signal is pre-processed as described in Section 3.2. However, in this case the analysis window has been selected equal to 256 with 50% of overlap. The above size, for a sampling frequency of 100 Hz, corresponds to 2.56 seconds instead of the length of 1.28 seconds used for

global motion mode recognition. Indeed a larger window allows achieving higher resolution for evaluating the FFT. In this case a better resolution is preferable since the frequency analysis will be exploited for extracting the step frequency as detailed in Section 4.6.

4.2.2 Features extraction for the walking case characterization

This section introduces the features that have been selected to recognize the different carrying modes and hand motions mentioned previously. These features are extracted by analyzing the IMU signal in the time, frequency and time-frequency domains applying the techniques presented in Section 2.5.

4.2.2.1 Signal Energy

The energy is computed here by squaring the norm of the accelerometer and gyroscope data and summing and normalizing them over a moving window as in (3.2). For completeness, the expressions of accelerometer and gyroscope energies are reported herein:

$$E_{s_0^a} = \frac{1}{N}\sum_{n=0}^{N-1} s_0^{a\,2}[n] \tag{4.2}$$

$$E_{s_0^{\omega}} = \frac{1}{N}\sum_{n=0}^{N-1} s_0^{\omega^2}[n] \tag{4.3}$$

This feature can be exploited to recognize different sensors' carrying modes. In fact, when a subject is walking with the IMU in the swinging hand, the angular rate and acceleration energies are much bigger than the ones experienced in the case of a sensor carried in the texting/phoning hand or in a bag.

This is clearly visible in Figure 2 where the gyroscope energies are reported for a sensor in the phoning and swinging hand of a subject walking along a straight line. In fact, when the sensor is in the user's texting hand, the inertial force is mainly due to the motion of the body's lower part, while the hand is not significantly moving. These considerations are also true for phoning and bag carrying cases. Indeed, all mentioned states are characterized by signal patterns similar to the body fixed case and, consequently, can be grouped as a unique class.

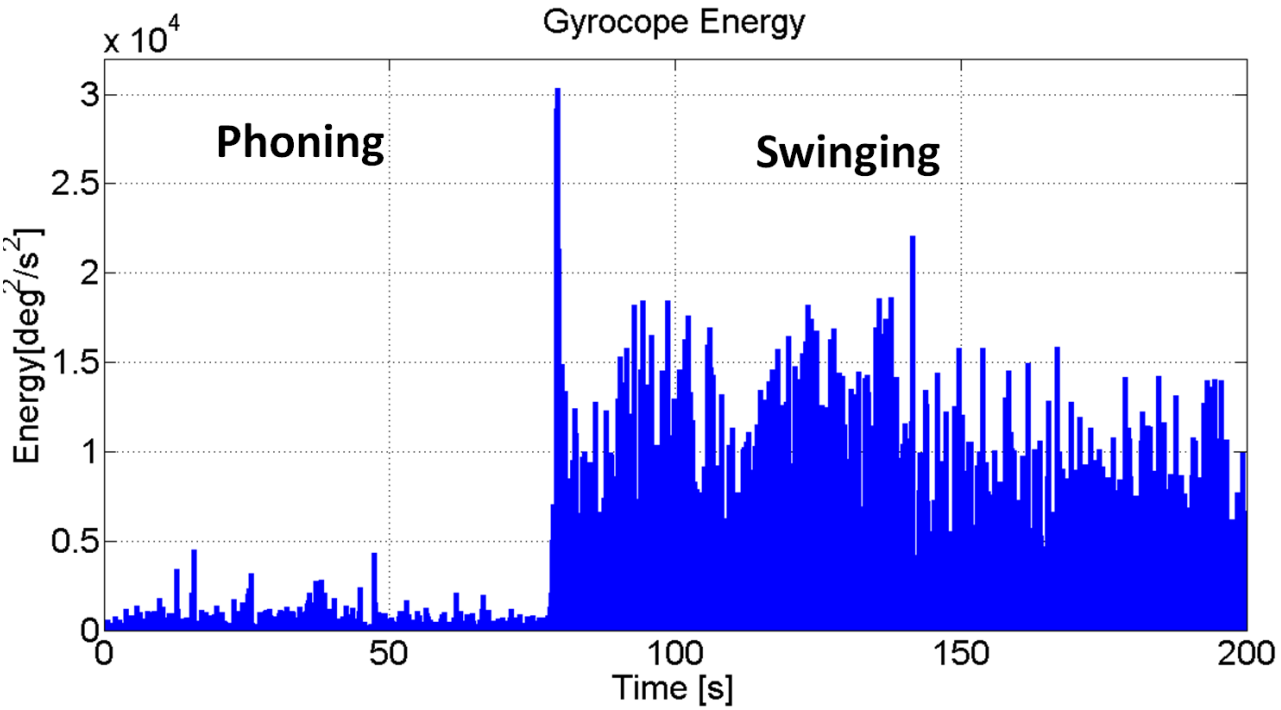

Figure 4-2: Energy of the gyroscope signal (norm) for a walking user with the IMU in the phoning and swinging hand.

4.2.2.2 Signal Variance

To increase the separability among different classes, the variance of the IMU signal has also been examined. The variance of a signal is a statistical measurement computed by averaging the squared differences of the signal from its mean. The variances of the accelerometer and the gyroscope signals are expressed as

$$\sigma^2_{s_0^a} = \frac{1}{N}\sum_{n=0}^{N-1}\left(s_0^a[n] - \frac{1}{N}\sum_{n=0}^{N-1}s_0^a[n]\right)^2, \quad (4.4)$$

$$\sigma^2_{s_0^\omega} = \frac{1}{N}\sum_{n=0}^{N-1}\left(s_0^\omega[n] - \frac{1}{N}\sum_{n=0}^{N-1}s_0^\omega[n]\right)^2 \quad (4.5)$$

Both gyroscope and accelerometer variances produce bigger values in the swinging case than in the texting, phoning and bag cases. This is observed in Figure 4-3 where the gyroscope variance is shown for a subject walking first with the sensors carried in the bag and then in a swinging hand. Furthermore, this feature allows identifying irregular motions.

In fact, the latter state generally corresponds to a sudden increase of the variance signal without any periodicity in the signals. To render the classification process more robust an analysis in the frequency domain is also performed and further detailed in Section 4.2.2.3.

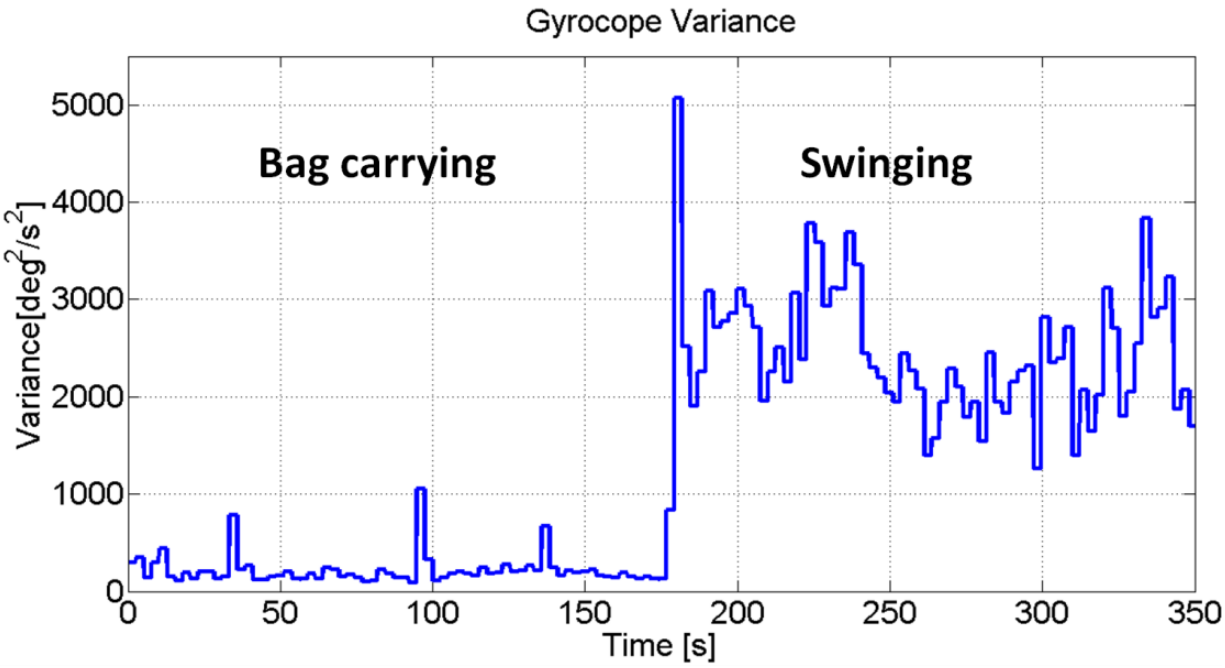

Figure 4-3: Variance of the gyroscope signal (norm) for IMU in the user's bag and in the user's swinging hand.

4.2.2.3 Frequency Analysis

As explained in Section 2.5, the frequency analysis of the IMU signal allows capturing the periodicity of signals produced by cyclic activities. However, non-stationary signals require also a time-frequency analysis that is able to catch the signal frequency variations over time. The frequency and time-frequency analyses are conducted using the Welch periodogram and signal spectrogram as described in Section 2-5. In Figure 4-4, the spectrogram of the accelerometer for a subject walking with the IMU in the hand is reported. The user is walking carrying the IMU first in texting mode and then in his swinging hand. A strongest frequency peak in the accelerometer spectrogram is showing the periodicity of the walking mode.

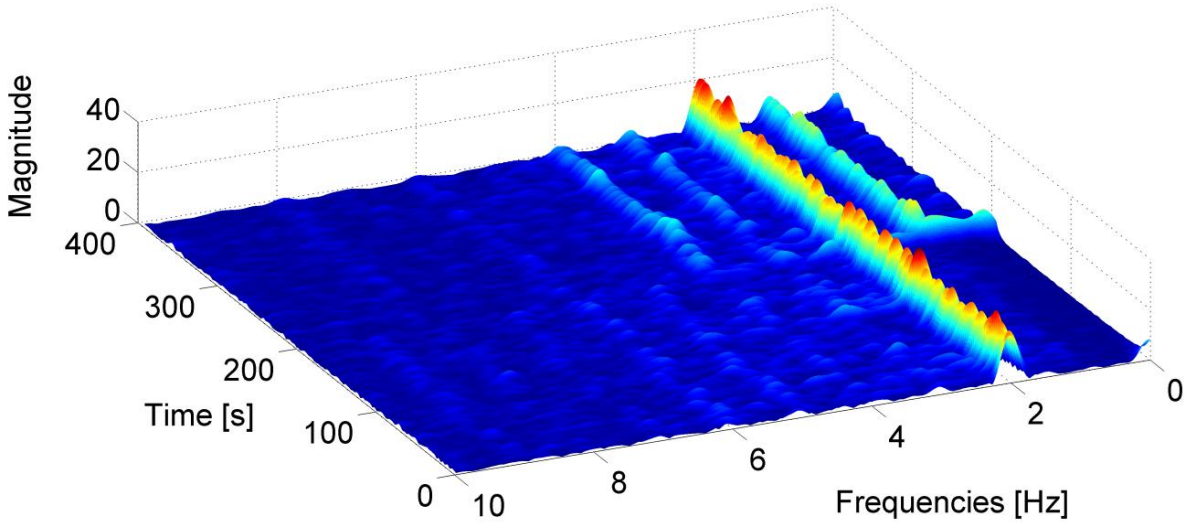

Figure 4-4: Spectrogram of the accelerometer signal for a walking user with the IMU in the hand.

For the swinging hand case, the three dominant frequencies are also analyzed over time and reported in Figure 4-5.

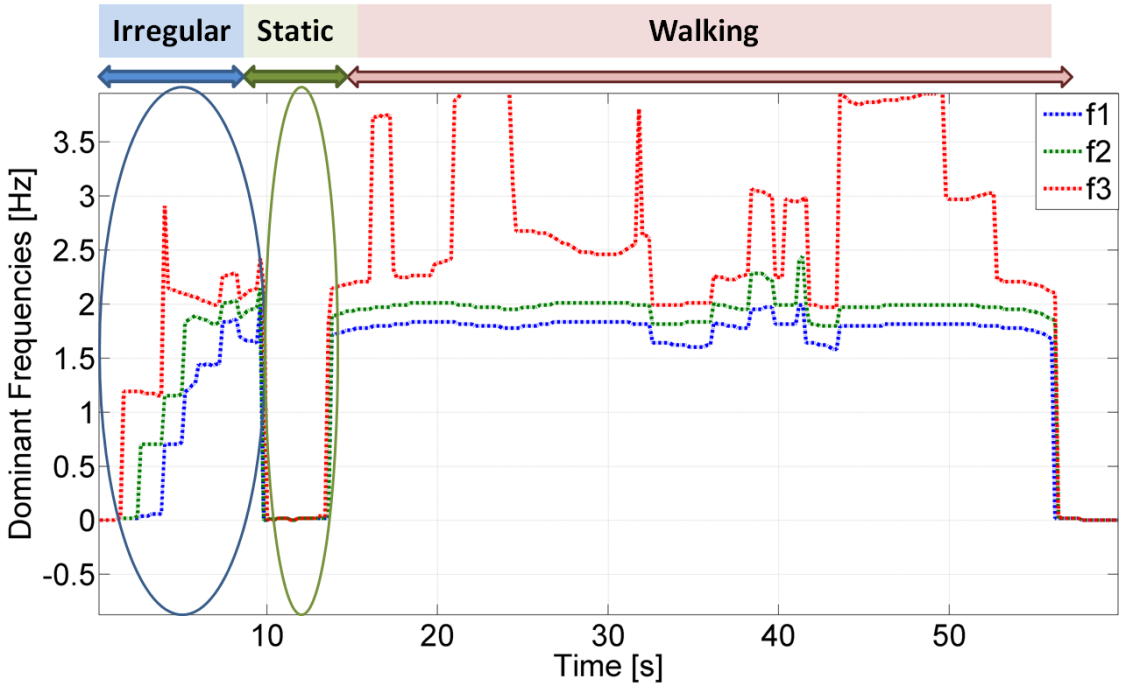

Figure 4-5: Dominant frequencies of the accelerometer signal over time. The IMU is carried in the user's hand

When the user is walking, the first two frequencies are almost stationary since the user is not significantly changing speed. If the user is performing an irregular motion, the two main frequencies follow a very irregular pattern. Finally, when the user is static the dominant frequencies assume values close to zero. A similar analysis has also been performed on the gyroscope's signal for a user walking with the sensors is a swinging hand.

The justification of this approach lies in the periodicity of the rotation of the arm, which is experienced in the swinging mode, and is reflected in the gyroscope signal producing

peaks in the frequency domain. This is shown in Figure 4-6, where the spectrogram of the gyroscope signal is reported. When the user is walking with the sensor in texting mode no peak is visible. Conversely, in the swinging case the peak produced by the arm's rotation is clearly observable.

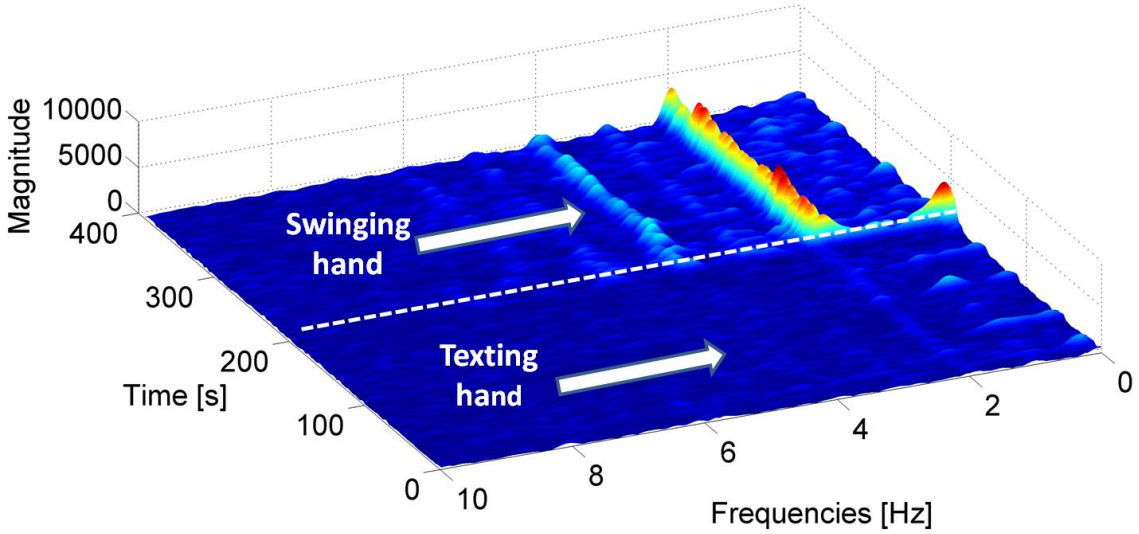

Figure 4-6: Spectrogram of the gyroscope signal for a walking user. The IMU is alternatively carried in the texting and swinging hand of the user.

4.2.3 Decision tree for motion mode identification in the walking case

In the next chapter it is shown that, for the recognition of the user's global motion, the decision tree classifier achieves the best results. In view of these results the features described in Section 4-2 have been integrated in a multivariate decision tree classifier whose structure is shown in Figure 4-7.

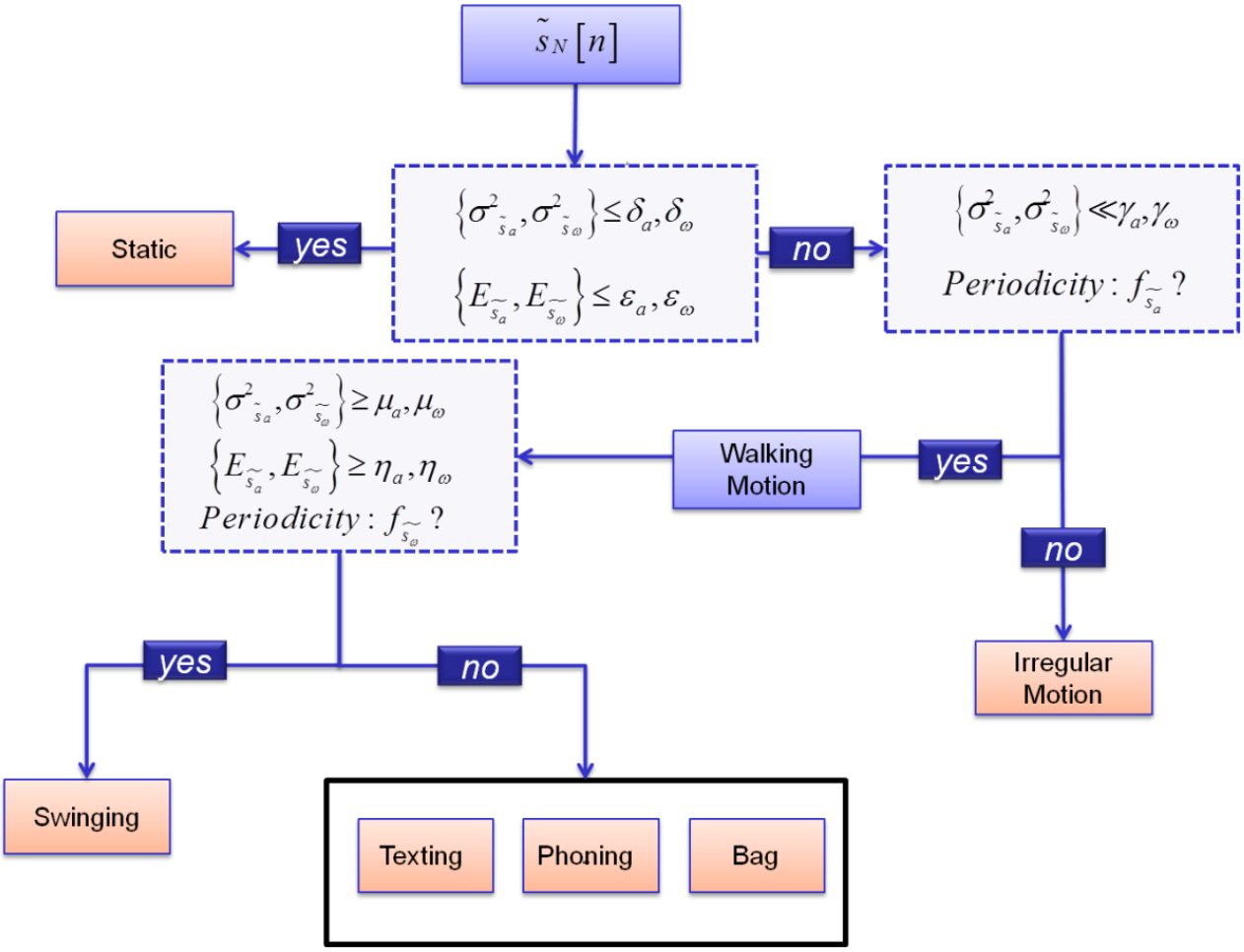

Figure 4-7: Decision tree for walking mode characterization

First of all the classifier distinguishes static and dynamic activities by comparing the energies and variances of gyroscope and accelerometer signals (Susi et al 2011b). Then, the gyroscope signals are evaluated to recognize walking with a swinging hand. In fact, as shown in Section 4-2, due to the periodic rotation of the arm during the swinging mode, the gyroscope signal shows frequency peaks that are not present when the arm is almost stationary. In addition, high values of the gyroscope and

accelerometer variance, induced by the motion of the arm, characterize the swinging mode.

Conversely, when the user is texting, phoning or walking with the mobile device in the bag the arm is not moving significantly and the IMU experiences low energies and variances. The latter cases show a similar pattern for both accelerometer and gyroscope signals. Consequently, they are considered as a unique class, as shown in **Error! Reference source not found.**. Finally, irregular motion modes are characterized by very high values of the gyroscope and accelerometer variances in short temporal periods. Texting, phoning and bag carrying do not show substantial difference between each other in the inertial signals patterns when dealing with step event detection. For this reason, the named activities are grouped into a unique class.

4.3 Step detection algorithm

After identifying the motion mode, next step for tracking the user's position consists in identifying user's step events. If the sensor is foot mounted, step events can be extracted by identifying the foot's stance phases corresponding to zero velocity periods. **When the sensor is in the hand, this method cannot be applied anymore since zero-velocity periods do not exists**.

However, the synchronization between upper and lower parts, confirmed by bio-mechanic studies (Park 2008), can be exploited to detect step events by analyzing the arm swinging. Indeed, a clear sinusoidal pattern is produced in the gyroscope signal by the cyclic rotation of the swinging arm. Consequently, identifying the peaks of the

gyroscope signal, the up and forward motions of the user's arm can be detected and used to mark the stance phases of the user's foot.

The gyroscope signal pattern changes for the case of a user walking on a straight line while texting a message, phoning or carrying the mobile phone in the bag. In fact, for the mentioned cases the signal provided by the gyroscope is mainly due to the noise components and to random motions of the hand. Consequently, in these situations gyroscope signals cannot be used for step events extraction. However, the torso's up and down motion still produces a sinusoidal pattern in the accelerometer signal which can be used for step detection. In both situations, step identification can be dealt as a peak detection problem.

In this thesis, signal peak detection is performed by recognizing a local maximum or minimum within the sliding window. The algorithm uses an adaptive threshold for being independent on variations of the signal energy, for example due to any change of the user's pace. To increase the robustness of the algorithm, a dedicated pre-processing phase of IMU signals is also performed.

Specifically, accelerometer and gyroscope signals are low-pass filtered using a 10th order Butterworth filter with a 3 Hz cut-off frequency. The aim of this pre-processing phase is to obtain an undistorted signal by extracting the signal's fundamental frequency that is induced by step events. After this pre-processing phase the algorithm evaluates the maximum value within the sliding window and uses this value as a threshold for the peak detection. Consequently, if a sample in the window assumes a bigger value than the computed maximum, a peak is detected. In the upper part of Figure 4-8, the norm of the gyroscope signal recorded by the IMU in the swinging hand

of the user is reported and the bottom part shows the norm of the acceleration signals recorded on the foot. Signals recorded in the hand and on the foot are synchronised.

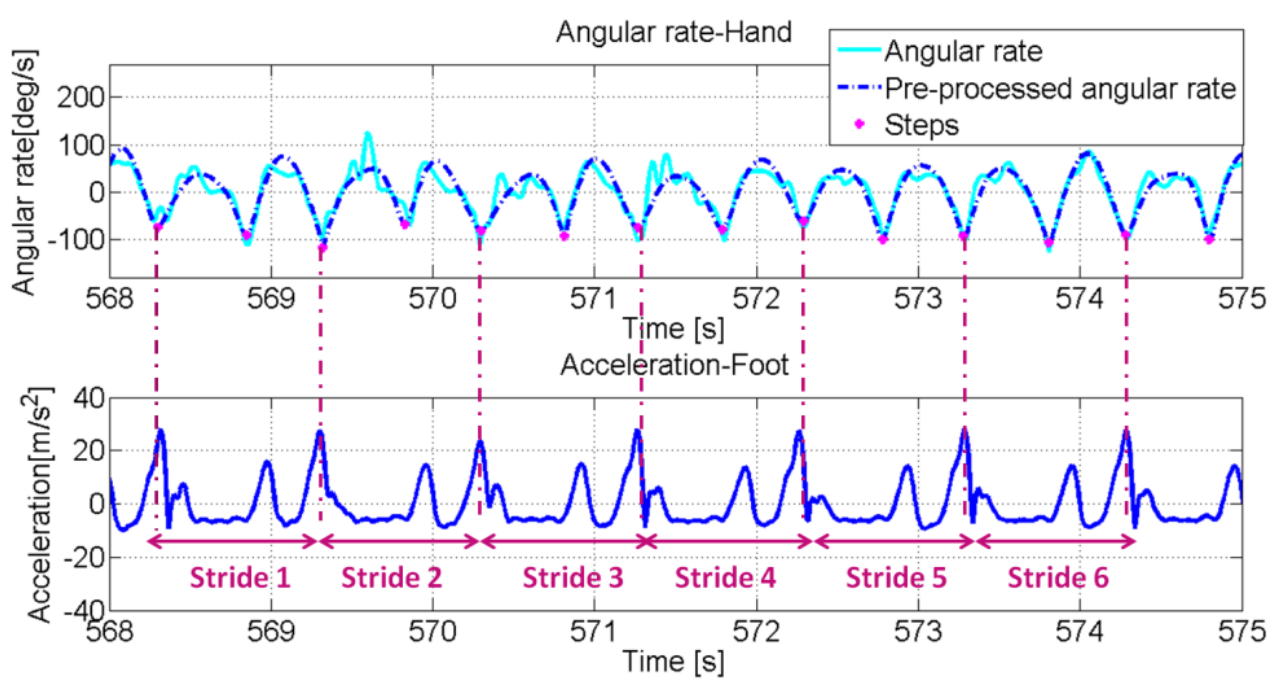

Figure 4-8: (Upper) Gyroscope signal (norm) recorded by the IMU in the swinging hand. The dots represent the detected step events. (Down)Accelerometer signal (norm) recorded by the IMU on the foot (the mean has been removed).

The magenta dots mark the minima extracted from the signal. By comparing the signals recorded in the hand and on the foot, the relationship between the above minima and stride events is assessed.

Indeed each minimum can be associated to a step event and subsequently for each couple of minimum points a stride can be identified. In Figure 4-9 (upper part), the norm of accelerometer signals recorded by the IMU in the texting hand is reported. Again in

this case, the magenta dots identify the minimum values of the signal that are related to the step events in the same way as for the swinging case.

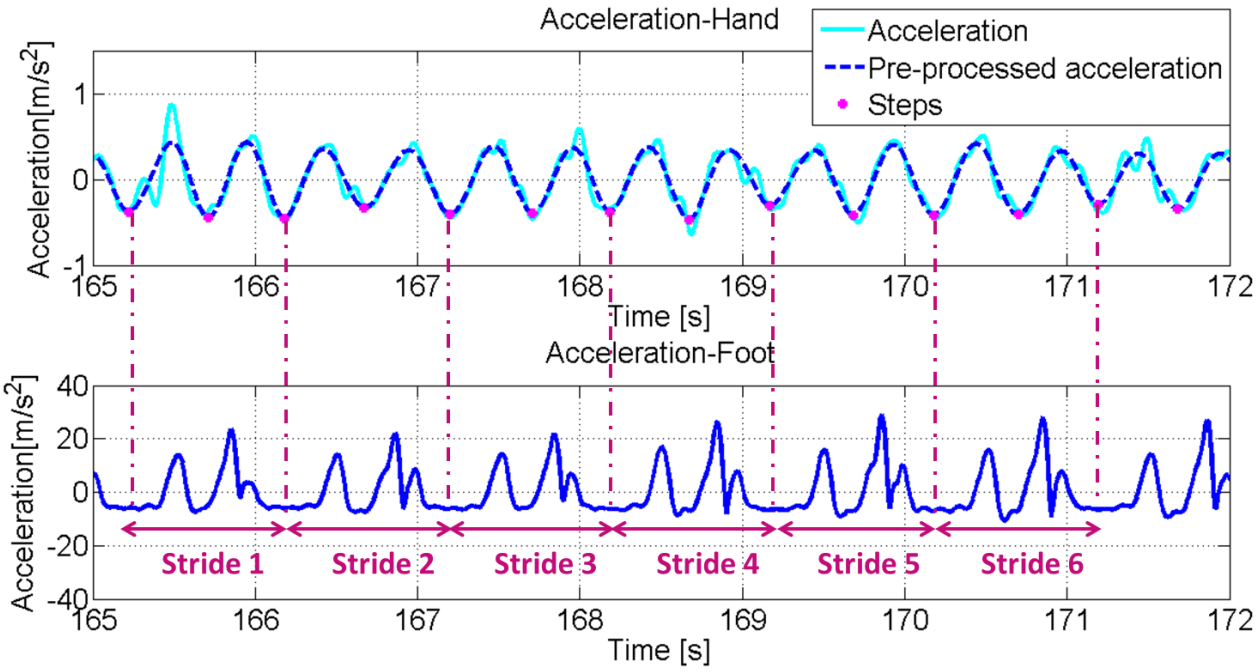

Figure 4-9: (Upper) Accelerometer signal (norm) recorded by the IMU in the texting hand. The dots represent the detected step events. (Down) Accelerometer signal (norm) recorded by the IMU on the foot (the mean has been removed).

4.4 Step length estimation: general overview

After detecting step events, the final stage for tracking user displacements consists in the **estimation of step lengths**. The evaluation of steps can be performed by using different approaches, which are strongly related to the sensor's position.

Most of the algorithms proposed in the literature are based on the assumption that the sensor is firmly attached to the user's body, generally mounted on the foot, or

close to COM, e.g., along the backbone, or distributed on the leg (Renaudin et al 2007,Tien et al 2010, Myazaky 1997, Jahn et al 2010). As pointed out in Chapter 1 these locations are particularly indicated for navigation purposes since in these cases the inertial force experienced by the sensor is directly produced by the gait cycle. More specifically, two main categories of step length models can be used for step length evaluation from a body fixed sensor: biomechanical and parametric models.

Usually biomechanical models assume that the sensor is attached close to the user's COM and model the user's leg as an inverted pendulum (Jahn et al 2010, Alvarez et al 2006). This model allows applying a simple geometric relationship between the COM's vertical displacement and the step length. Alternative geometric based approaches are also proposed in (Zijlstra et al 2008, Kim et al 2004).

Parametric models compute step length by exploiting parameters, such as the step frequency and the accelerometers variance (or their combination) (Shin et al 2007, Sun et al 2008). However, also in these cases, the sensor is generally mounted on the belt. As already pointed out, body fixed locations are not realistic for handheld devices applications. However, only a few studies consider the case of non-body fixed sensors for step length modeling.

Furthermore, even if the sensor is not body fixed its location is generally constrained to a body position where the device is relatively stable while the user is walking. A classical example is when devices are carried in the user's trouser pocket (Steinhoff et al 2010) or constrained close to the ear while phoning or pointing toward the walking direction. The reason is that in these cases the IMU signal patterns of the device are similar to the ones produced by body fixed sensors and subsequently similar

approaches can be adopted. Conversely, the cases of the sensor held in a swinging hand and when the sensor's location can change while the user is walking are generally ignored. In (Ayub et al 2012) different sensor carrying modes are analyzed, including carrying the sensor in the swinging hand. However, in this work traditional techniques, generally adopted for body fixed sensors, are applied. These techniques, designed for body fixed sensors, achieve lower performance if applied to the handheld case. In view of the limitation of the method proposed in the literature to evaluate step lengths by handheld devices a dedicated and extensive analysis of the hand case has been performed herein.

4.5 Step model

The linear relationship existing between step length and step frequency is often exploited to estimate step length (Shin et al 2007). Indeed if a subject walks faster, both step's length and step frequency will increase. After a dedicated analysis, it was found that this approach can also be extended for the handheld case.

Finally another physiological element has been considered. Biomechanical studies have demonstrated that generally the user's step length is proportional to the length of the user's leg and subsequently to the user's height (Rose & Gamble 2006). Using both elements, a novel step length model for handheld devices has been both theoretically and experimentally developed herein. It is based on the combination of the step frequency and the user's height.

Experimentally tests, reported in Chapter 5, have shown that the best linear relationship between frequency and step length is the one weighted by the user's height and is given by:

$$s = h \cdot (a \cdot f_{step} + b) + c \quad (4.6)$$

$$\text{with } k=\{a,b,c\} \in \mathbb{R}$$

where h is the user's height, f_{step} is the step frequency and k is a set of parameters. In Figure 4-10 the three phases, namely sensor carrying mode/hand motion identification, step detection and step length estimation necessary to model the step length, are also represented.

The sensor carrying mode/hand motion identification is used to select the step detection algorithm, which is based on the peak detection of the gyroscope or the accelerometer signal respectively, for the swinging case and for the texting, phoning, carrying the bag cases. Then, as shown, In Figure 4-9 the step event is sent to the step length evaluation block. The latter combines the step frequency, evaluated as described in Section 4.6, and the user's height with the set of constants k, as in (4.5).

These constants can be trained rendering the model ***universal***, since the set of parameters k is the same for any subject. Alternatively the model can be ***calibrated*** fitting the constants for each single person.

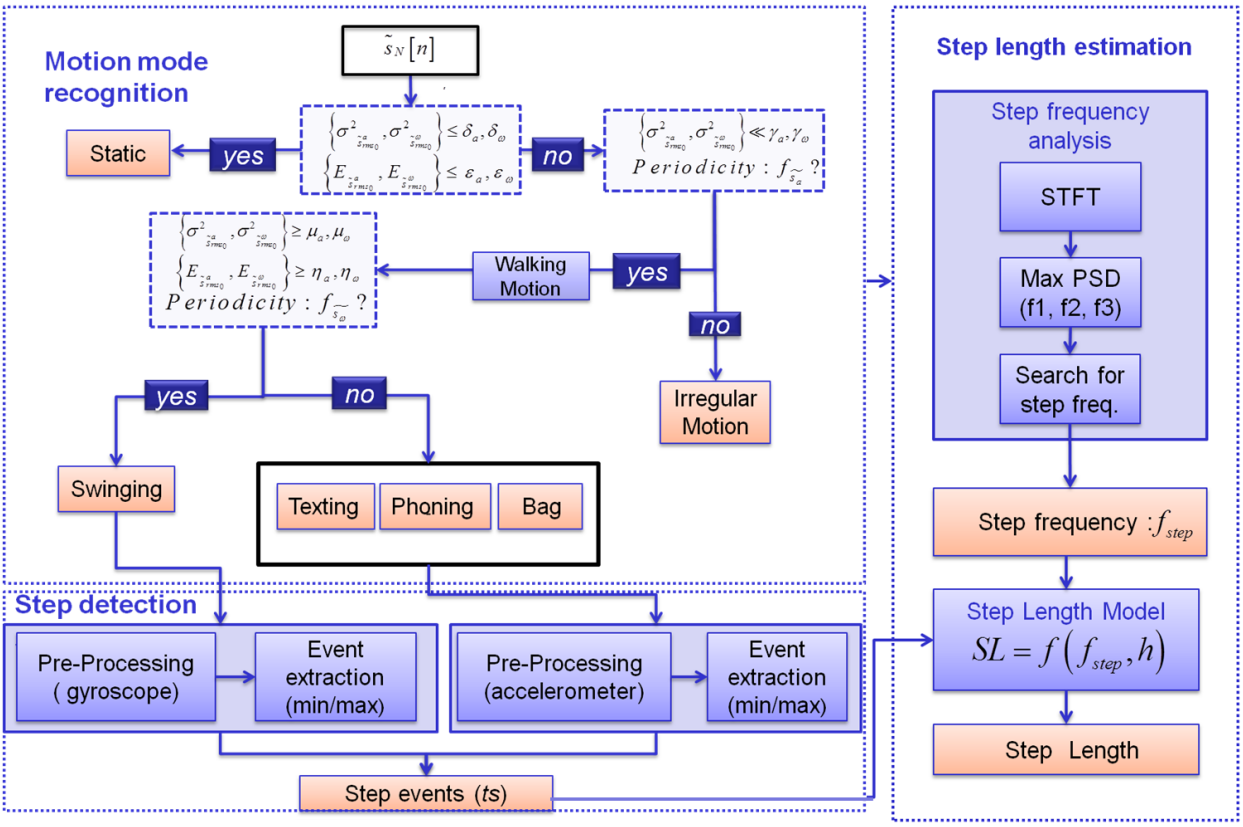

Figure 4-10: General scheme of the algorithm for the computation of the linear travelled distance

In this thesis both universal and calibrated models are proposed. The universal model could be exploited as an initial solution for any filter that would provide adaptive capabilities. As detailed in Chapter 5 the universal model relies on a set of constants trained using 12 test subjects while the calibrated model fits the set of constants to the single user by applying a Recursive Least-Squares (RLS) (Teunissen 2003) technique. The latter consists on the iterative evaluation of the optimum parameters by minimizing the sum of squared residuals between the true step length and the foreseen step length.

The initial solution x_0 is given by the universal set of parameters *k* as.

$$\hat{\mathbf{x}}_{t+1} = \hat{\mathbf{x}}_t + \left(\mathbf{H}^T\mathbf{H}\right)^{-1}\mathbf{H}^T\,\mathbf{s} \tag{4.7}$$

with:

$$\begin{aligned}
\mathbf{x}_0 &= \begin{bmatrix} a & b & c \end{bmatrix}^T_{universal}, \\
\mathbf{H} &= \begin{bmatrix} h_{user_1} f_{step_1,user_1} & h_{user_1} & 1 \\ \cdots & \cdots & \cdots \\ h_{user_n} f_{step_k,user_n} & h_{user_n} & 1 \end{bmatrix}, \\
\mathbf{s} &= \begin{bmatrix} s_{user_1,1} & \cdots & s_{user_n,t} \end{bmatrix}^T.
\end{aligned} \tag{4.8}$$

- s includes the true step lengths computed for all subjects

- the matrix **H** comprises the step frequencies and users' heights for *n* test subjects over t epochs. The set of fitted parameters is determined when the convergence criteria over $\left(\hat{\mathbf{x}}_{k+1} - \hat{\mathbf{x}}_k\right)$ is achieved. True step lengths are evaluated following a specific procedure described in Chapter 5, while predicted step lengths are obtained using the model in (4.6).

4.6 Step frequency evaluation

The proposed step length requires the extraction of the user's step frequency with the IMU handheld device. For this purpose an analysis has been conducted to investigate the relationship between hand and foot frequencies. The spectrograms of the accelerometer signals have been evaluated for a sensor placed in a hand and on the

foot of a walking subject. In Figure 4-11, where the spectrogram of the accelerometer is reported for the foot mounted IMU case, three dominant frequencies can be identified.

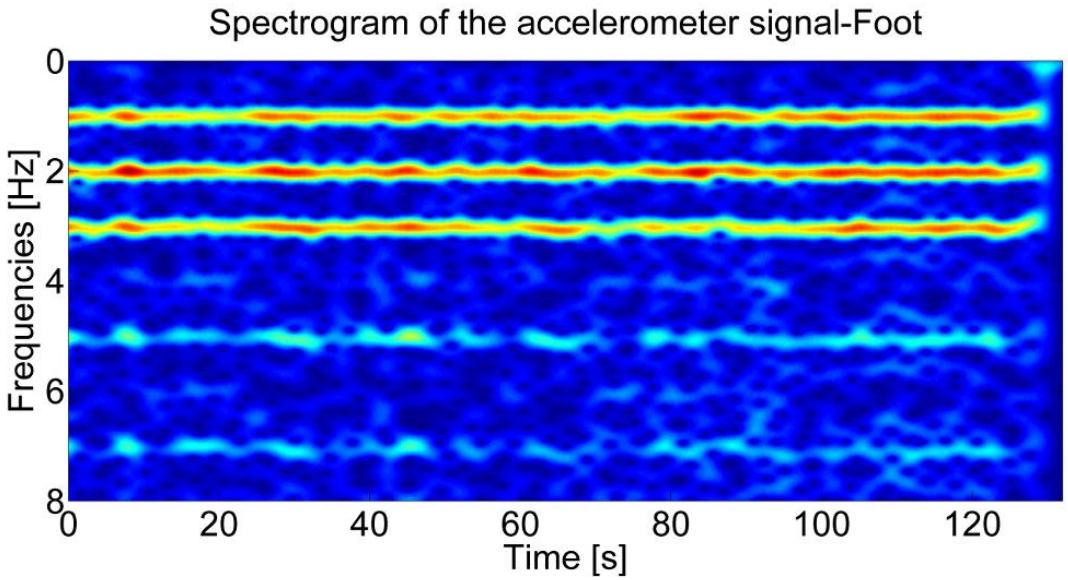

Figure 4-11: Spectrogram of the accelerometer signal for the sensor mounted on the walking user's foot.

As shown in Figure 4-12, when the sensor is held in the hand, three dominant frequencies are also identifiable in the spectrogram of the accelerometer signal for a subject walking alternatively with the sensor in the swinging and in the texting modes

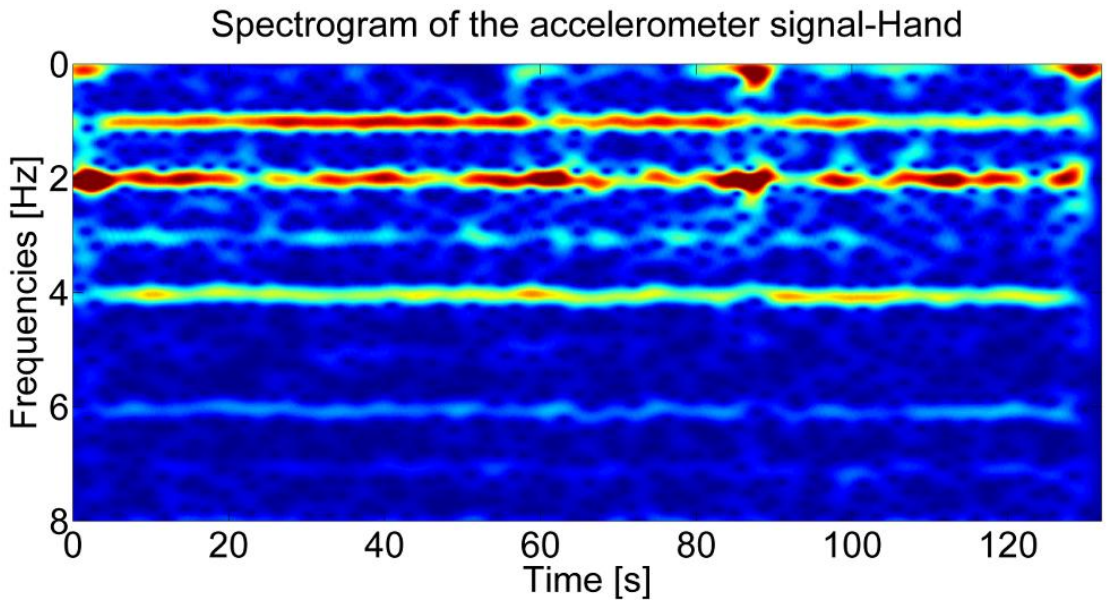

Figure 4-12: Spectrogram of the accelerometer signal for the sensor placed in the walking user's swinging hand.

A specific study has been conducted to relate the hand frequencies to gait events, such as user's step and stride. In Figure 4-13, the PSDs are shown for the accelerometers of both IMUs in the swinging and texting cases. Dominant frequency peaks are centered on the same values for both sensors showing that the step frequency can be evaluated even if the sensor is not foot mounted or non-body fixed. It has also been observed that the strongest frequency of the accelerometer signal, i.e., the frequency with the maximum power, is not always coupled with the same event of the walking gait cycle. Sometimes it is coupled with the step event (Figure 4-12) and sometimes, especially for faster speeds, with the stride event.

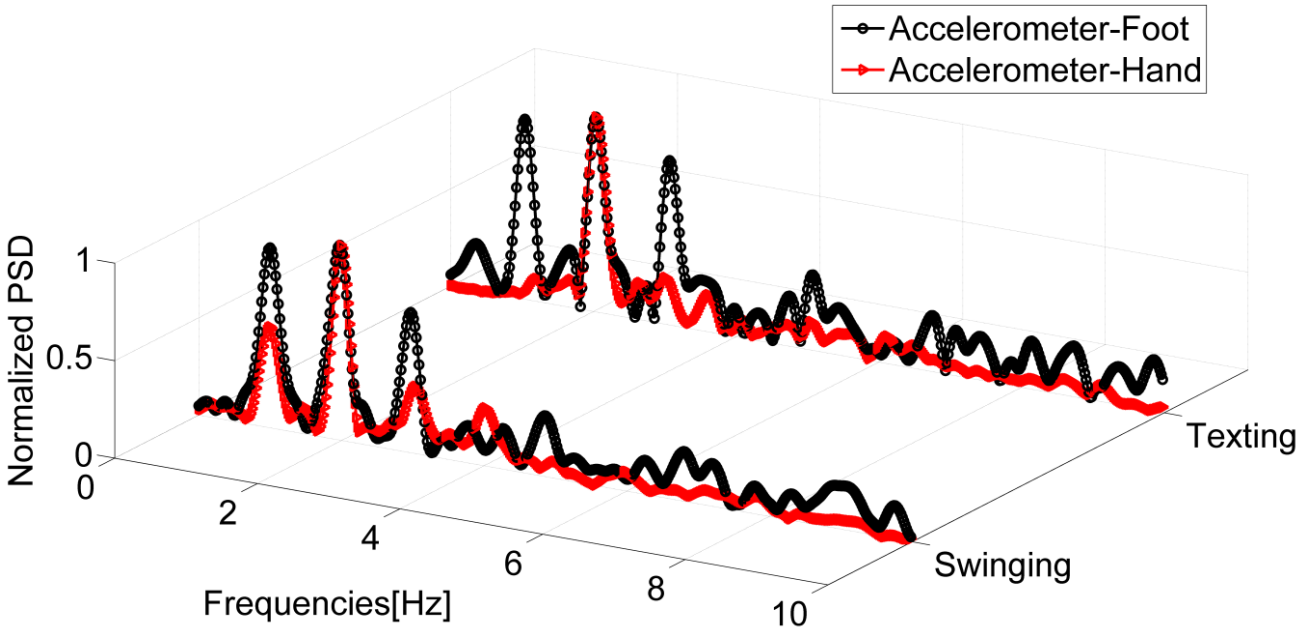

Figure 4-13: Normalized PSD of the accelerations sensed by the foot mounted sensor and the one in the swinging and texting hand. For both motion modes, the strongest frequency is coupled with the step event.

This is further illustrated in Figure 4-14 where the PSD extracted from the signal of a sensor in the user's swinging hand is reported. The PSD is estimated using the Welch periodogram technique, detailed in Section 2.5. The spectrum analysis shows that increasing the users speed, it is more likely that the strongest frequency and stride event are coupled

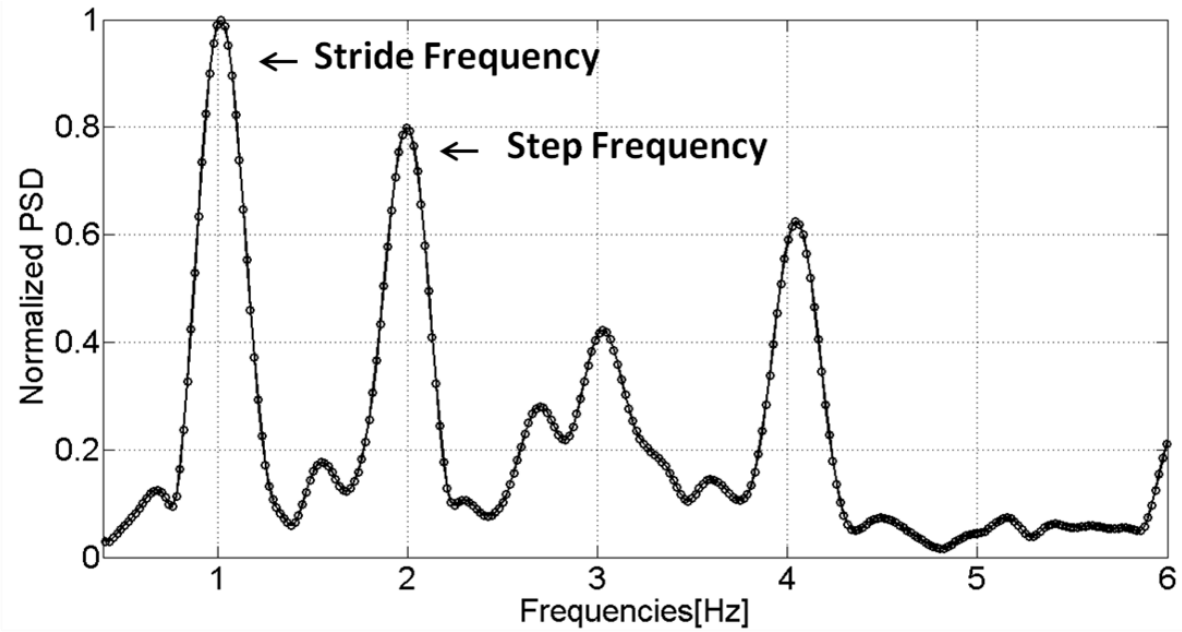

Figure 4-14: Normalized PSD for the accelerometer sensed by the user's swinging hand. Here, the strongest frequency is coupled with stride events.

To mitigate this coupling problem and to achieve robust evaluation of the step frequency from the hand frequency, a binary classifier has been designed. The classifier first of all extracts the strongest frequency and then applies the following decision rules:

$$\begin{cases} \text{if} \quad f_{strongest} > \tau \Rightarrow f_{strongest} = f_{step} \\ \text{if} \quad f_{strongest} < \tau \Rightarrow f_{strongest} = f_{stride} \end{cases} \tag{4.9}$$

A 1.4 Hz threshold τ has been selected considering that in the normal walking case the step frequency was above 1.6 Hz for all test subjects. However, further investigation should be performed to understand how the user age affects the step frequency. If the detected frequency corresponds to a stride frequency, the classifier computes the final

step frequency by multiplying the strongest frequency value by two. In Figure 4-15 the step frequencies, extracted after applying the binary classifier, true step lengths and the estimated ones using the step length model and the universal set of parameters are reported for a subject walking with the sensor in his swinging hand.

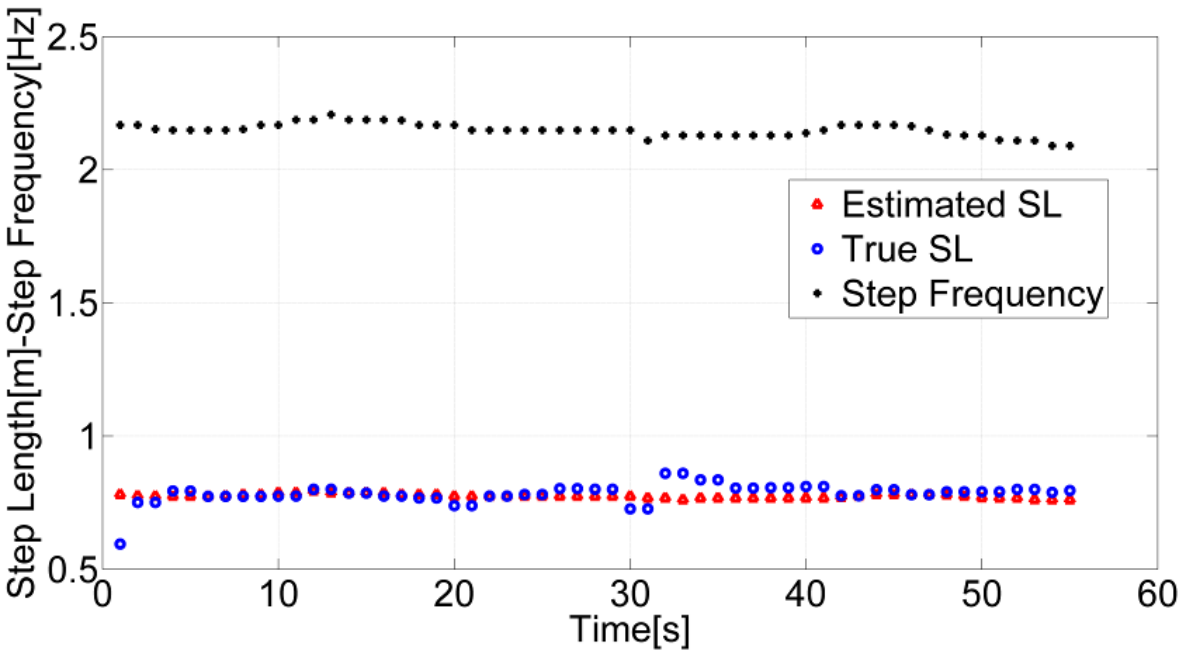

Figure 4-15: Estimated, true step lengths and step frequencies computed with signals from a handheld IMU when the user is walking with his hand swinging.

4.7 Summary

In this chapter an algorithm to evaluate the linear distance travelled by a walking subject has been presented. The algorithm is composed of the following three stages

- Sensor carrying mode/hand motion identification
- Step detection
- Step length estimation

The step length estimator combines the step frequency and user's height by using a set of three constants. In order to evaluate the step frequency even if the sensor is in the hand a dedicated analysis is proposed to relate step and hand frequencies. In particular, it has been observed that the step frequency is sometimes coupled with the stride and sometimes with the step events. A dedicated binary classifier has been developed to mitigate this ambiguity. In Chapter 5, performances of the proposed algorithms are assessed in the position domain.

Chapter Five: Field tests and experimental results

This chapter presents the results obtained from the assessment of the algorithms introduced in Chapter 3 and Chapter 4. Specifically, in Section 5.1 the field tests performed to train and test the classifiers for global motion mode recognition, proposed in Chapter 3, are described. Then, the performances of the above classifiers are compared and discussed. Section 5.2 describes the training and testing phases of the step length model introduced in Chapter 4. Since the step length model is based on three modules, namely carrying mode/hand motion identification, step detection and step length estimation, the assessment of each module has been carried out with dedicated field tests. A detailed description of these tests and related results is reported. Finally, overall performances of the step length model are evaluated in the position domain using ten test subjects.

5.1 Motion mode recognition: training and assessment

This section describes the equipment set up used for training and testing the motion mode recognition algorithms proposed in Chapter 3. Then, the methodology adopted to perform the test fields is detailed. In particular, since different IMU locations produce different signal patterns, the classifiers are tested for different sensor locations. The criterion used for the sensor position selection is explained herein. Finally, the results obtained from the classifiers' assessment phase are discussed and compared.

5.1.1 Data collections set up

In order to collect enough data for training and testing the motion mode classifier proposed in Chapter 3, different data collections have been carried out by seven subjects, two females and five males, of ages ranging between 20 and 35. For the field tests, Crysta MEMS IMUs (Bancroft 2010), produced by Cloud Cap technology, have been used. The sensors were connected via cables to a small laptop storing the IMU data. Then, the laptop and the battery to power all the equipment were carried by the user in a backpack, as shown in Figure 5-1. All cables connecting the IMUs to the laptop were firmly fixed to the user's body in order not to affect the user walking style and consequently the classifiers' performance.

Figure 5-1: Test set up: the IMUs are connected to a laptop carried inside a backpack

5.1.2 Data collection methodology

The proposed classifiers for motion mode recognition have been designed to identify five activities, namely standing, walking, running, climbing and descending stairs. During each data collection the subjects were asked to perform the mentioned activities carrying three IMUs placed in three different locations of the user body: on the foot, in the pocket and in a swinging hand. The impact of the above sensor locations on the human activity recognition is explained herein. Then, the procedure followed to collect the data is described.

5.1.2.1 Sensor on the user foot

The inertial force experienced by a foot mounted sensor reflects the subject's leg and, consequently, the user's global motion. Indeed, in this case the IMU signal is generally undistorted rendering the identification of the mentioned activity easier. Moreover, since the sensor is body fixed its orientation does not change over time. This aspect is particularly relevant for the identification of the stair case. In fact, climbing and descending stairs are identified, also exploiting the correlation between acceleration components. As detailed in Section 3.5.2, this feature depends on the sensor orientation and, consequently, its effectiveness could decrease if the sensor orientation changes, which is likely to happen for unconstrained devices. In view of the above observations, this foot sensor location was selected for producing the reference data used to assess the performances of the developed algorithms.

5.1.2.2 Sensor in the user trouser pocket

Conversely to the foot situation, the trouser pocket represents a typical placement for mobile devices. Furthermore, although a sensor in the user's pocket is not body fixed, it is mainly subject to the user's global motion and consequently, this location induces IMU signal patterns similar to the body fixed case. This explains why the published studies dealing with non body fixed sensors generally assume that the sensor is located in the user's pocket.

5.1.2.3 Sensor in the user swinging hand

Human activity recognition by using a sensor in the user swinging hand represents the most complicated case to be analyzed. Indeed, the hand motion can hide the global user's motion, thereby producing distorted signal patterns. Moreover, the hand motion can be decoupled from the global user's motion rendering the activity identification complex. However, this is the most interesting case for portable device applications.

5.1.2.4 Data collection procedure

During the test fields, the subjects were required to perform the examined activities, in a sequential way, without receiving any instruction about the sensor orientation. Furthermore, they were also allowed to stop or change direction. While the users were performing the activity they were time tagged and the performed activity was recorded by a second person as in (Ravi et al 2005). Figure 5-2 shows an outdoor data

collection and the different sensor locations. In this case, the test subject is walking at different speeds carrying the backpack with the equipment described in Section 5.1.

Figure 5-2: Outdoor data collection: (a) the test subject is carrying the backpack with a small laptop and a GPS antenna used as reference. The subject carries a foot mounted IMU (b), an IMU in his pocket (c) and an IMU in a swinging hand (d).

5.1.3 Assessment criterion and results

The collected data have been divided in two subsets: training and testing data. The choice of the dimension of the above two data sets is a critical point in pattern recognition. A common rule of thumb is to use 70% of the database for training and 30% for testing (Fukanaga 1990). This rule is applied for the analysis described here. Different algorithms have been designed and implemented to recognize the user activities, namely the *k* nearest neighbour, the decision tree and the Naïve Bayes, all detailed in Chapter 3. The performances of the mentioned classifiers have been compared by computing their probability of correct identification, i.e. accuracy that is the number of correctly identified test samples normalized by the total number of test samples. For each sensor location, the latter results have been averaged over the

different motion modes encountered by the pedestrians leading to a “mean accuracy” indicator. The results are reported in Table 5-1.

Table 5-1: Accuracy of classifiers for motion mode recognition

	Naïve Bayes			Decision Tree			K Nearest Neigbour		
Sensor Location	**Swinging Hand**	**Pocket**	**Foot**	**Swinging Hand**	**Pocket**	**Foot**	**Swinging Hand**	**Pocket**	**Foot**
Static/ Standing	95%	97%	98%	99%	100%	100%	97%	97%	100%
Walking	89%	94%	95%	96%	98%	98%	93%	95%	98%
Running	93%	87%	94%	94%	96%	97%	91%	94%	98%
Descending stairs	72%	90%	85%	92%	94%	95%	84%	90%	95%
Ascending stairs	68%	88%	90%	82%	90%	93%	80%	88%	92%
Mean Accuracy	**83.4 %**	**91.2%**	**92.4%**	**92.6%**	**95.6%**	**96.6%**	**89%**	**92.8%**	**96.4%**

Furthermore, to have a better insight into the classifiers’ performance, in Tables 5-2, 5-3, and 5-4 the confusion matrices are also provided for the sensor in a swinging hand representing the most critical case. The use of confusion matrices is a common approach for evaluating classifier performance. The rows of the confusion matrix show the actual classes while the columns report the predicted classes. Consequently, the principal diagonal of the confusion matrix reports the classifier accuracy or probability of detection (P_{det}) for each state. The off diagonal elements report the percentages of misclassification (P_{md}). These evaluation metrics will be adopted also for the assessment of the sensor carrying mode classifier and the step detection algorithm presented in Section 5.2.3

In Tables 5-2-5-4, the colors key is based on the percentage of correct state prediction. Specifically, the green color along the principal diagonal refers to high percentages of accuracy. Conversely, the blue color in correspondence of the off diagonal elements is indicating a low level of miss classification.

Table 5-2: Confusion matrix-Naïve Bayes classifier (IMU in a swinging hand)

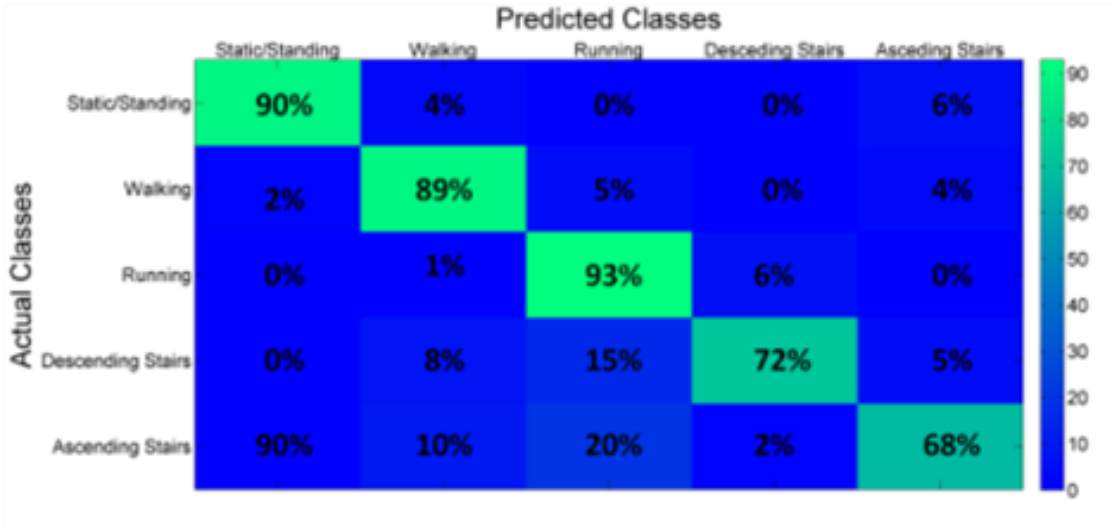

Table 5-3: Confusion matrix- Decision Tree classifier (IMU in a swinging hand)

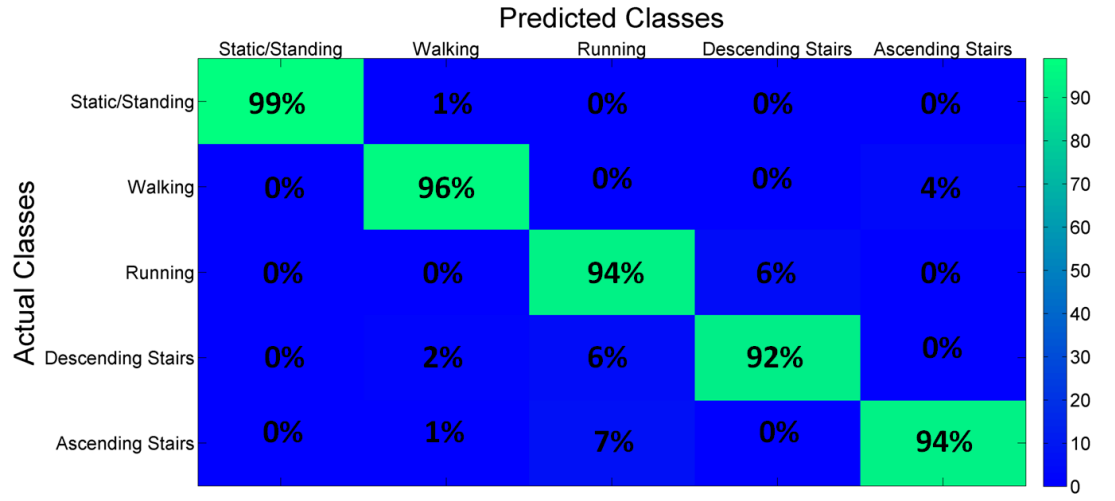

Table 5-4: Confusion matrix- K-Nearest-Neighbour classifier (IMU in a swinging hand)

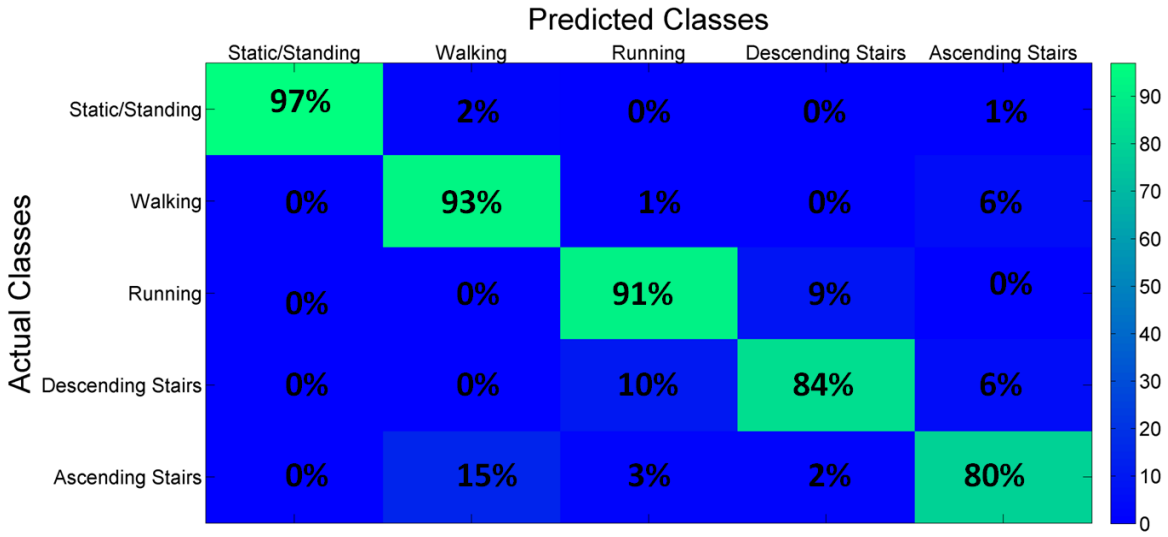

By analysing the above results, it is clear that the decision tree achieves the highest performances regardless of the activity. **For the case of freely carried sensors, the results obtained with the decision tree are comparable with the ones achieved in the literature for body fixed sensors (Yang 2009, Frank et al 2011).**

For all classifiers the lowest identification accuracy is achieved in the stair cases. In particular, a higher miss classification between descending the stairs and running and between climbing the stairs and walking on a flat plane has been observed. The latter can be attributed to similar values of the sub-band energy ratios for the mentioned activities. In order to reduce the ambiguity in the recognition of the mentioned classes the total energy has also been evaluated. The total and sub-band energies for the stair case are reported in

Figure 5-3 (upper part) where the automatic classification performed by the decision tree is also showed.

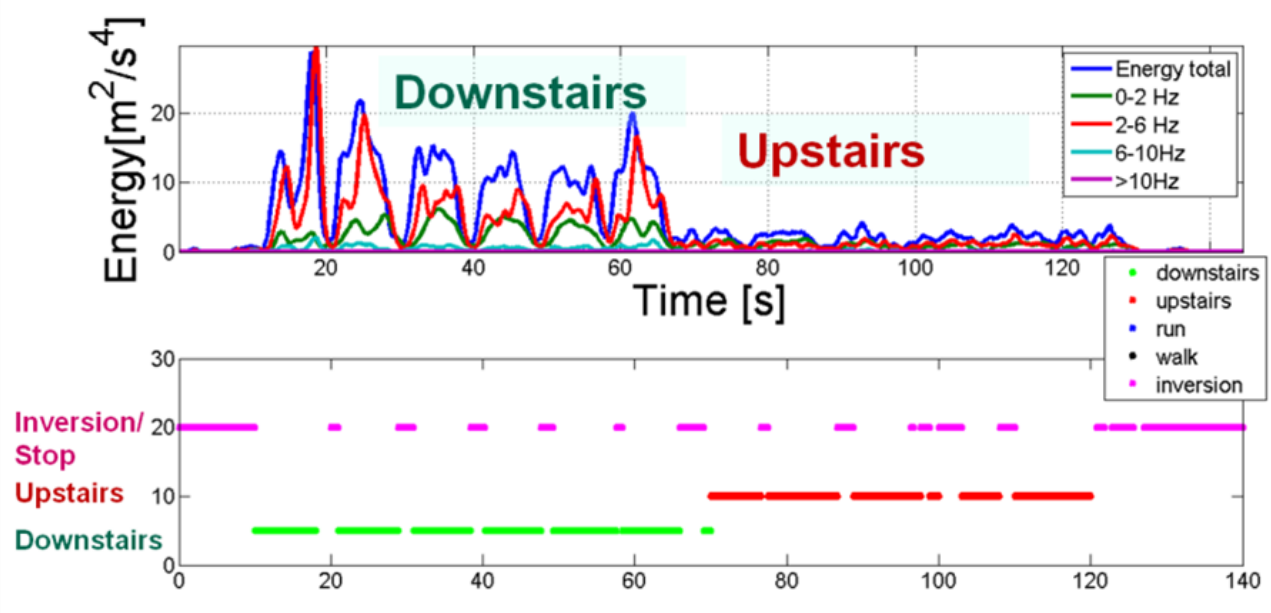

Figure 5-3: (Upper part) Total and sub-band energies; (lower part) classification results of the decision tree classifier for a user descending and climbing stairs with the sensor in a swinging hand.

A certain ambiguity persists between climbing up the stairs and walking when the total energy is similar for the two modes. The latter situation can occur, for example, in the slow walking case. With the proposed algorithm, after the energy evaluation, the dominant frequencies are also analyzed. But this feature does not allow all uncertainty to be totally removed, therefore the correlations between accelerometer components have been also evaluated. This is the most effective feature to identify the stair cases. However, it is worth pointing out that the stair case is particularly hard to identify when the sensor is in the hand and the user is frequently changing the sensor's orientation.

As explained in Section 3.5.2, the reason is that when the sensor orientation varies the cross-correlation terms can be less effective since they relies on the signal' single components.

Despite these limitations, in general, even for the stair cases, the decision tree provides a good accuracy, as shown in Figure 5-3. It is worth pointing out that for the staircase the use of additional sensors, such as a barometer, could remove any ambiguity in the recognition process. In fact, despite of its sensitivity to weather pattern and pressurization level of building ventilation systems (Morrison et al 2012), a barometer can be useful to sense altitude variations such as those due to a change of floor.

Moreover, by comparing the results of the three classifiers, it can be observed that the Naïve Bayesian achieves the lowest performance. This is likely due to the weak assumption of independent features as explained in Section 3.6.1.

The performance of the *k*-nearest-neighbour classifier is strictly related to the *k* parameter value. As reported in Section 3.6.3, for simplicity in the algorithm implemented in this thesis, *k* has been selected as 1. Further analyses are required to evaluate how the classifier performance changes for different values of *k*. Finally, as expected, all classifiers achieve the worst performance when the sensor is in the user's swinging hand. Conversely, the best performances are obtained for the body fixed sensor, namely the foot mounted sensor.

5.2 Step length evaluation: training and assessment

As shown in Figure 4.9, the algorithm for the evaluation of the user's step length requires the identification of the sensor carrying mode/hand motion and step events performed through dedicated modules. The present section describes the tests conducted for training and testing each single module. Then, the assessment of the step length model in the position domain is described and related results are discussed.

5.2.1 Data collection set up

All data collections described in this section were performed using the NavCube, a multi-sensor navigation platform described in (Morrison et al 2012). The NavCube includes a Novatel receiver and is able to support up to 10 six-degree of freedom Analog Devices ADIS16375 inertial sensors. Each sensor weighs 100 grams and offers a very good compromise in terms of size/weight and performance.

All collected data are synchronized with GPS time and consequently can be used for comparison purposes. A shown in Figure 5-4, the system can be worn on the user's waist without changing a natural walk mainly thanks to its low weight of 2.7 kg.

Figure 5-4: (Left)Test subject wearing the NavCube at the waist, two IMUs are foot mounted and two IMUs are in the user's hand; (Right) Zoom on the NavCube

5.2.2 Criterion for the sensor location selection

As for the global motion recognition case, different tests have been carried out to collect sufficient data for training and testing the step length model. During the data collections each subject was carrying at least one IMU in the hand and one mounted on the foot. Similarly to the data collections described in Section 5-1, the wires connecting the NavCube to the IMUs were rigidly fixed to the user's body for keeping the natural walking style. Details about the selection criterion of the sensor locations are provided herein.

5.2.2.1 Sensor on the foot

The foot mounted sensor was used as a reference. The true pedestrian's gait cycle was identified by using moving variances on the norm of the foot mounted accelerometer's signal. This is a consolidated approach used in the literature for detecting step events with foot mounted sensors (Skog et al 2010). Even if the process of detecting stance phases with foot mounted sensors is not error free, when test subjects are walking at a normal speed on a flat plane, which is the situation considered here, this error can be neglected with good approximation. In Figure 5-5 the IMU mounted on the user's foot during one of the test fields is shown.

Figure 5-5: ADIS 16375 IMU attached on the foot and used as a reference for the step detection algorithm.

5.2.2.2 Sensor in the user hand

The sensor in the hand was used to test the algorithm for the hand swinging and texting cases. As explained in Section 4-2, during the texting mode, the sensor is quite stable while the user is walking. Texting mode is also representative of the other states considered in the design of the carrying mode classifier, namely phoning and bag carrying. In fact all these modes have been included in a unique class. Furthermore, empirical tests have shown that also the trouser pocket case can be included in the above class since, as the previously mentioned states, it induces IMU signal patterns similar to the body fixed case.

5.2.3 Sensor carrying mode identification and step detection algorithms: training and assessment

In this section the data collections performed to train and assess the carrying mode/hand motion classifiers and the step detection algorithms are described. Then, the performances of these algorithms are reported and discussed.

5.2.3.1 Data collection methodology

A first series of data collections were performed for training the sensor carrying mode/hand motion classifier. Two women and two men were required to walk along two routes of about 50 and 120 metres carrying the NavCube. During the first run the subjects walked with the IMU in their swinging hands. During the second and third runs the users walked pretending to type a message on the smart-phone (IMU) and

phoning. For the fourth run, the pedestrian was carrying the IMU in a backpack (for the men) or in a purse (for the women). During the fifth run, a phone call was simulated. Specifically, the user started walking with the IMU in the bag, answered a phone call while walking and then put the IMU back in the bag. The first five runs were conducted over the shortest path, illustrated in black in Figure 5-6. The last run, illustrated in red in the same figure, consisted of a free motion. The subjects started at the location marked with the flag "Start" in Figure 5-6 and walked back to the initial point performing a "U turn" in the middle of the path. All motions were time tagged and annotated similar as in Section 5-1.

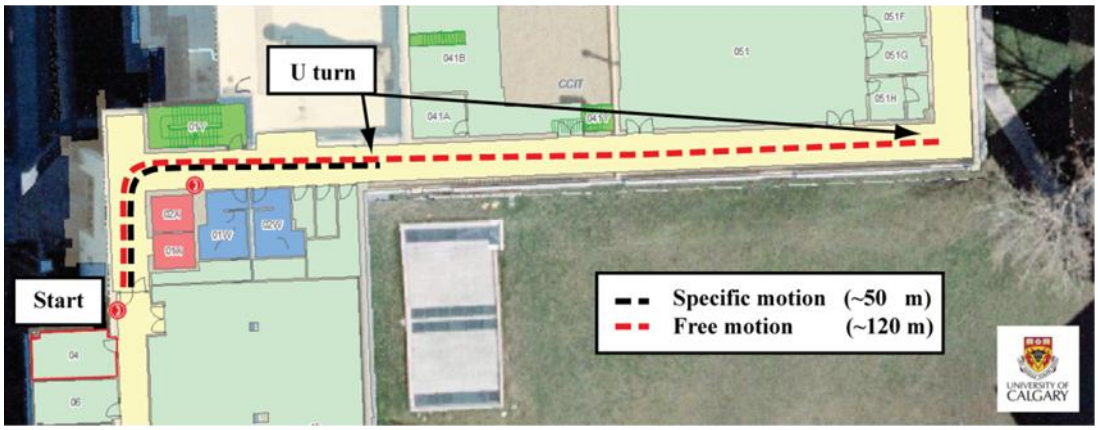

Figure 5-6: Indoor map of the handheld data collection with two pedestrian routes.

As shown in Figure 5-7, a second series of data collections was performed in a parking lot for assessing both algorithms, namely for motion recognition and step detection. Four different subjects, two men and two women were asked to perform a

free motion walk in a parking lot, which is an open sky environment. The users were walking for about 300 metres carrying the IMU in their hands and without receiving instruction about the sensors orientation. The users were required to perform all mentioned motions but they could choose the sequence of occurrence. Also this time, the time of occurrence of each activity was carefully annotated.

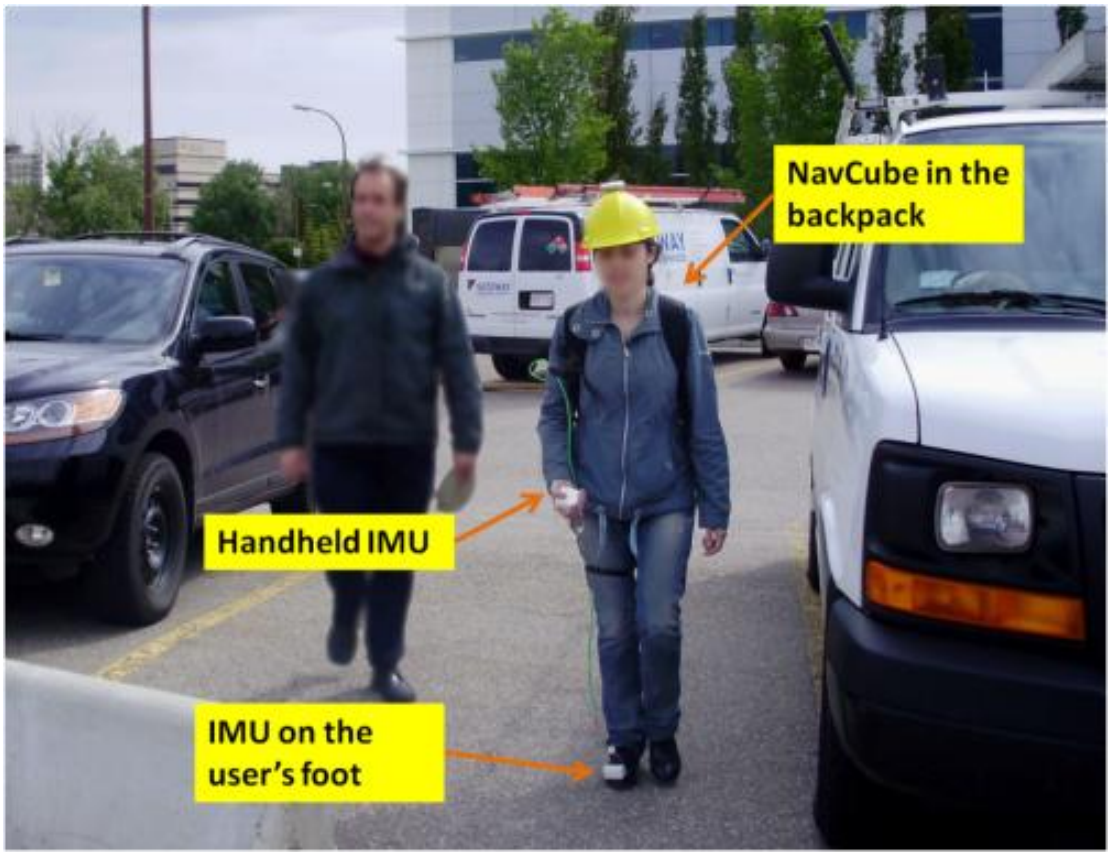

Figure 5-6: Outdoor data collection for testing the carrying mode/hand motion identification and step detection algorithms

5.2.3.2 Sensor carrying mode classifier assessment

The data collected during the outdoor test fields described in Section 5.3 were used to assess the performance of the algorithm for the sensor carrying mode/hand

motion identification. The outcomes of such analysis are summarized in the confusion matrix given in Table 5-5.

The proposed algorithm was able to identify the performed activities with accuracy higher than 94%. The worst performance was obtained for the identification of irregular motion where the activity was misclassified 6% of the time. This result is due to similar features characterizing swinging and irregular motions. Thus, if an irregular motion occurs during hand swing it can be easily miss detected.

However by analyzing the periodicities of the gyroscope signal for both states, the above ambiguity decreases in most of the analyzed cases. Indeed walking with swinging hands is a periodic activity while irregular motions are random by definition. For texting/phoning/bag cases, most of misclassifications occur when the subject is changing his direction.

Table 5-5: **Confusion matrix for the sensor carrying mode/hand motion classifier**

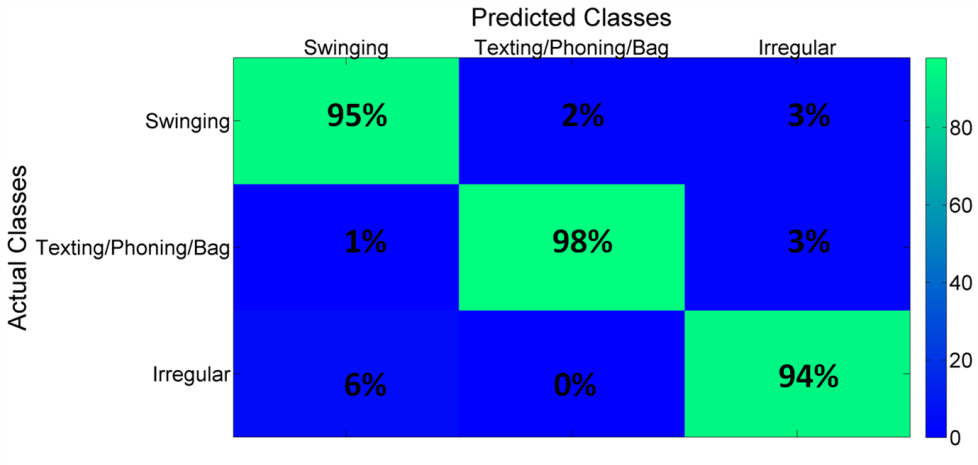

5.2.3.3 Step detection assessment

The data used for testing the algorithm for sensor carrying mode/hand motion identification has also been used to assess the step detection algorithm proposed in Chapter 4. For this purpose, the step events detected from handheld device have been compared with the ones identified for the foot mounted IMU case.

The results of this analysis are summarized in Table 5-6 where the P_{det} and the P_{md}, defined in Section 5.1.3, are reported. In particular, in this context the probability of detection corresponds to the percentage of correctly identified samples with respect to the ones identified with the sensor on the foot.

In addition, the probability of false alarm (P_{fa}) representing the percentage of incorrectly identified samples is also reported. It can be seen that for each motion mode the step detection accuracy is higher than 98%. Finally, it is worth pointing out that the performance of the algorithm is high regardless of the type of activity performed by the pedestrian.

Table 5-6: Step detection algorithm performance

steps in ...	...hand swinging	...texting	...phoning	...bag
P_{det}	99%	100%	99%	97%
P_{fa}	1%	0%	0%	1%
P_{md}	1%	0%	1%	3%

5.2.4 Step length model training

The last stage to evaluate the travelled distance is to estimate the user's step length. In Chapter 4 a step length model for handheld device has been proposed. The model is based on the combination of user' height and step frequency by using a set of three constants. As detailed in Chapter 4 both universal and calibrated models are proposed.

The set of universal parameters *k* defined in (4.5) has been found using the data collected by 12 subjects, six men and six women between twenty and forty years old. The test subjects were required to walk along a 200 m straight line on a parking lot, at three different speeds, for a total length of approximately 600 m. As shown in Figure 5-8, a second person was pacing the subject using a wheel speed sensor, which was also used for measuring true step lengths. This wheel encoder provides the pedestrian's walking speed with an accuracy of ±4×10-3 m/s.

The records were time tagged with GPS time. The test subjects walked at different speeds, namely at slow speed (about 0.8 km/h), intermediate speed (about 1.8 km/h) and fast speed (about 4 km/h) with the hand in texting and in the swinging motion mode. Universal parameters for *k* were found by fitting the handheld MEMS based step length model to all datasets. The optimum fitting of the step length model as function of the product of the user's height with the step frequency is shown in Figure 5-9.

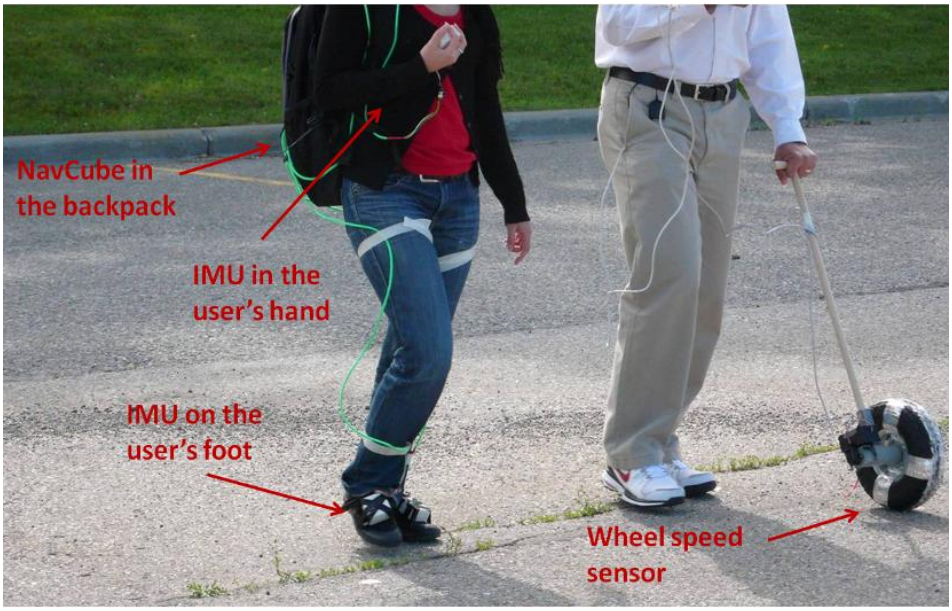

Figure 5-7: Data collection set up for training the parameters of the step model. The subject walks at different speeds with one IMU in the hand and one on the foot. A second person paces the test subject by using a wheel speed sensor.

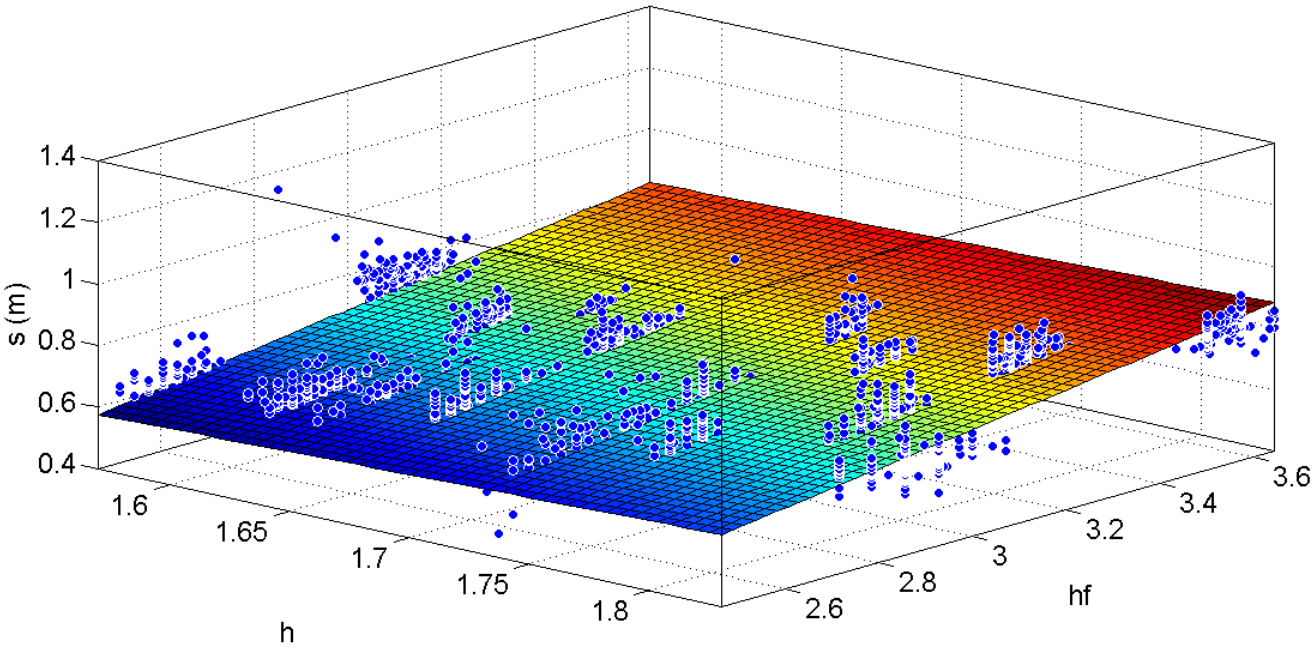

Figure 5-8: Linear fitting of the true step lengths (blue dots) with the user's height (h) and the product of the strongest dominant frequencies with the user's height (hf) at different walking speeds and hand's motions. The outcome is the universal set K in the step length model.

The performance of the proposed step length model has been computed in the position domain. For this purpose new data collections were conducted with 10 subjects: 5 men and 5 women different from the ones that participated to the training phase. The same number of male and female subjects was selected in order to test the validity of the algorithm regardless the subject's sex. Furthermore, the use of 10 subjects allowed extensively assessing the model.

The test subject age varied between 20 and 35. Test fields were carried out in an open sky soccer field and the data were collected with the NavCube. This location was selected to guarantee the availability of GPS data, used for heading determination, as detailed herein.

The subjects were asked to walk twice along the curved route of the soccer field. Each route corresponds to about 300 metres for a total length of 600 meters. As shown in Figure 5-10 for one subject, during the first run, the test subjects walked with the IMU in their swinging hand while in the second run they walked carrying the sensor in texting mode. Pedestrians observed no break between the two runs and changed the carrying mode while walking.

Figure 5-9: (Left) Test subject walking with the IMUs in his swinging hands; (Right) Test subject walking with the IMUs in his texting hands.

The subjects were also asked to perform two straight paths for the purpose of finding individual calibrated set *k*. "True" step lengths were computed by interpolating post-processed differential GPS positions over each detected step. Then, a Recursive Least Square (RLS) technique was performed to find the calibrated set k_n, with a convergence achieved at the n^{th} iteration.

5.2.5 Step length model assessment

In order to evaluate the step length model, the sensor carrying mode/hand motion and step events must first be identified. To investigate the contribution of these two modules to the overall error budget, their performances are evaluated individually for these data sets. The results of the classifier assessment are reported in the confusion

matrix shown in Table 5-7. It can be observed that the classifier achieves high accuracy for both analyzed modes, i.e. texting and swinging.

Table 5-7: Confusion matrix of the algorithm for the identification of the sensor carrying mode/hand motion.

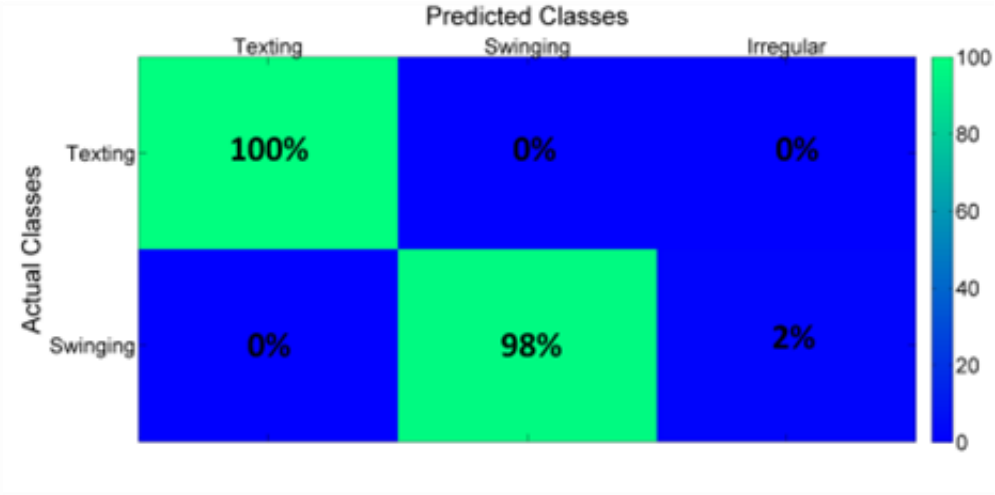

In Table 5-8 the percentage of correct detection (P_{det}) for each motion mode performed by the 10 test subjects and the percentages of correct step detection are shown. In order to assess the step length estimation model, the percentage of error over the travelled distance has been evaluated for all subjects by applying the following:

$$\varepsilon = \frac{d_{handheld}}{d_{GPS}} \tag{5.1}$$

where

- $d_{handheld}$ is the travelled distance obtained by applying the equation (4.1) and using the proposed step length model.

- d_{GPS} is the reference distance computed by using post-processed GPS carrier phase signals in a differential mode. The accuracy of the post-processed solution with a 1 km baseline under open sky was better than 1 cm.

A PDR technique has been applied to obtain the total travelled distance. As seen in (4.1) the latter is based on the recursive sum of each step displacement combined with the walking direction over each step. The heading is here obtained from the GPS trajectory post-processed in differential mode. This approach allows mapping the estimated displacement in position domain. Furthermore, the use of these post-processed headings does not affect the computation of the distance travelled error, as it can be seen in equations (4.1) and (5.1). In Table 5-8 the error percentages over the travelled distance are shown for all test users for the universal and the fitted set of parameters. Men are indicated with “M” and women with “W”. The table reports also the number of iterations necessary to achieve RLS convergence in the calibration phase.

From the results we can see that both universal and calibrated models achieve travelled distance errors between 4 and 6% for the majority of subjects. The larger errors correspond to the male subjects M4 and M5 achieving errors of 8 and 9% for the universal model. However, by applying the calibrated model the errors significantly decrease and the highest percentage is then 5%. **The results obtained are comparable with the ones reported in the literature for the body fixed case**. The number of iterations required for estimating the fitted solution can also be used for assessing the effectiveness of the model. By observing Table 5-5, where the number of iterations required for each subject is reported, it can be observed that the mean

number of iterations necessary to converge to the calibrated solution is equal to four. These results further confirm the validity of the model.

Table 5-8: Metrics for Evaluating the Handheld Based Step Length Model

Subject	$\%P_{det}$ (motion)	$\%P_{det}$ (steps)	%DistanceTravelled		Convergence Iterations
			Universal Model	Fitted Model	
M1	100	99	5.8	5	4
M2	100	100	4.8	4.3	3
M3	99	100	5	4.5	3
M4	100	99	8	4.2	6
M5	100	100	9	3.8	7
W1	98	97	5.2	4.3	4
W2	100	100	3.2	2.5	3
W3	98	99	4.5	4	3
W4	100	98	5.6	5	3
W5	100	100	5.8	5	4
Mean	99.6	99.2	5.7	4.2	4

To further assess the quality of the model the absolute differences between fitted and universal parameters have been evaluated for all subjects. The results of such analysis are shown in Figure 5-11 reporting the minimum, maximum and mean values of the differences between fitted and universal parameters.

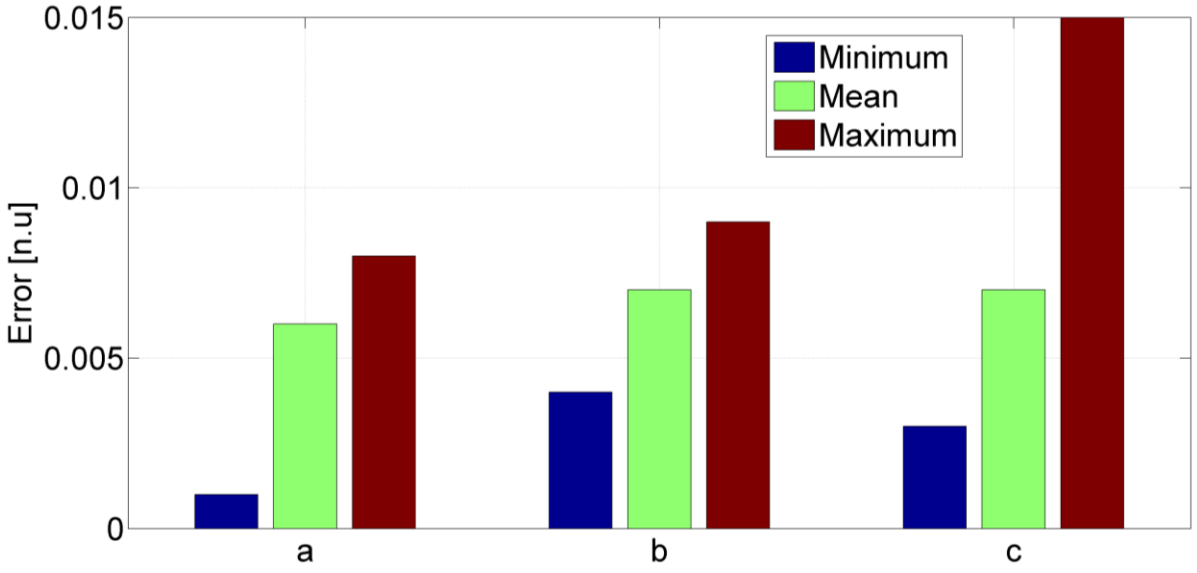

Figure 5-10: Minimum, mean and maximum absolute differences between "fitted" and "universal" parameters of the proposed step length model.

Figure 5-12 shows the three travelled paths for the worst results case (M5). We can see that the path is overestimated by the universal model. However, the fitted model significantly increases performance.

Figure 5-11: Reference path in green and estimated trajectories: modelled step length with the universal parameters in red and with the calibrated parameters in blue for the test subject with the worst performance (M5).

A possible reason for the worst performance obtained by M5 is likely to be the height of this test subject, who is significantly taller than the other test subjects. Consequently, by increasing the number and the typology of the test subjects, higher performance would be expected.

5.3 Summary

This chapter described the training and assessing phases of the algorithms proposed in Chapter 3 and Chapter 4. Three different classifiers, namely a decision tree, a k nearest neighbour and a Naive Bayesian classifier have been proposed to identify different motion modes, i.e. standing, walking, running, and climbing/descending stairs. The decision tree achieved the best performance with an accuracy higher than 90% for all examined states also when the sensor is handheld, which is the most critical case. Then the performances of the step length model described in Chapter 5 have been assessed. Before evaluating the distance walked over a step, the sensor carrying mode/hand motion is identified in order to adapt the step detection algorithm to the specific case. Experimental tests showed a classification accuracy above 94% for all states and a percentage of correct step event detection above 97% irrespective of the sensor carrying mode. Then, the step length model proposed in Chapter 4 has been assessed in the position domain. The model achieves error percentages over the travelled distance between 2.5% and 5%. These percentages are similar to the ones obtained in the literature for the body fixed case. Thus, these results show that an inertial sensor can be exploited for autonomous navigation and tracking of pedestrians using handheld devices, i.e. for smart phones applications. In addition, the proposed algorithms analyze the signals in windows between 1.2 to 2.5 seconds, which is also compatible with real time implementation.

Chapter Six: Conclusions and Recommendations

This thesis investigated the use of low cost MEMS handheld inertial sensors for pedestrian navigation. In particular, the research work focused on the characterization of user's motion mode and evaluation of the linear travelled distance of a subject walking on a flat ground. The present chapter summarizes the main contribution of this research work. Finally recommendations for further enhancing the proposed algorithms and integrating these in a complete pedestrian navigation system are made.

6.1 Conclusions

On the basis of the analysis and outcomes presented in this thesis the following conclusions can be drawn:

1. The literature review of pedestrian navigation techniques based on MEMS inertial sensors has highlighted that the existing research works are mainly focusing on the use of body fixed sensors. The few published documents exploiting non-body fixed sensors for pedestrian navigation are generally assuming sensor locations where the device is quasi-stable while the user is walking, for example a trouser pocket. A complete characterization of the handheld case was therefore proposed herein through the analysis of different sensor carrying modes that are typical of handheld devices applications. In particular, the case of sensors carried

in a user's swinging hand is also examined whereas it had been generally ignored in the previous literature.

2. A specific IMU signal pre-processing was found to be necessary for coping with the consumer grade nature of the inertial sensors used in smartphones. In Chapter 2, details were provided about the signal processing techniques used for denoising the signal. Furthermore the use of the pre-processed IMU signal norm was found to be effective for removing any dependence on the sensor orientation.

3. The recognition of the global user motion mode, performed with handheld devices, requires the selection and extraction of features irrespective of the sensor carrying mode. Indeed, when the sensor is freely carried, its position can quickly change. Features able to characterize the global user motion mode with high accuracy regardless not only of the sensor position but also of the user walking style have been extracted and presented in Chapter 3.

4. By exploiting the above features, three classifiers, namely the *k* nearest neighbour, the decision tree and the Naïve Bayes have been designed and implemented in order to identify the following global motion modes, namely standing, walking, running and climbing/descending stairs. As reported in Chapter 5, the decision tree classifier showed the highest accuracy.

5. Knowledge about the sensor carrying mode has been exploited to better characterize gait cycle and, consequently, detecting step events. This knowledge

has been achieved through the design of a dedicated classifier, described in Chapter 4, which is able to distinguish different sensor carrying modes/hand motions. In particular, the situation of the sensor carried in a swinging hand has been distinguished from the case when the user is interacting with the mobile device. The latter is, for example, the situation of a subject walking while phoning or texting a message on his/her mobile device. In these cases the patterns induced in the IMU signal have been found similar to the ones produced by body fixed sensors. Consequently, in these situations the human gait cycle can be analyzed by using techniques designed for the body fixed sensor case. Conversely, these techniques are a suboptimum choice for the swinging hand case.

6. The identification of “irregular motions” has been found necessary in order to discard parasite motions in the navigation process. This class includes all motions inducing an inertial force on the sensor that does not reflect a real change of user’s position. The identification of this type of motion is usually neglected in PDR algorithms but it is essential for avoiding faulty propagation of the user position in time.

7. After detecting steps, the step length needs to be evaluated. A step length model for handheld inertial sensors was established and detailed in Chapter 4. The model combines the user step frequency and the user height with a set of three constants.

8. In order to evaluate the user step frequency with handheld devices, a dedicated analysis was carried out to relate hand and foot frequencies. This analysis showed that the strongest hand frequency, i.e. the frequency with maximum power, can be coupled with the stride frequency or with the step frequency. In particular, it has been observed that the strongest hand frequency is likely coupled with the stride frequency for higher user's speed, especially if the sensor is carried in the user swinging hand. Following these outcomes, a specific step frequency detector has been implemented to evaluate the step frequency even if the sensor is in the user hand.

9. A universal and a calibrated version of the step length model are proposed. The universal model has been designed by training the set of constants using twelve subjects while the calibrated model is based on fitting the constants for each single test subject. The model has been assessed in the position domain with 10 persons, different from the ones that participated to the training phase. The percentage of error over the travelled distance is between 2.5% and 5% which is comparable with the results achieved in the literature using body fixed sensors. These results show that the proposed algorithms can be applied to autonomous navigation and tracking of pedestrians using smartphones. Finally, the analysis windows used to analyze the IMU signals are between 1.2 and 2.5 seconds, which render the algorithms suitable for real time applications.

6.2 Recommendations

In view of the above conclusions, the following recommendations are suggested for future work:

1. The classifier for the global motion mode identification relies only on accelerometer measurements. To achieve higher performance, especially for climbing and descending stairs mode identification, the use of additional sensors is suggested. Specifically, for the identification of the two mentioned states the use of a barometer, able to sense the change of pressure between floors, is expected to increase the classifier accuracy.

2. The algorithm for the evaluation of the travelled linear distance exploits the sensor carrying mode knowledge for identifying step events. For characterizing the human gait cycle the distinction between the swinging case and situations similar to the body fixed case, as described in Point 6 of Section 6.1, was found to be relevant. However for heading determination purposes, it could be of interest to increase the classification levels by assigning activities such as phoning and texting to different classes. In fact, the orientation of the device's compass depends greatly on how the user is holding the device. Texting and phoning, for example, usually cause significant differences in the orientation.

3. The step length model is based on the evaluation of the user step frequency by a dedicated binary classifier. The latter uses a trained threshold to distinguish step and stride events. However the age of the test subjects used was between 20 and 35. Further analysis should be carried out to investigate as the subject age could affect the value of this threshold. The use of younger and older subjects could complete the analysis.

4. The algorithm for the linear distance evaluation was designed for the normal walking case. Further studies should be performed to adapt such algorithms to other situations, such as running, climbing and descending stairs. Then, the knowledge of the global motion mode, acquired through the classifier presented in Chapter 3, could be exploited to adapt the algorithm for the travelled distance estimation to the specific case.

5. The universal step length model could be used as first approximation for any navigation filter that would offer tuning functionalities. Further enhancement of the universal model performance could be achieved by increasing the typology of subjects used in the training phase. Finally, as pointed out at in the ninth conclusion, the algorithm for computing the linear distance evaluation has been designed for real time application. Thus, real time implementation of such algorithm should be tested.

6. Finally, in order to implement a self-contained pedestrian navigation system for GNSS denied environments, the algorithm for the evaluation of the linear travelled distance should be integrated with an algorithm for heading determination, for example based on gyroscopes and/or magnetometers.

References

Ayub, S., X. Zhou, S. Honary, A. Bahraminasab, and B. Honary (2012) *Sensor placement modes for smartphone based pedestrian dead reckoning.* Computer, Informatic, Cybernatics and Applications-Springer, vol 107, pp. 123–132.

Alonso J. M., M. Ocana, M. A. Sotelo, L. M. Bergasa, and L. Magdalena (2009) "WiFi Localization System Using Fuzzy Rule-Based Classification," in *Computer Aided Systems Theory - Eurocast 200*9, Moreno Diaz, R., F. Pichler, and A. Quesada Arencibia, eds., Springer-Verlag Berlin, Berlin, pp. 383-390

Alvarez, D., R. C. Gonzalez, A. Lopez, and J. C. Alvarez (2006) "Comparison of step length estimators from wearable accelerometer devices," in Proceeding of 28th In Engineering in Medicine and Biology Society, 2006.EMBS '06. 28th Annual International Conference of the IEEE, pp. 5964–5967.

Aminian, K., B. Najafi, C. Büla, P.F. Leyvraz, and P. Robert (2002) "Spatio-temporal parameters of gait measured by an ambulatory system using miniature gyroscopes" *Journal of Biomecanics*, vol 35, pp. 689–699.

Bao, L. and S. S. Intille (2004) "Activity recognition from user-annotated acceleration data" in Proceeding of Second International Conference on Pervasive Computing (PERVASIVE), April, Vienna, Austria, pp. 1-17

Bancroft, J.B. (2010) *Multiple Inertial Measurement Unit Fusion for Pedestrian Navigation*. PhD Thesis, Department of Geomatics Engineering, University of Calgary, Canada. (Available at http://plan.geomatics.ucalgary.ca)

Beauregard, S. (2007) “Omnidirectional pedestrian navigation for first responder,” in *Proceedings of the 4th Workshop on Positioning, Navigation and Communication (WPNC 2007),* March 22,Hannover, Germany, pp 33-37.

Bylemans, I., M. Weyn, and M. Klepal (2009) “Mobile Phone-Based Displacement Estimation for Opportunistic Localisation Systems,” in *Proceedings of the Third International Conference on Mobile Ubiquitous Computing Systems Services and Technologies*, IEEE, no. 10, pp113-118.

Bourke, A. K., and G.M. Lyons (2006) “A threshold-based fall-detection algorithm using a bi-axial gyroscope sensor,” *Medical Engineering & Physics*, vol. 30, issue 1, pp. 84–90.

Chowdhary, M., M. Sharma, A. Kumar, K. Paul, M. Jain, C. Agarwal, G. Narula (2009) “Context detection for improving positioning performance and enhancing user experience,” in *Proceedings of the 22nd International Meeting of the Satellite Division of the Institute of Navigation*, September, Savannah, GA, pp. 2072 - 2076

Cohen L. (1995) “Time-Frequency Analysis: Theory and Applications*” Prentice-Hall, Inc.,* Upper Saddle River*, NJ, USA*

Do, T. N., and S. Y. Suh (2012) "Gait Analysis Using Floor Markers and Inertial Sensors," *Sensors* 12, no. 2:, pp. 1594-1611.

El-Sheimy, N. (2004) *Inertial techniques and INS/DGPS Integration,* ENGO 623-Course Notes, Department of Geomatics Engineering, University of Calgary, Canada

Ermes, M., J. Parkka, J. Mantyjarvi, and I. Korhonen (2008), “Detection of daily activities and sports with wearable sensors in controlled and uncontrolled conditions” *IEEE Trans.Inf.Technol*,B12, pp. 20–26.

Foxlin, E. (2005), “Pedestrian tracking with shoe-mounted inertial sensors,” *IEEE Computer graphics and applications*, vol. 25. no 6, December 200, pp. 38-46

Frank K., M. J. V. Nadales, P. Robertson, and M. Angermann (2010) “Reliable real-time recognition of motion related human activities using MEMS inertial sensors”, in *Proceeding of the 23rd International Technical Meeting of The Satellite Division of the Institute of Navigation*, Portland, OR, 21- 24 September

Gabaglio, V. (2002) *GPS/INS integration for pedestrian navigation,* PhD Thesis Ecole Politechnique Federale De Lausanne, Department of Engineering of the Environment, Switzerland

Godha, S. and G. Lachapelle (2008) "Foot mounted inertial system for pedestrian navigation," *Measurement Science and Technology*, vol 19, pp. 1-9.

Good, P. (2009) “Robustness of Pearson correlation,” Available on line at http://interstat.statjournals.net,

Gusenbauer, D., C. Isert, and J. Krosche (2010) “Self-Contained Indoor Positioning on Off-The-Shelf Mobile Devices,” in *International Conference on Indoor Positioning and Indoor Navigation,2010* , September, pp. 15–17

Hide, C., T. Botterill, and M. Andreotti (2010) “Low cost vision aided IMU for pedestrian navigation,” in *Proceeding. of UPINLBS*, Kirkkonummi, Finland, October, pp. 1 –7

Inoue, Y., A. Sashima, and K. Kurumatani (2009) "Indoor Positioning System Using Beacon Devices for Practical Pedestrian Navigation on Mobile Phone," in *Proceedings of the 6th InternationalConference on Ubiquitous Intelligence and Computing, UIC'09*, Brisbane, Australia, 7–9 July, pp. 251-265.

Jahn, J., U. Batzer, J. Seitz, L. Patino-Studencka, and J.G. Boronat (2010) “Comparison and Evaluation of Acceleration Based Step Length Estimators for Handheld Devices,” in *Proceeding of IEEE 2nd Conf. on Indoor Positioning and Indoor Navigation,* Zurich, Switzerland, Sep. 15-17, 2010, pp. 1-6.

Jain K. (2000) “Statistical pattern recognition: Review” *IEEE Transaction on pattern analysis and machine intelligence,* Vol. 22, No. 1

Karantonis D. M., M. R. Narayanan, M. Mathie, N. H. Lovell and B. G. Celler (2006). “Implementation of a real-time human movement classifier using a triaxial accelerometer for ambulatory monitoring” *IEEE Transactions on Information Technology in Biomedicine,* Vol. 10, No. 1, January, pp. 156–167

Kim, J.W., H.J. Jang, D. Hwang, and C. Park (2004) “A step, stride and heading determination for the pedestrian navigation system” *Journal of Global Positioning. Syst*em, vol 3, pp. 273–279.

Kraft, M. (1997) *Closed Loop Digital Accelerometer Employing Oversampling Conversion*, PhD Thesis, School of Engineering, Coventry University, UK.

Kwakkel S.P. (2008) *Human lower limb kinematics using GPS/INS*, MSc Thesis, Department of Geomatics Engineering, University of Calgary, Canada (Available at http://plan.geomatics.ucalgary.ca).

Lachapelle, G. (2007) "Pedestrian navigation with high sensitivity GPS receivers and MEMS." *Personal and Ubiquitous Computing*, vol 11, pp. 481-488.

Lara, O.D. and M. A. Labrador (2012) “A Survey on Human Activity Recognition based on Wearable Sensors”. *IEEE Communications Surveys and Tutorials*

“

Luimula, M., K. Saaskilahti, T. Partala, S. Pieska, and J. Alaspaa (2010) "Remote Navigation of a Mobile Robot in an RFID-augmented Environment," *Pers. Ubiquitous Comput.,* vol 14, no 2, February, pp. 125-136

Mannini, A., A.M. Sabatini (2010) “Machine learning methods for classifying human physical activity from On-Body Accelerometers,” *Sensors 2010*, vol 10, pp.1154-1175.

Mathie, M.J. (2003) *Monitoring and interpreting human movement patterns using a triaxial accelerometer*, Ph.D. thesis, University of New South Wales.

Mathie, M.J., B.G. Celler, N.H. Lovell and A.C.F. Coster (2004) “Classification of basic daily movements using a triaxial accelerometer”, *Med. Biol. Eng. Comput*. 42 (5), pp. 679–687

Miyazaki, S. (1997) “Long-term unrestrained measurement of stride length and walking velocity utilizing a piezoelectric gyroscope” *IEEE Transaction on Biomed. Eng*ineering, vol 44, pp. 753–759.

Morrison, A., V. Renaudin, J.B. Bancroft, and G. Lachapelle (2012) “Design and testing of a multi-sensor pedestrian location and navigation platform” *Sensors 2012*, 12, pp.3720–3738.

Nijsen T.M E., R. M. Aarts, P.J. M. Cluitmans, and P.A. M. Griep (2010) “Time-frequency analysis of accelerometry data for detection of myoclonic seizures”, *IEEE Transactions on Information Technology in Biomedicine*, Vol. 14, No. 5, September, pp. 1197–1203

Park,J. (2008) “Synthesis of natural arm swing motion in human bipedal walking,” *Journal of Biomechanics*, vol. 41, no. 7, pp. 1417-1426, Apr. 2008.

Park, M. and Gao, Y. (2008) “Error and Performance Analaysis of MEMS-based Inertial Sensors with a Low-cost GPS Receiver.” *Sensors* 8, no. 4,pp. 2240-2261

Pei L., R. Chen, J. Liu, W. Chen, H. Kuusniemi, T. Tenhunen, T. Kröger, Y. Chen, H. Leppäkoski and J. Takala (2010) “Motion recognition assisted indoor wireless navigation on a mobile phone,” in *Proceeding of the 23rd International Technical Meeting of The Satellite Division of the Institute of Navigation*, Portland, OR, September, pp. 3366–3375 2010.

Proakis, J.G., and Manolakis, D.G. (1996) Digital Signal Processing: Principles, Algorithms and Applications , 3rd Edition, Pearson Education

Ravi, N., N. Dadekar, P. Mysore, and M.L. Littman (2005) “Activity recognition from accelerometer data,” *in Proceedings of 17th Innovative Applications of Artificial Intelligence Conference*

Renaudin, V., O. Yalak, P. Tomé, and B. Merminod (2007) “Indoor navigation of emergency agents,” *European Journal of Navigation*, vol. 5, pp. 36- 45.

Renaudin, V., M. Susi and G. Lachapelle (2012) "Step Length Estimation Using Handheld Inertial Sensors." *Sensors*, no. 7, pp 8507-8525.

Rose, J. and J. G. Gamble (2006) *Human walking* ,Third edition, Lippincott Williams and Wilkins, Baltimore

Sabatini, A.M., C. Martelloni, S. Scapellato, F. Cavallo (2005) “Assessment of walking features from foot inertial sensing” *IEEE Transaction on Biomedical Eng*ineering, vol 52, pp. 486–494

Sabatini, A.M (2006) *Inertial sensing biomechanics: a survey of computational techniques bridging motion analysis and personal navigation*, Computational Intelligence for Movement Sciences: Neural Networks and Other Emerging Techniques, Idea Group Publishing, Hershey, PA, USA, pp.70–100. /http://www.idea-group.comS.

Skog,I., P. Händel,J.O. Nilsson, and J. Rantakokko (2010) “Zero-velocity detection - an algorithm evaluation,” *IEEE Trans. on Biomed. Eng*., vol. 57, no. 11, pp. 2657–2665,

Shen, G. W., R. Zetik, O. Hirsch, and R. S. Thoma (2010) "Range-Based Localization for UWB Sensor Networks in Realistic Environments," *EURASIP Journal on Wireless Communications and Networking*, vo. 2010, Article ID 476598, pp 9

Silverman, B. (1986) “Density Estimation for Statistics and Data Analysis”, Monographs on Statistics and Applied Probability, Chapman and Hall, London, UK

Steinhoff, U. and B. Schiele (2010) “Dead Reckoning from the Pocket—An Experimental Study” in *Proceedings of 2010 IEEE International Conference on Pervasive Computing and Communications (PerCom),* Mannheim, Germany, 29 March–2 April, pp. 162–170.

Suh, Y.S. and S. Park, (2009) “Pedestrian Inertial Navigation with Gait Phase Detection Assisted Zero Velocity Updating”, In *Proceedings of the Fourth International Conference on Autonomous Robots and Agents*, Wellington, New Zealand, pp. 505-510

Susi, M., D. Borio and G. Lachapelle (2011a) “Accelerometer Signal Features and Classification Algorithms for Positioning Applications,” in *Proceedings of International Technical Meeting, Institute of Navigation*, January 24-26, San Diego, CA, USA, 12 pages.

Susi, M., V. Renaudin and G. Lachapelle (2011b) “Quasi-static detection from MEMS handheld devices,” in *Proceedings of the International Conference on Indoor Positioning and Navigation (IPIN),* 21-23 September, Guimarães, Portugal, 9 pages.

Tao, W., T. Liu, R. Zheng and H. Feng (2012) “Gait Analysis Using Wearable Sensors,” *Sensors* 2012, 12, 2255-2283.

Teunissen, P.J.G. Adjustment Theory: An Introduction; Series on Mathematical Geodesy and Positioning; University of Delft: Delft, The Netherlands, 2003.

Tien, I., S.D. Glaser, S.D, R. Bajcsy,D.S. Goodin, M. J. Aminoff (2010)" Results of using a wireless inertial measuring system to quantify gait motions in control subjects" *IEEE Trans. Inf. Technol. Biomed*., 14, pp. 904–915.

Titterton, D. H., and J. L. Weston (2004) Strapdown Inertial Navigation Technology, 2nd Ed., Institution of Electrical Engineers, Stevenage

Tunçel,O., K. Altun, B. Barshan (2009) "Classifying human leg motions with uniaxial piezoelectric gyroscopes," *Sensors*, vol 9, pp. 8508-8546,.

Veltink P.H., H.B.J. Bussmann, W. De Vries, W.L.J. Martens and R.C. Van Lummel (1996) "Detection of static and dynamic activities using uniaxial accelerometers," *IEEE Transactions on Rehabilitation Engineering*, Vol. 4, No. 4, December, pp. 375–385

Webb A. (2002) "Statistical pattern recognition,"John Wiley & Sons, New York, USA

Weinberger, K.Q., J. Blitzer, and L. Saul. (2005) "Distance metric learning for large margin nearest neighbour classification" In *Advances in Neural Information Processing Systems* 18.

Winter, D.A. (1990) *Biomechanics and Motor Control of Human Movement*, (3rd Edition), New York, Wiley-Interscience Publishings.

Yin J., Q. Yang, and J. J. Pan (2010) “Sensor-based abnormal human-activity detection”, *IEEE Transactions on Knowledge and Data Engineering*, Vol. 20, No. 8, August, pp. 1082–1090

Zijlstra, W. and A.L. Hof (1997) “Displacement of the pelvis during human walking: experimental data and model predictions*” Gait Posture* 1997, 6, pp. 249–262.